Effect of polycations on stability and bioactivity of polyelectrolyte multilayers with thermoresponsive cellulose sulphate

Dissertation

Zur Erlangung des
Doktorgrades der Ingenieurswissenschaften
(Dr. Ing.)

der

Naturwissenschaftlichen Fakultät I – Biowissenschaften –

der Martin-Luther-Universität
Halle-Wittenberg,

vorgelegt

von Herr Dipl. Ing. Falko Doberenz

Gutachter:

Prof. Dr. rer. nat. habil. Thomas Groth

Prof. Dr. rer. nat. habil. Steffen Fischer

Priv.-Doz. Dr. Christian Schmelzer

22.11.2024

Table of contents

Abbreviations

ATP	adenosine triphosphate	**LCST**	lower critical solution temperature
RGD	arginine–glycine–aspartate	**NMR**	nuclear magnetic resonance
BMP	bone morphogenic proteins	**PCS**	PNIPAM-grafted-cellulose sulphate
CS	cellulose sulphate	**PZC**	point zero charge
CHI	chitosan	**PNIPAm**	Poly(N-isopropylacrylamide)
CST	critical solution temperature	**PEM**	polyelectrolyte multilayer
DQ	degree of quaternization	**PLL**	poly-L-lysin
DS	degree of substitution	**PG**	proteoglycan
EDTA	ethylenediaminetetraacetic acid	**QCHI**	quaternized chitosan
ECM	extracellular matrix	**QCM**	quartz crystal microbalance
FGF	fibroblast growth factor family	**RI**	refractive index
FN	fibronectin	**SPR**	surface plasmon resonance
FA	focal adhesion	**TCPS**	tissue culture polystyrene
GAG	glycosaminoglycans	**TE**	tissue engineering
GPI	glycosylphosphatidylinositol	**TGF**	transforming growth factor family
GF	growth factor	**UCST**	upper critical solution temperature
HEP	heparin	**VEGF**	vascular endothelial cell growth factor family
LbL	Layer-by-Layer	**WCA**	water contact angle

Abstract

The thermoresponsive Poly(N-isopropylacrylamide) (PNIPAm) is widely utilized in hydrogels and surface modification, enabling controlled drug release, cell sheet engineering, and tissue engineering. Due to its lower critical solution temperature near 32 ℃, close to body temperature, PNIPAm shows promise in adjusting the physiochemical properties of biomaterial surfaces. Nonetheless, existing methods to create PNIPAm-modified surfaces are often inefficient or costly and lack bioactivity, limiting their use as stimuli-responsive substrates regulating cell activities. A novel approach is explored here, integrating semi-synthetic glycosaminoglycans (GAGs) to facilitate the cost-effective fabrication of bioactive PNIPAm-containing polyelectrolyte multilayers (PEMs) using the layer-by-layer (LbL) technique. This involves the sequential adsorption of oppositely charged polyelectrolytes (PELs). The study investigates the PEM assembly using PNIPAm-containing PELs by conjugating PNIPAm with the polyanion cellulose sulphate (CS). CS, which resembles GAGs with excellent bioactivity, is used to mimic surface coatings using native GAGs to enhance bioactivity. In the framework of this research, two new synthetic pathways to prepare PNIPAm-grafted-cellulose sulphate (PCS) as a polyanion are developed, differing in the degree of substitution of PNIPAm and amount of sulphate groups. These variations aim to achieve both thermoresponsive and bioactive PEMs via the LbL technique. Lower sulphated PCS 1 (DS 0.41) and higher sulphated PCS 2 (DS 0.93) are used to investigate their ability to form PEMs with various polycations (chitosan, CHI, quaternized chitosan, QCHI, or poly-L-lysine, PLL). The resulting behavior, structure, stability, and surface properties of the PEMs strongly correlate with the sulfation degree, polycation type, and presence of PNIPAm. Notably, the highly sulphated PCS 2 effectively surpasses the steric hindrance of PNIPAm, enabling greater adsorption of both polycations and forming more stable PEMs compared to the less sulphated PCS 1 after exposure to pH 7.4. Moreover, the smaller molecule PLL tends to form more intertwined PEMs than the larger QCHI, significantly affecting surface properties. The surface characterization study is further linked to the toxicity and biocompatibility of the PEMs with cells from three different germ layers. The PEMs combined with PLL exhibit higher toxicity to 3T3, HepG2, and HaCaT cells, particularly when paired with PCS1, while the combination of QCHI and PCS2 demonstrates excellent biocompatibility, promoting cell adhesion and proliferation over 7 days. Immunofluorescence staining of the cytoskeleton and focal adhesions of 3T3 cells supports these findings regarding the superior biocompatibility and enhanced cell adhesion of QCHI and PCS 2. In summary, this thesis

introduces newly developed thermoresponsive coatings capable of modulating surface properties and enhancing bioactivity by incorporating PNIPAm-modified CS, a semi-synthetic GAG. These coatings hold immense potential as cell culture substrates for delivering growth factors, cell production, and as bioactive wound dressings for tissue regeneration.

Zusammenfassung

Das thermoresponsive Polymer Poly(N-isopropylacrylamid) (PNIPAm) findet breite Anwendung in Hydrogelen und bei der Oberflächenmodifizierung und ermöglicht die kontrollierte Freisetzung von Medikamenten, die Herstellung von Zellschichten und die Gewebezüchtung. Aufgrund seiner niedrigen kritischen Lösungstemperatur von etwa 32 °C, die nahe der Körpertemperatur liegt, hat PNIPAm das Potenzial, die physikochemischen Eigenschaften von Biomaterialoberflächen zu verändern. Bestehende Methoden zur Herstellung von PNIPAm-modifizierten Oberflächen sind jedoch oft ineffizient oder kostspielig und weisen eine geringe Bioaktivität auf, was ihre Verwendung als stimulierende Substrate zur Regulierung zellulärer Aktivitäten einschränkt. In dieser Arbeit wird ein neuartiger Ansatz untersucht, der halbsynthetische Glykosaminoglykane (GAGs) einbezieht, um die kostengünstige Herstellung von bioaktiven PNIPAm-haltigen Polyelektrolyt-Multischichten (PEMs) mit Hilfe der Layer-by-Layer-Technik (LbL) zu ermöglichen. Dies beinhaltet die sequentielle Adsorption von entgegengesetzt geladenen Polyelektrolyten (PEL). In der Studie wird der Aufbau von PEMs mit PNIPAm-haltigen PELs durch Konjugation von PNIPAm mit dem Polyanion Cellulosesulfat (CS) untersucht. CS, das den GAGs ähnlich ist und eine ausgezeichnete Bioaktivität aufweist, wird verwendet, um Oberflächenbeschichtungen mit nativen GAGs nachzuahmen und die Bioaktivität erheblich zu verbessern. Im Rahmen dieser Forschungsarbeit werden zwei neue synthetische Verfahren zur Herstellung von PNIPAm-gepfropftem Cellulosesulfat (PCS) als Polyanion entwickelt, wobei sich die Verfahren durch den Grad der Substitution von PNIPAm und die Menge der Sulfatgruppen unterscheiden. Diese Variationen zielen darauf ab, mit Hilfe der LbL-Technik sowohl thermoresponsive als auch bioaktive PEMs herzustellen. Weniger sulfatierte PCS 1 (DS 0,41) und stärker sulfatierte PCS 2 (DS 0,93) werden verwendet, um ihre Fähigkeit zur Bildung von PEMs mit verschiedenen Polymeren (Chitosan, CHI, quarternisiertes Chitosan, QCHI oder Poly-L-Lysin, PLL) zu untersuchen. Das daraus resultierende Verhalten, die Struktur, die Stabilität und die Oberflächeneigenschaften der PEM stehen in engem Zusammenhang mit dem Grad der Sulfatierung, dem Typ des Polykations und der Anwesenheit von PNIPAm. Am Auffälligsten war die Beobachtung, dass das stark sulfatierte PCS 2 das sterische Hindernis von PNIPAm wirksam überwindet, eine stärkere Adsorption von Polymeren ermöglicht und stabilere PEMs bildet als das weniger sulfatierte PCS 1, nachdem die Multischichten dem pH-Wert 7,4 ausgesetzt wurden. Darüber hinaus neigt das kleinere Molekül PLL dazu, mehr ineinander verschlungene PEMs zu bilden als das größere QCHI, was die Oberflächeneigenschaften erheblich beeinflusst. Die

Oberflächencharakterisierung steht in einem weiteren Zusammenhang mit der Toxizität und Biokompatibilität der PEMs mit Zellen aus drei verschiedenen Keimblättern. Die mit PLL kombinierten PEMs zeigen eine höhere Toxizität gegenüber 3T3-, HepG2- und HaCaT-Zellen, insbesondere in Kombination mit PCS1, während die Kombination aus QCHI und PCS2 eine ausgezeichnete Biokompatibilität aufweist und die Zelladhäsion und -proliferation über 7 Tage fördert. Die Immunfluoreszenzfärbung des Zytoskeletts und der fokalen Adhäsionen von 3T3-Zellen unterstützt diese Ergebnisse hinsichtlich der überlegenen Biokompatibilität und der verbesserten Zelladhäsion von QCHI und PCS 2. Zusammenfassend werden in dieser Arbeit neu entwickelte thermoresponsive Beschichtungen vorgestellt, die in der Lage sind, die Oberflächeneigenschaften zu modulieren und die Bioaktivität durch die Integration von PNIPAm-modifiziertem CS, einem halbsynthetischen GAG, zu verbessern. Diese Beschichtungen haben ein enormes Potenzial als Zellkultursubstrate für die Bereitstellung von Wachstumsfaktoren, die Zellproduktion und als bioaktive Wundauflagen für die Geweberegeneration.

1. Introduction

The treatment of severe medical conditions, especially regarding organ failure, damaged tissues after accidents, or other medical related shortcomings of patients is based on the application of biomaterials. Hudecki et al. followed the definition of the "Biomaterials" journal and described a biomaterial as "substance that has been engineered to take form, which, alone or as part of a complex system, is used to direct, by control of interactions with components of living systems, the course of any therapeutic or diagnostic procedure"[1]. In the past decades, the number of applicable and applied biomaterials has rapidly increased[2]. Hence, this field greatly impacted the area of biomedical research. The development of synthetic or biological materials, the development of new and more fitting structures for the area of application in living systems or the enhancement of biocompatibility and degradability of biomaterials employs research facilities and groups all over the world. In this section, the reader is provided with the basic knowledge for the understanding of this doctoral dissertation.

1.1. Regenerative medicine and tissue engineering

As described above, an enormous number of biomaterials are part of medical treatments. A wide variety of biomaterials (and medical devices), from sutures to close wounds, to stents to widen narrowed arteries up to pacemakers and artificial joint replacements, are basically used on a daily basis[3]. However, the human body is designed to reject all foreign materials and so it shows manifold adverse reactions towards implantable biomaterials, e.g., an immune response and so-called foreign body reaction. The immunological rejection can cause great pain and hinders the regeneration and functionality of tissue. Especially for the application of biological materials, including donated tissue or organs, patients must be treated with immune suppressive medicine to enable or facilitate the acceptance of the transplanted organs or implanted material into the patient's body. Circumventing the immune reaction is made possible by using autologous implants (derived from the same organism). However, the availability of such transplants is strongly limited. In addition to the rejection reaction, many biomaterials are non-compatible with blood, leading to blood coagulation on their surface causing enhanced risk of thrombotic complications[4]. Due to these adverse effects, biomaterials with basically inert surface are often applied, which minimizes the risk of an immune reaction or blood clotting[5]. However, inert materials are not integrated into the tissue as cell adhesion is minimized, which is not beneficial for bone and other tissue implants. Over the past years, the development of new materials and the focus on biocompatible and bioactive surface

coatings enhanced the possibilities and application of biomaterials[4,6]. Furthermore, the field of regenerative medicine, focusing on the use of patient derived cells, enabled new therapeutic methods[7], especially in cases, where tissues in the human body cannot be replaced by artificial implants.

Mason und Dunnill (2008) discussed a brief definition for regenerative medicine and narrowed it down to the following: "regenerative medicine replaces or regenerates human cells, tissue or organs, to restore or establish normal function"[8]. To maximize the effect of regenerative medicine approaches, transplanted cells ideally are effective at the desired site until the tissue or organ is regrown, repaired or replaced. The widely used approach for cell transplantation is as suspension, which is probably due to their convenient application. However, the use of cell suspensions often leads to marginal effects, because many cells are known to be lost soon after transplantation[7,9]. Tissue engineering and the production of artificial organs[10], emerged as a promising biomedical area aiming to close the gap left by implants and transplants and overcoming their drawbacks. Tissue engineering, evolving from biomaterial research and being a part of regenerative medicine, combines cells and bioactive components with so-called scaffolds and aims for the replacement, reconstruction or regeneration of damaged tissue or organs (by disease, trauma, etc.) using patient-specific tissue substitutes[11,12]. The use of scaffolds, desirably biodegradable ones, as anchoring or depot for cells or bioactive components could solve the issue of cell loss as it is the case for cell suspensions, making tissue engineering a promising research field[9]. However, the scaffold-based TE relies on the development of a fine balance between the rate of scaffold degradation and the growth of tissue from the cells[13]. Hence, in the past 30 years, researchers even aimed for scaffold-free "cell sheet engineering" approaches. The method was introduced by T. Okano and aims for the fabrication of tissue replacements based on the cultivation of cell mono- or multilayers, combining or using them as functioning tissue replacement[14].

Conventionally, cells for TE purposes are cultivated in polystyrene cell culture flasks, fed with cell culture medium (containing nutrients and bioactive substances), and grown to a certain density inside the flask (depending on the cell type). Afterwards, the cells are harvested, traditionally using enzymes like trypsin. These so-called proteases enzymatically degrade proteins of the extracellular matrix (ECM), cell adhesion receptors and transport proteins, leading to cell detachment from the culture flask surface. Additionally, chelating agents like ethylenediaminetetraacetic acid (EDTA) bind cations like Mg^{2+} and/or Ca^{2+}, weakening the cell-cell-junctions. This allows the harvest of separated cells for further use[15,16]. However, the use of proteases and chelating agents always leads to nonspecific effects, damaging ECM components, cell adhesion receptors, transport proteins and subsequently

6

cells[17]. Using Trypsin or EDTA is not suitable for the use in scaffold-free TE, when aiming for the use of intact cell sheets. In the past years, manifold research groups came up with new surfaces or strategies for cell harvest, such as thermoresponsive surfaces, fibrin-coated dishes and vitamin C treatment[18]. At this point, cell sheet engineering on thermoresponsive surfaces, especially using Poly-N-isopropylacrylamide, were used for manifold cell sheet engineering applications[19,20]. The cell sheet engineering allows for the direct fabrication of diverse tissue constructs that enable to regenerate, rebuild, or even replace damaged or malfunctioning tissues. While culturing the cell sheets before their application, cells start to build their extracellular matrix (ECM) and secrete ECM components, mainly proteins. When harvesting these sheets for applications, they can retain this secreted ECM, allowing for easier use in vivo as the presence of ECM components forms a "biological glue" (Kushida, Yamato, et al. 1999), as the re-attachment on surfaces or even stacking of sheets is promoted[21]. This allows for a second great advantage for the use of cell sheets, as they allow stacking of several homotypic or even heterotypic sheets. Allowing the combination of different cell types, depending on the tissue they are ought to replace. However, this approach is mainly used in tissues with a lower amount of ECM, such as epidermis and other tissue rich in epithelial cells (e.g., liver, or mucous membranes). ECM-rich tissues, such as bones or cartilage, where the ECM is also responsible for a certain mechanical stability, the use of scaffolds is necessary to provide this stability, hence the use of cell sheets is rather limited in these fields of tissue engineering. Nevertheless, the possibility to use intact cell sheets for biomedical applications has great potential, fabricating diverse tissues "ready-to-use" and patient specific[22].

This work is part of this trend and aims for the fabrication of new kind of biological active surface coating with thermoresponsive properties for the harvest of intact cell sheets for tissue engineering purposes.

1.2. Tissue structure based on extracellular matrix and cells

For the use of biomaterials in living systems, be it implants, surface coatings, or other components interacting with cells, and particularly cell sheet engineering it is imperative to understand the basic interactions of cells with their environment. Under "artificial" conditions (e.g., application of implants or in vitro culture) cells do not interact with surfaces directly, but rather with the protein adsorption layer. These proteins are either produced by the cells themselves or adsorbed to the surface from blood and tissue fluids or, *in vitro*, from the serum used in the cell culture medium[23,24]. *In vivo*, the cells encounter a highly complex environment that is called the extracellular matrix (ECM). The ECM is an important component, present in all tissue and organs, playing a major role in tissue morphogenesis, in cell adhesion, growth,

differentiation, migration, and in homeostasis by providing pivotal biochemical and biomechanical cues[25]. The complexity and function of the ECM is however depending on the tissue. For connective tissue (3D), the ECM is plentiful, enriched by many fibrous polymers (mostly collagen), which provide the tissue with the necessary mechanical stability and the cells are seldomly in contact to one another but rather distributed in the abundant matrix. In contrast, for epithelial tissue (2D) cells are tightly bound to another and form sheets, while the ECM is called a basal lamina, only providing minimum biological cues and the mechanical stress is mostly born by the cells[26]. Nevertheless, the ECM contains depending on the tissue, a plethora of proteins, e.g., collagens, glycoproteins[27] and proteoglycans (protein backbone with glycosaminoglycan (GAG)[28] side chains), which are the main components of the ECM[29] and mediate the interactions of cells with biomaterial surfaces or support the cell-cell interactions.

For connective tissue, the structure of the ECM is dominated by fibrillar collagens and partly elastin, building the scaffolding of the matrix, and providing mechanical strength. More than 20 genetically different collagens are known and are present in the ECM in different composition, depending on the cell type/tissue. While collagens are mostly responsible for the ECM structure, adhesive glycoproteins, such as laminin and fibronectin and the proteoglycans, specifically interact with the collagen. The plethora of proteins provides the ECM with manifold cues that enable specific interactions with cells present in or adjoining the matrix[30]. As an example, collagen and fibronectin contain specific sequences (e.g. RGD) onto which cell receptors such as integrins can bind[6].

A major component in cells, the basal lamina and the ECM of connective tissue are proteoglycans (PG) and GAGs. PGs are built by GAGs (e.g., chondroitin sulphate, dermatan sulphate, heparan sulphate, heparin, hyaluronic acid, and keratan sulphate), which are covalently bound to a core protein[6]. Even though the core protein contributes to the properties of PGs, their main functionality depends on the GAGs attached to the core. A PG can contain several GAGs as side chains, providing different properties and enabling different interactions[31]. Their presence contributes significantly to the structural organization of the ECM, playing a crucial role in stabilizing interactions among various ECM components such as collagen, fibronectin (FN), laminin, and glycoproteins[32,33]. PGs and GAGs are considered highly bioactive. The bioactivity arises from the diverse functional groups present in their structures. The GAGs contain sulphate, carboxyl, and hydroxyl groups that confer negative charges, allowing them to interact with positively charged regions of a wide range of biomolecules, including ECM proteins, growth factors, other GAGs, cytokines, and other signaling molecules. The variability in their structures and sulfation patterns also contributes

to their specificity in binding to various ligands and receptors, thereby regulating numerous biological processes[31,34]. Regarding cell adhesion, proliferation, growth, and differentiation and the interaction with growth factors, especially two cell surface PGs are most relevant, syndecans and glypicans. Syndecans and glypicans are both types of transmembrane or cell-surface PGs, involved in cell signaling and interactions within the extracellular matrix[28]. Syndecans are integral membrane proteins that participate in cell adhesion (formation of focal adhesions), migration, and signal transduction by binding to various molecules like growth factors (GFs) and matrix proteins. They have a unique structure with a cytoplasmic domain that interacts with the cell's internal machinery and an extracellular domain that binds to outside signaling molecules. This allows syndecans to either directly (by binding GF through heparan sulphate or chondroitin sulphate) or indirectly (by supporting integrins or GF receptors) activate cell signaling cascades[28,33,35]. On the other hand, glypicans are anchored to the cell membrane via a glycosylphosphatidylinositol (GPI) linkage. These proteins also play crucial roles in cell signaling by regulating the activity of signaling molecules (e.g., GFs like bone-morphogenic protein or fibroblast growth factor). Glypicans are involved in cell growth, differentiation, and development by modulating the gradient and availability of these signaling molecules[33,35]. Additionally, other proteoglycans like aggrecan, neurocan, and brevican also contribute significantly to cell-ECM interactions, growth factor binding, and modulation of signaling pathways, albeit their major functions might be more specific to specific tissues (e.g., aggrecan regulates cartilage development, growth, and homeostasis and neurocan/brevican inhibit neuronal attachment and neurite outgrowth)[33].

Table 1: Overview of some of the proteoglycans, grouped by their location, linked with the GAGs mainly responsible for their properties and with an overview of the functions they have in vivo. The table was filled by the adaptation of a figure from Rnjak-Kovacina et al. (2017)[34]. Abbreviations: CHS = chondroitin Sulphate, DS = dermatan sulphate, HS = heparan sulphate, KS = keratan sulphate

Location	Proteoglycan	Glycosaminoglycans	Proteoglycan functions
Intracellular	Serglycin	CS/DS/HS/heparin	• Binding of growth factors, cytokines, chemokines and morphogens and protection against proteolysis • Formation of morphogen gradients
Cell surface	Syndecans 1-4	HS	
	Glypicans 1-6	HS	
	Betaglycan	CS/HS	
	Phosphacan	CS	
Pericellular	Perlecan	HS/CS/KS	
	Agrin	HS	
	Collagen XVIII	HS	
	Collagen XV	CS/HS	

Extracellular	Aggrecan	CS/KS	• Co-receptors for growth factor signalling
	Versican	CS	• ECM assembly
	Neurocan	CS	• Basal lamina assembly
	Brevican	CS	• Direct cell interactions or modulation of cell interaction with other ECM molecules
	Biglycan	CS	
	Decorin	DS	
	Lubricin	CS/KS	
	Fibromodulin	KS	
	Lumican	KS	• Biophysical roles in tissue hydration, compression, and lubrication
	Keratocan	KS	
	Osteoadherin	KS	
	Epiphycan	DS/ CS	
	Testican 1-3	HS	

Depending on the composition of the ECM, it possesses different mechanical properties, which play an important role in controlling cell function and fate. Each cell must balance the external forces exerted on them by the mechanical properties of their environment, which includes for example the stiffness of the ECM, and by neighboring cells. To achieve this balance, cells regulate the tension of their cytoskeleton which generates internal forces that are transmitted through adhesion sites. These sites link the cytoskeleton to the ECM, which in turn results in an interplay between cells and their microenvironment. This generates cytoskeletal tension that allows cells to maintain their shape and to dynamically response to external forces, leading to a fine regulation of cellular behaviour[36]. This interplay, also known as mechanotransduction, is very complex and only mentioned briefly. But it allows to understand that, since each tissue has a specific stiffness that is regulated by the ECM composition and organization, cellular behavior differs on differently stiff ECMs[37]. A widely known example is the differentiation of stem cells on different substrata. They tend to differentiate towards osteoblasts when cultured on substrates that possess similar stiffness values as bone, but on the other hand the same cell type differentiates into adipocytes or chondrocytes when the culture substrate is soft[38,39]. This emphasizes the influence of the mechanical properties of the ECM.

Beside the provision of topographical cues and mechanical strength, the ECM acts as a reservoir for cytokines, such as growth factors (GFs), which control the cell fate. The manifold functions of GF include, e.g., stimulation of cell growth and differentiation, and influencing survival, but they are also involved in processes like inflammation and tissue repair. For

normal tissue cells to proliferate and survive, multiple types of GFs are necessary. Some ECM components, e.g., fibronectin, vitronectin and the proteoglycans, can bind a variety of GFs from different classes. Important classes to concisely introduce here are the fibroblast growth factor family (FGF), the transforming growth factor family (TGF), which includes bone morphogenic proteins (BMPs) and the vascular endothelial cell growth factor family (VEGF)[40–42]. For tissue engineering and regenerative medicine, GFs have become a critical component, providing necessary signals to cells in their microenvironment, which causes accelerated wound healing. Furthermore, the growth of tissue can be influence by presence of growth factors in or on the substrate they are cultivated on[43]. As a detailed explanation of GFs would surpass the scope of this thesis, a comprehensive review in literature is referred[40]. The ECM is responsible for the controlled availability of GFs, acting as a reservoir by saving the GFs in an inactive state and releasing them for cells in a spatially and timely controlled manner. As matrix proteoglycans are playing a key role in this process, the ECM shows another important feature in delivering and realizing GFs on demand by proteolytic activity and other processes[6,25].

Plentiful ECM components, especially collagen, laminin, fibronectin, vitronectin, and fibrinogen, show specific sequences that allow specific interactions with cells[44]. Interactions with proteoglycans are diverse so that proteoglycans containing heparan sulphate are
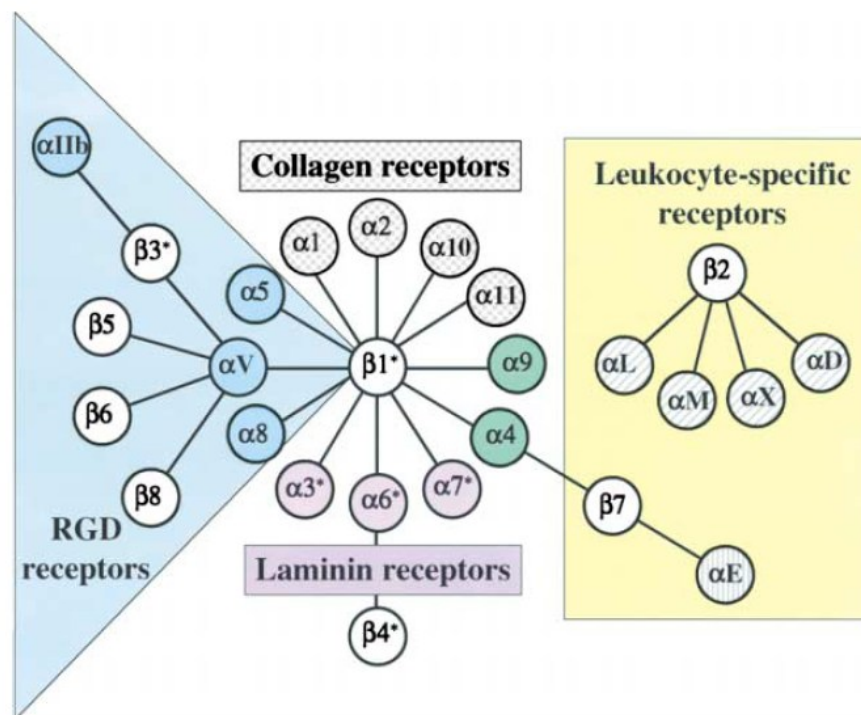

Figure 1: Overview of all integrin receptors and their affinity towards certain ECM components. Reprinted from Hynes et al. (2002)

facilitating cell attachment, while those with chondroitin sulphate domains show opposite effects[44].

The interaction between the ECM components and the cells is mediated by certain heterodimeric transmembrane receptors, in particular the so called integrins[45]. While their main task is mediating cellular adhesion, they also form transmembrane connections to the cytoskeleton of cells and activate intracellular signalling pathways. Recognized in the later 1980s by Hynes et al.[46], they have since become the best-understood cell adhesion receptors and their role in multiple biological processes like immune response, haemostasis or cancer, just to name a few, has been accounted for[47]. Integrins are αβ heterodimers. In mammals, 8β and 18α subunits comprise the full set of 24 known integrins (see Figure 1[47]). These 24 integrins can be grouped in RGD (amino acid sequence Arg-Gly-Asp, linked to cellular adhesion[48]), laminin, collagen, and leukocyte-specific receptors. Integrins are the leading adhesion molecules and provide mechanical continuity between the inside and the outside of the cell., e.g., ECM, but also other cells. The integrins basically serve as transmembrane link, connecting the ECM components with the cytoskeleton inside the cell. For most integrins, this connection is established with the actin microfilament system[47] via a variety of linker proteins, such as talin, vinculin and paxillin[30]. The integrin connections to ECM ligands also trigger several signal transduction pathways with profound effects on cell survival, cell proliferation, structure and functional activity of the cytoskeleton, and gene transcription. These integrin-mediated cell-ECM adhesion sites, named focal adhesions[49], are among other things also responsible for the aforementioned mechanotransduction. The interaction of ECM and cells via integrins is the basis for the anchorage dependence of cell survival and proliferation (describe as Anoikis mechanism by Frisch and Screaton[50]). In addition to integrins which mainly form focal adhesions, interacting with the ECM, other transmembrane proteins such as cadherins are responsible for the cell-cell interaction in tissue. They are of outmost importance for epithelial tissue, as they allow the formation of a tight epithelial cell barrier[51]. Cadherins are calcium-dependent homotypic cell-to-cell adhesion molecules, which localize in so called adherence junctions. There, cadherins can establish linkages to other cells with actin-containing cytoskeletons[49]. Cadherins of opposing cells form complexes and align in "zipper"-like manner side by side. Cadherins play a crucial role in tissue organization but also for regulation of signalling cascades, making them very important transmembrane molecules in the maintenance of normal tissue structures[49]. The cadherin superfamily comprises many different cadherins, such as classical cadherins, protocadherins, desmosomal cadherins, and cadherin-like proteins. Best known are the classical cadherins E-, N- and R-cadherins, derived from epithelial, neural and retinal, the tissue they are most prominent in[52].

12

So, for epithelial tissue, E-cadherins are mostly responsible for the cell-cell adhesion, tissue organization, maintenance of the epithelial barrier and signal transduction[51].

1.2.1. Cell-surface interactions

As expected from the stages of interactions of biomaterials with blood, serum or cell culture media, protein adsorption is preceding cellular adhesion, but can be followed by activation-depending events like coagulation, inflammation and, of course, cell adhesion[22,53]. After adhesion, cell activation related to morphological changes, proliferation and differentiation of tissue cells follows[54,55], making protein adsorption a vital process for cell and tissue formation on biomaterial surfaces. Therefore, understanding protein adsorption and manufacturing biomaterial surfaces to which proteins can adsorb and induce the desired effects on cells and tissue is crucial for biomedical applications.
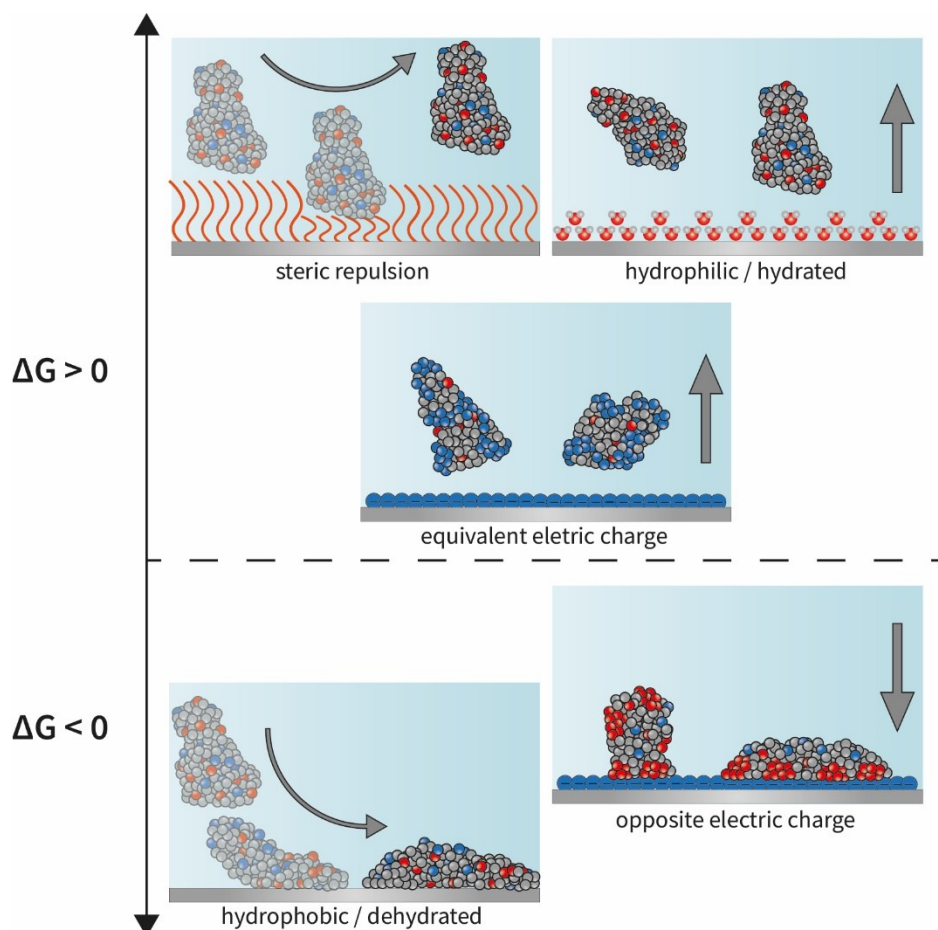

Figure 2: Surface or protein properties related to their resulting Gibbs free energy, subsequently hindering, or facilitating protein adsorption. If delta G > 0, protein adsorption is hindered, if delta G < 0, it is promoted. Especially surface wettability (hydration forces), electrostatic (Coulomb) interactions and steric repulsion of polymeric chains are important factors influencing protein adsorption on surfaces. Figure taken from Doberenz et al. (2020)[22].

Proteins are macromolecules composed of amino acids with side groups that may be polar or non-polar, positively, or negatively charged, which means they are amphiphilic and amphoteric, respectively. These properties make proteins prone to adsorb to interfaces[56]. It

enables proteins to engage in manifold interactions with other molecules or surfaces driven by interfacial energy differences, increasing entropy, Coulomb and other interactions, which are summarized with regard to their Gibbs free energy (ΔG) in Figure 2[22,57,58]. The Gibbs free energy is defined as $\Delta G = \Delta H - T\Delta S$ (H: enthalpy, T: temperature, S: entropy). Protein adsorption is driven by interfacial energy differences, which is related to a ΔG decrease[56,59]. The interaction of hydrophobic polymers or other surfaces with proteins in aqueous solutions leads to spontaneous protein adsorption. The adsorption leads to a decrease in ΔG, since water molecules shielding the hydrophobic surface and additionally water molecules from hydrophobic amino acid residues (e.g., lysins, tryptophan, etc.) of the protein are released, increasing the entropy of the system (which in summary leads to ΔG < 0)[60]. For hydrophilic surfaces, protein adsorption is hindered because the low interfacial energy between surface and aqueous phase promotes the formation of a thin layer of water molecules on the surface, which ultimately generates a very strong repulsive barrier known as hydration force[61]. Another hindrance for protein adsorption is the presence of hydrophilic macromolecules of certain length covering the surface. The compression of these macromolecules decreases the entropy of the system, raising the Gibbs free energy and making protein adsorption unfavorable. This phenomenon is called "steric repulsion"[4,62]. Lastly, the influence of the net charge of proteins needs to be addressed. Electrostatic interaction can promote protein adsorption, if the electrokinetic potentials of surface and protein are of opposite value[56]. It has been observed, that especially positively charged surfaces can adsorb large amounts of proteins[63], relating to the fact that many proteins have a net negative charge at physiological pH values[4]. On the contrary, protein adsorption is hindered if the net charges are equivalent. Norde and Lyklema (1991) explained in more detail, which subprocesses are involved in protein adsorption and are referred here for more insight[56]. Generally, protein adsorption is an important prerequisite for cell adhesion. As explained in the former section, cell receptors specifically interact with certain proteins present in their environment. The presence of proteins matching these receptors can even enhance cell adhesion (e.g., fibronectin, containing the RGD-motif matching to certain integrins, drastically facilitates cell adhesion and spreading)[59,64,65].

For the fabrication of bioactive coatings, it is detrimental to understand the in vitro cell adhesion mechanisms. In most of the cases, cells are present in some kind of physiological medium and statically interact with the surface[66]. These surfaces might be bioactively modified to present additional specific peptide sequences ("Adhesion sequences") to the cells, in addition to the unspecific protein adsorption that occurs from the physiological fluid used in the cell culture process. The first cue for cell adhesion is based on electrostatic interaction

14

of the cells with the surface. This is followed by the initial stage of cellular adhesion; whereby the cell body attaches to the substrate. The interaction of cells with the surface at this stage is driven by specific integrin-mediated adhesion, starting with the binding of single receptor-ligand pairs. In quick succession, receptor-ligand bonds are formed, which rapidly increase in number, increasing the adhesion strength. This is followed by the change in cell shape from a spherical to a flattened geometry, decreasing cell height and increasing surface-contact area. Initiated by the binding of integrins, stress fibers and subsequently focal adhesions form. Spreading is driven by further adhesion and the reorganization and distribution of the actin fibers around the cell's edges, finally reaching full spread and maximum adhesion. This process strongly relies on the presence of biological cues, such as, e.g., the aforementioned proteins and glycosaminoglycans (as functional side chains of proteoglycans in ECM). Hence, to control cellular response, a precise control of the substrate surface and the presence of specific bioactive peptide sequences that facilitate cell adhesion is striven for. Thereafter, the adsorption of specific proteins onto a surface is a crucial process. However, the ECM cells interact with in vivo is a highly complex network of proteins and polysaccharides, and in vitro approaches often need to address issues such as nonspecific protein adsorption, the density and kind of present adhesive peptides and the dynamic nature of the ECM[67]. This makes the fabrication of a bioactive surface with the goal of a specific cellular response highly complex and challenging[22,45,47,54,68–71].

1.2.2. Engineering surfaces

The objective of this work is the fabrication of thermoresponsive surface coatings for use in cell sheet tissue engineering. The lack of functionality of the biomaterial surface leads to unpredictable interactions with the multitude of proteins present in the body fluids, and cell culture media. With the help of chemical, physical or biological surface modifications, materials surface properties can be modified to achieve desired effects on protein adsorption, cell adhesion and growth or presenting biological cues for cell differentiation[72].

Over the past decades several methods for the generation of functional groups or the grafting of other molecules onto biomaterial surfaces have been developed. These methods include chemical etching, plasma treatment and polymerization, ion beam, UV or visible light irradiation, and surface grafting[6]. In contrast, for biological surface modifications or biological-based applications, the harsh processing conditions and the harmful solvents of these methods are often damaging the biomolecules or need to be extensively removed, as they are mostly cytotoxic[73]. In contrast, physical modification methods rely on physical interactions like Van der Waals forces, hydrogen bonding and electrostatic interactions and

are considered simple, inexpensive and mild (in terms of toxicity and processing conditions)[6,73–77]. In recent years, especially one method gained much interest in the field of surface coatings for biomedical applications, now known as the layer-by-layer (LbL. Originally inspired by the idea to mimic natural layered structures, the alternate adsorption of oppositely charged polyelectrolytes – polyanions and polycations – on a substrate was introduced. Basically, two or more constituents are sequentially added to the surface of a
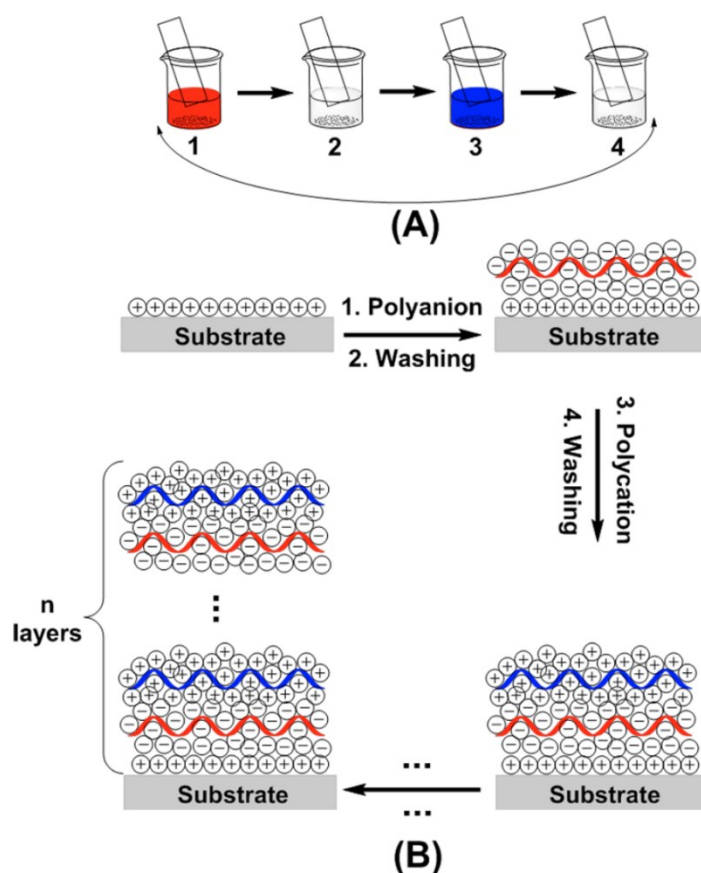
Figure 3: Schematic principle of the layer-by-layer technique. Substrates can be dipped in the polyelectrolyte solutions as depicted (A) or generally immersed for a certain time. For the layer formation, alternating deposition of polyanion and polycation, in each case followed by washing is performed, repeated until n layers are deposited (B). Reprinted from Borges and Mano (2014).

substrate as many times as desired, until the stacked layers form a multilayer thin film. As early as 1966, Iler *et al.* made first attempts of fabricating multilayer thin films[78]. With further developments by Decher and Hong *et al.*, this method of thin film fabrication became known as layer-by-layer (LbL)[79–81]. Since then, it has become one of the most prominent and researched surface modification strategies in material science and biomedical applications. The capability to fabricate surface coatings with desired properties in an easy, reliable, versatile, and cost-effective way with nanoscale control over the film thickness at non-harmful conditions are good reasons for the popularity.

The fundamental principle of LbL adsorption is the use of two or more materials that possess complimentary interactions and the multitude of forces that occur between them. The most exploited interactions are of electrostatic origin, but they also include hydrophobic, charge-transfer, host-guest, biologically specific and coordination chemistry interactions. Furthermore, hydrogen bonding, covalent binding, stereo complexation, and sol-gel process can be the driving forces of the multilayer formation. Often times, the formation is driven by a combination of several forces. Borges and Mano (2014) impressively reviewed the multitude of molecular interactions driving the LbL assembly[82]. Since a detailed description of all these interactions and factors goes beyond the scope of this dissertation, the review is heartly recommended for explicit details. In this work, multilayered films are fabricated using LbL mainly driven by electrostatic interaction between oppositely charged polyelectrolytes. This approach is especially suitable for surfaces designed for biomedical applications, since it enables the manufacture of multilayers with well-controlled composition, structure, and thickness, by simple, alternate immersion of a charged substrate in dilute solutions of oppositely charged molecules. Basically, aqueous solutions of anionic and cationic polymers are sequentially introduced to the substrate. Due to the opposite charge, a certain amount of polymer chains is adsorbed to surface. In between these adsorption steps, washing with a salt containing buffer solution is necessary to remove weakly or unbound molecules and enable the interaction between the subsequently introduced oppositely charged molecules. Beside the electrostatic, short-range interactions such as Van der Waals forces and hydrogen bonding may impact the multilayer formation. These days it is commonly acknowledged that the release of counterions leads to a gain in entropy. This gain is a decisive factor in the LbL adsorption process, which leads to the organization of the multilayer in a more coiled and interdigitated conformation with reduced degree of freedom of the polyelectrolytes involved[73,82]. A multitude of charged molecules are suitable for electrostatic layer deposition, including polysaccharides, polypeptides, nucleic acids, and viral components. However, the use of synthetic polyelectrolytes has been given some preference. Especially the combination of poly (styrene sulfonate) and poly (allylamine hydrochloride) (PSS-PAH) has been widely investigated and is considered as a model for multilayered thin films. These synthetic materials are highly versatile and can be tailored with specific properties, enabling the analysis of the system und influence of different intrinsic or extrinsic parameters and how they impact, and perhaps, change the dynamic of the deposition process and/or multilayer structure[73]. The parameters are manifold, as are their influences upon the polyelectrolyte

multilayer (PEM) systems. Hence, they have been summarized in Table 2, presenting the parameters and linking them to their impact of the PEMs.

Table 2: Overview of the intrinsic (polyelectrolyte) and extrinsic (environmental) parameters and the PEM property they are directly affecting.

Parameter		Effect on PEM	
Extrinsic	**Solution pH**	-	growth mechanism
		-	level of interpenetration depths
		-	surface wettability
	Temperature	-	stability
		-	internal structure
		-	morphology
		-	growth mechanism
		-	thickness
	Ionic Strength & electrolyte species (salt type and concentration)	-	stability
		-	permeability
		-	internal structure
		-	function
		-	growth mechanism
		-	thickness
	Solvent Quality & adsorption time	-	structure
		-	growth mechanism
Intrinsic	**Charge density**	-	growth
		-	internal structure
		-	morphology
		-	thickness
	Molecular weight	-	growth
		-	internal structure
		-	morphology
		-	chain mobility
		-	thickness
	Chain architecture	-	growth
		-	thickness
		-	internal structure

These manifold possibilities make it imperative to closely examine the physicochemical properties. New combinations of biopolymers, integration of charged biomolecules, such as

growth factors or loaded lipoplexes, or newly synthesized co-polymers, as in this work the combination of cellulose sulphate with thermoresponsive PNIPAm, need to be examined to understand what intrinsic and/or extrinsic parameters might influence the multilayer properties. Furthermore, if PEM films are used for biomedical applications, extensive biological examinations have to follow to determine their impact on cells and subsequently the living tissue.

2. Biopolymers for biomimetic surface coatings

Biopolymers are produced in microorganisms, plants, and animals. Over the past decades, due to their biological origin and, related to that, their bioactivity, biopolymers have been extensively studied, and applied in the biomedical field. The bioactive domains found in these biopolymers, in combination with biocompatibility, 3D structure, antigenicity, non-toxicity of biodegradation by-products, and the intrinsic structural resemblance to the natural occurring ECM are motivating to look for natural polymers to be used for regenerative medicine[83,84]. In contrast, biopolymers possess some noteworthy disadvantages, limiting their application potential in tissue engineering. The key disadvantages are microbial contaminations, e.g., endotoxins, disease transmission from other species (due to their extraction from animal or human resources), decreased tuneability (in contrast to synthetic polymers), immunogenic reaction, uncontrollable degradation rate, and poor mechanical strength (limitation especially for TE of hard tissue like bone)[84]. Overall, biopolymers greatly contribute to the field of TE and biomedicine, for example in form of delivery systems, bioactive surface coatings, and hydrogels for diverse TE applications[84-86]. This work focuses on polysaccharide-based polymers. Polysaccharides are long-chain polymeric carbohydrate molecules, comprised of monosaccharide or disaccharide units. The combination of different saccharide isomers by utilizing a range of different chemical bonds results in a wide variety of structurally diverse biopolymers[84,87]. In terms of diversity and heterogeneity, their chemistry is comparably rich as that of proteins, but their sources are more abundant and renewable. Furthermore, they are biocompatible and biodegradable (to some extent) and possess structural and functional similarities to the extracellular matrix (this effect is linked to their glycan units[88]), making them promising materials for TE purposes[89]. They are often applied in form of hydrogels, as they form loose viscoelastic gels in aqueous vehicles via non-covalent interactions (especially alginate, methylcellulose, chitosan)[90]. The high charge density of some polysaccharides enables the easy fabrication of surface coatings via electrostatic interactions[90]. However, it should not be overlooked that polysaccharides, beside all their benefits, come with some restrictions. They come often with high batch-to-batch

differences, since distribution, branching, and sequence of molecular weight are often not consistent, making the reproducibility on industrial scale quite complicated. This is
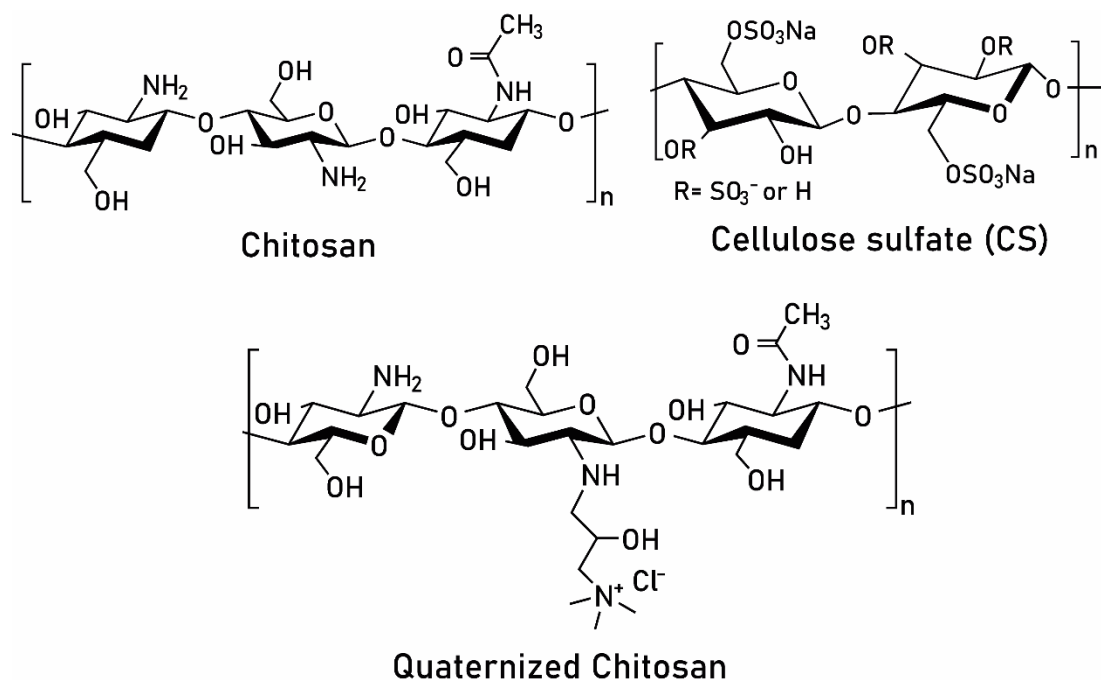

Figure 4: Structural chemical formula of biopolymers chitosan (CHI), quaternized chitosan (QCHI), cellulose sulphate (CS) and poly-L-lysin (PLL).

detrimental for biorecognition events and affects the rheology, and important property for scaffold and surface fabrication. They present a further disadvantage in terms of biodegradability, as some natural occurring polysaccharides are not biodegradable after introduction to mammalian species and need further chemical modification[84]. Nevertheless, the application and amount of research of polysaccharides in the biomedical field has steadily increased over the last 20 years[89]. In this work, the focus lies on two abundantly available polysaccharides, namely chitosan and cellulose sulphate.

Chitosan is a linear polysaccharide consisting of randomly distributed D-glucosamine and N-acetyl-D-glucosamine residues. Derived from chitin by deacetylation, it is soluble in mild acidic aqueous solutions. The deacetylation procedure introduces functional amino groups, which, in combination with hydroxyl groups and their distribution on the polymer backbone, provide chitosan with many beneficial physicochemical and therefore biological properties, such as biocompatible, biodegradable, cell adhesive and antimicrobial. It is one of few naturally derived polycationic polysaccharides, enabling electrostatic interaction with anionic biopolymers for layer-by-layer fabrication of polyelectrolyte multilayers, or for interesting interactions in physiological environments, since most biomolecules are anionic[89]. Chitosan has been used for a plethora of biomedical applications, such as drug delivery (e.g., gene, antibiotic, antitumor drug, and protein drug delivery), vaccine delivery, antimicrobial

hydrogels or nanoparticles, and for diverse TE purposes[91].Chitosan can be further modified, either to achieve solubility in water, or to aid in scaffold manufacturing. The pKa-value for chitosan is ~6.5, explaining its insolubility in water above pH 6.5 due to the deprotonation of amine groups[92]. Quaternized chitosan has been introduced as water soluble chitosan modification, enabling chitosan solutions with neutral pH value for physiological applications and stability of polycationic character at physiological pH[93]. With regard to surface coating based on electrostatic interaction, the quaternary ammonium group introduced to the chitosan (hence the name quaternary chitosan) retains its positive charge characteristic and enables the interactions with polyanions even at physiological pH[94], making quaternary chitosan interesting for biomedical surface coatings based in electrostatic interactions (e.g., layer-by-layer technique for polyelectrolyte multilayers).

The second biopolymer of greater interest is cellulose, often lauded as the most abundant renewable biomaterial on the earth[31,89]. It is an unbranched polysaccharide build-up of β-(1→4)-linked-D-glucose units that is found in nature as microfibrils in the cell wall of wood, plants, and algae and produced by some bacteria, fungi and rarely in sea animals (e.g., tunicates)[95]. Cellulose is not water-soluble and subsequently of less interest for biomedical applications. But, the monomer of cellulose possesses three hydroxyl groups that can fully or partially react with chemical agents to form diverse derivatives with a wide range of degrees of substitution[96]. One of these derivatives is cellulose sulphate (CS), a semi-synthesized cellulose derivative, possessing a simple chain structure and unique biological properties. In contrast to other cellulose derivatives, it is only produced in lab scale, but research has shown that it is anticoagulant, antiviral, contraceptive, and a microbicide against human immunodeficiency virus (HIV). Additionally, it is soluble in water, antibacterial, excellent biocompatible, biodegradable and as polyanion able to form films based on electrostatic interactions[87,96,97].

As material for bioactive coatings, CS is excellently suited. The introduction of sulphate groups not only make it anionic, but when sulphate groups are introduced to the anhydroglucose units, CS possesses biological activities like those of glycosaminoglycans (GAGs). GAGs were discussed earlier as one of the functional components of the extracellular matrix (ECM) interacting with a plethora of regulatory proteins, e.g., growth factors. As GAGs are limited in their availability, the synthesis of CS with analogous function is very attractive. CS with a sulfation on the 2-O-position and 6-O-position showed similar properties to heparin[98], including binding of ECM proteins (e.g. fibronectin) and growth factors[99,100]. When used for surface coatings, the affinity to bind growth factors would allow for the production

of highly bioactive surfaces with the potential to modify cellular functions (e.g., growth, differentiation). The defined chemical structure and easy separation/purification make it predestined for industrial-scale production and significantly more affordable than the naturally occurring GAGs[31,96]. [96,101]

Chitosan and cellulose sulphate present, not only because of their abundance, but foremost based on their promising properties, excellent candidates as biomaterials for TE applications and due to their potential for electrostatic interactions, as polymers for simple polyelectrolyte multilayer surface coatings[102–104]. For application in biomedical research, especially in the field of polyelectrolyte multilayers, the cationic poly-amide poly-L-lysin is of great popularity. Especially due to the polycationic properties, it has been used in several studies as counterpart to anionic glycosaminoglycans, such as chondroitin sulphate, heparin and hyaluronic acid[105–108]. Especially for the layer-by-layer techniques it presents an easy-to-use biopolymer as it is water-soluble. The positive charge of poly-L-lysin is due to the protonated free amines on the side chain and allows electrostatic interactions with anionic materials. It is profoundly bioactive and allows interaction with anionic molecules and hence has been used as carrier material for genes and drugs[109]. Poly-L-lysin is additionally used as coating of cell culture substrates to enhance cell adhesion due to the electrostatic interaction with the anionic membrane of mammalian cells[110]. Unfortunately, this interaction exhibits a cytotoxic effect when poly-L-lysin is in solution and not bound to the surface. PLL can lower the cells ATP level, leading to energy crisis, cell dysfunction and eventually cell death[109].

2.1.1. Stimuli-responsive polymers for surface coatings

Stimuli-responsive polymers are polymers that sharply respond to small changes in their immediate environment with often reversible, large changes of their physical or chemical properties. The stimuli-responsive polymers, also known as smart polymers, can react to single or multiple environmental changes, including temperature, pH, magnetic or electric fields, biomolecules (e.g., enzymes), light intensity, or even mechanical stress[111–113]. The stimuli cause the material to macroscopically respond, often in form of swelling, collapsing, sol-gel-transitions or other conformational changes depending on the physical state of the polymer chains[113]. This often causes changes in solubility/phase separation in aqueous solutions, adsorption or chemically-grafting onto solid surfaces, or the building of networks based on chemical crosslinking, H-bonds, and/or physical entanglement and the subsequent formation of hydrogels[111]. Their properties alone are quite interesting for biomedical applications, but they can be further enhanced through combination with bioactive molecules by physical mixing, chemical conjugation, or complexation. The bioactive molecules include nucleic acids (e.g., DNA, RNA), small organic molecules (e.g., drugs, steroids, cell membrane receptors),

22

proteins (e.g., enzymes, antibodies, growth factors) and carbohydrates (e.g., heparin, hyaluronic acid, polysaccharides)[111]. This makes the stimuli-responsive polymers a versatile and promising biomaterial. Wei et al. list some of their applications, such as biosensors, controlled drug delivery systems, environmental remediation, chemo-mechanical actuators and many other, for example as substrates for cell culture or tissue engineering[112,113].

From the multitude of possible stimuli, one has been of particular interest and has been extensively studied and is well understood: the response to temperature. So called thermoresponsive polymers undergo solubility changes, along with conformational alterations in their structure, depending on the environmental temperature. This certain temperature, at which structural or solubility alterations happen, is called transition temperature. As it is often the case that the solubility of the polymer changes, it is also known as critical solution temperature (CST). Thermoresponsive polymers are generally divided into two groups regarding their CST: polymers with lower critical solution temperature (LCST) and polymers with upper critical solution temperature (UCST). These are completely opposite behaviors with different underlying mechanisms and driving forces. Polymers with UCST are soluble in water above this temperature and phase separation occurs below it. UCST behavior is enthalpy-driven and requires strong supramolecular interactions, which are weakened upon heating, leading to phase separation[114]. Polymers with UCST are rather rare, and with regard to biomedical use, UCST behavior harder to achieve at physiological temperatures. The main type of polymers with UCST behavior soluble in water are zwitterionic polymers[115,116]. Polymers with UCST behavior are explained in detail in the review of Seuring and Agarwal (2021), presenting comprehensive explanations on the physical/chemical principle, the application and the limitations of these polymers[117]. More suitably to the scope of this dissertation, the opposite LCST behavior is explained in more detail.
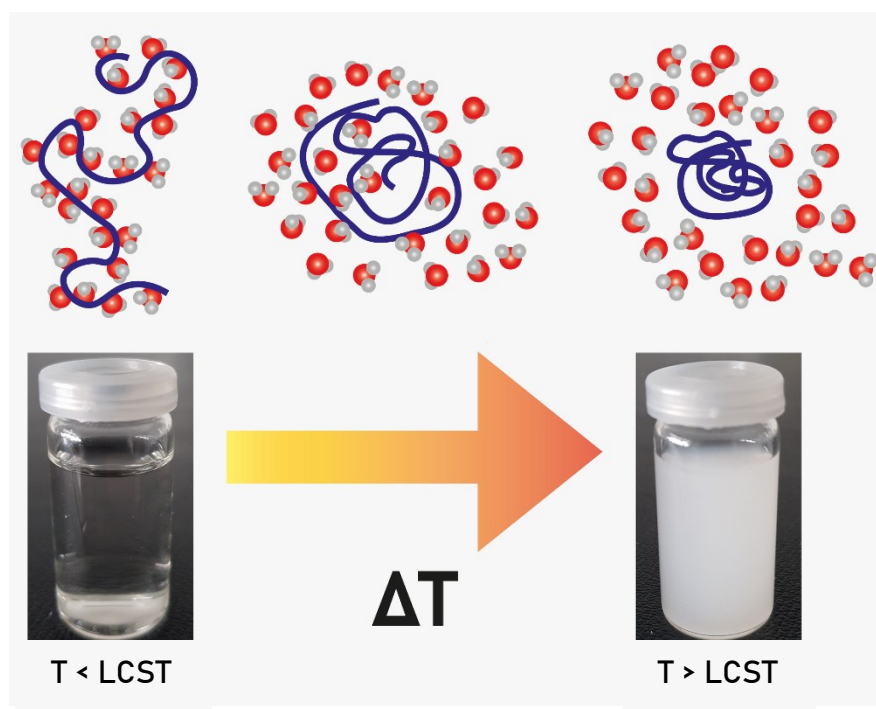
Figure 5: Schematic representation of LCST behavior. With increasing temperature, thermoresponsive polymers hide hydrophilic chain segments and expose hydrophobic ones. This leads to aggregation of the polymer chains. A formerly clear dilution of thermoresponsive polymer becomes turbid.

When a polymer possesses a LCST phase transition, it is completely miscible in a solvent below the transition temperature and phase separates above it. This can be explained by the hydrophobic effect and from a thermodynamical point of view. The Gibbs free energy (known from the part concerning protein adsorption: $\Delta G = \Delta H - T\Delta S$) is negative for the dissolution of the polymer below the LCST but becomes positive with increasing temperature. Below the LCST, the enthalpy term (ΔH) is negative, because hydration, the hydrogen bonding of water to the polymer chain, is favorable. Additionally, the entropy contribution (ΔS) is negative too because water loses entropy while binding to the polymer chain. Hence, the polymer is dissolved in aqueous solution below the LCST. With increasing temperature, the hydrogen bonding interaction will become less, decreasing ΔH. The decisive factor is the entropy term ($-T\Delta S$), which increases because it is energetically more favorable for the water molecules to assume a higher state of disorder and go back to the bulk water, leaving partially dehydrated polymer chains behind. The dehydrated polymer chains collapse and aggregate into a polymer-rich phase, leaving behind a phase separated solution[22,113,118]. Polymers never fully dehydrate, and the hydrophilicity of the polymer chains influences the dehydration: the more hydrophilic the polymer is, the more water is retained in the collapsed chains. This process can be easily observed, since the solution changes from clear, transparent, and homogenous to cloudy and heterogenous. Hence, the LCST is sometimes referred to as cloud point. There are several known factors that influence the LCST: polymeric properties like nature of

substitute groups, chain length and molecular weight and additive properties like salt concentration, co-solvents, and surfactants. For example, increasing molecular weight of a polymer decreases its hydration due to more polymer-polymer interactions and therefore lead to a decreasing LCST. As explained before, hydrophilic groups can bind more water, making the dehydration process more energy consuming, leading to a higher LCST[113].

In particular, one thermoresponsive polymer with LCST behavior attracted much research interest, namely Poly (N-isopropylacrylamide), or also known in its abbreviated form as Poly-NIPAm or PNIPAm. The transition temperature at roughly 32 °C (only slightly lower if dissolved in physiological saline) and the LCST being independent of the molecular weight and concentration made it a promising candidate as thermoresponsive biomaterial. Besides the LCST being in the physiological range, it is quite popular because of its excellent biocompatibility[119–122]. The thermoresponsive behavior of PNIPAm can be explained by looking at the functional groups present in the polymer. PNIPAm is amphiphilic, which means, that it possesses both, hydrophilic (amide groups) and hydrophobic (isopropyl groups) chains. When passing the LCST by increasing the temperature, solubility and wettability are altered, based on the conformational changes the PNIPAm chains undergo, also known as coil-to-globule transition[123,124]. This structural change to a more globule form buries most of the amide groups inside, accompanied by significant release of water molecules (dehydration), hiding the hydrophilic chains, and exposing the hydrophobic ones. By lowering the surrounding temperature, this process can be reversed. PNIPAm chains extend to their globule form, driven by hydrogen bonds, exposing the amide groups again. The polymer hydrates, regaining solubility, and wettability. When talking about the transition of PNIPAm, it is often proclaimed as a transition from hydrophilic to hydrophobic behavior. This is misleading, as Pelton *et al.* (2010) described in a small, published communication. With regard to the definition of hydrophobic behavior, it was pointed out that PNIPAm is indeed never hydrophobic[125]. But it is correct, that it becomes less hydrophilic when the environmental temperature is increased and the LCST passed.

PNIPAm might be the dominating thermoresponsive polymer in terms of research effort and biomedical applications, there are still other interesting materials, such as Poloxamers, poly (N-vinylcaprolactam) (PNVCL) and elastin-like polypeptides (ELP). Poloxamers are co-polymers of highly water-soluble poly (ethylene oxide) (PEO) and hydrophobic poly (propylene oxide) (PPO)[126]. These amphiphilic co-polymers show LCST behavior, whereas the transition temperature can be adjusted between 10 – 100 °C by combining PEO-PPO in different ratios[127]. In contrast to PNIPAm, the transition behavior of poloxamers is described

as reverse thermal gelation (RTG). When the temperature is raised, passing the LCST, viscosity of a poloxamer solution (containing a critical number of polymers) is drastically increased. The driving forces for the RTG behavior are thought to be multiple. Investigations proposed that changes in the micellar properties and the formation of three-dimensional networks and a gain in entropy (similar to PNIPAm) are responsible for the behaviour[128–131]. The combination of PEO and PPO to so-called tri-block polymers (PEO-PPO-PEO) with different hydrophilic and hydrophobic segments allows to manufacture materials with desired properties concerning LCST and assumed viscosity. Ideally, the materials form a semi-solid gel at physiological temperatures. This enables the injection of the material with low viscosity at lower temperatures and the gel formation at body temperature. Poloxamers are used for drug delivery/release, tissue engineering and wound dressing applications[22]. One material with these properties, which is also commercially available, is the tri-block polymer known as Pluronics®. At a minimum concentration of 15-20 % it achieves a solution-gelation (sol-gel) transition. By adjusting the concentration, desired viscosities suitable for different applications can be achieved. The Pluronic with the name F127 is of particular interest for biomedical applications, because it possesses a LCST at 30 ℃. It shows excellent biocompatibility, enhances protein stability and is neither myotoxic nor immunotoxic[132]. For those reasons, it has been extensively used as vehicle in drug delivery applications[133–135]. Furthermore, poloxamers found their way in the application as TE scaffold material, mainly in form of hydrogels[136,137] and 3D-printed scaffolds[138–140].

Poly (N-vinylcaprolactam) is another interesting thermoresponsive polymer. PNVCL shows similar characteristics as PNIPAm, such as LCST between 32 and 34 ℃ and a reversible transition from swelling to collapsing at the LCST when dissolve in water. Its lack in popularity is due to the difficulties in polymerization of the monomer in controlled manner. Since the thermoresponsive properties, in contrast to PNIPAm, rely on molecular weight and dispersity, a controlled polymerization process is important. This has been achieved over the past years, but the use of PNVCL is still limited due to the slightly enhanced cytotoxicity above 37 ℃[22,141]. Nevertheless, it has been used for multiple biomedical applications in form of thermoresponsive surface coating[142,143], hydrogel for TE[144] and transdermal drug delivery system[145], just to name a few.

Another thermoresponsive polymer and as that quite popular, are the elastin-like polypeptides (ELP). Elastin is a structural protein of the extracellular matrix in all vertebrate connective tissues. It is built up in the extracellular space by strong crosslinking of its soluble precursor tropoelastin through the action of lysyl oxidase[146]. Tropoelastin, like the aforementioned polymers, is amphiphilic, being composed of hydrophilic and hydrophobic

26

crosslinking domains. ELPs, which are repetitive artificial polypeptides, are derived from a certain amino acid sequence found in the hydrophobic domains of tropoelastin. The sequence is composed of the amino acids Valine (Val), Proline (Pro), Glycine (Gly) and one more amino acid other than Pro (Xaa) in the order Val-Pro-Gly-Xaa-Gly. They cannot be fabricated by conventional synthesizing or polymerization procedures. But they are genetically encodable, enabling a controlled synthesize (e.g., with specific molecular weights and amino acid sequences) in heterologous hosts, such as bacteria or eukaryotic cells. Exploiting their thermoresponsive phase transition behavior, they can be purified after simple high yield production from Escherichia coli bacteria[147]. The similarity to the ECM protein, biocompatibility, biodegradability, and non-immunogenicity[148] are a few reasons for ELPs attractivity for TE and drug delivery applications[149–155].

In the following section, the focus lies on biopolymers and PNIPAm and their use as biomaterial surface coatings before the application of thermoresponsive polymers and especially the current state-of-the-art is critically reviewed in a separate section.

2.2. Poly (N-isopropylacrylamide) for thermoresponsive surface coatings

PNIPAm is mainly used as thermoresponsive surface modification, introduced by Yamada *et al.* in 1990 and since then further developed by Okano *et al.*[156–158]. They grafted NIPAm monomers covalently to polystyrene (commonly used as tissue culture substrate) with the aim to harvest cells and/or cell sheets without the use of harmful enzymes for tissue engineering purposes. Using electron beam irradiation, they polymerized NIPAm and simultaneously grafted it to the substrate. On these grafted surfaces, they successfully cultivated cells and recovered them by simply change the environmental temperature from 37 °C (conventional cell culture temperature regime) to room temperature (or below). The conformational change of PNIPAm while passing the LCST and the subsequent change in wettability and hydration caused the cells to slowly detach from the surface[22,158,159]. The cells play actually and active role in this process. The process is indeed initiated by the weakened ECM-substrate interaction due to the hydration of the PNIPAm surface, but an active, ATP-consuming reorganization of the cells cytoskeleton and signal transduction is necessary. Integrins connect the cells inner actin-based stress fibers of the cytoskeleton with the surrounding ECM, exerting traction and contraction forces. Since PNIPAm hydration weakens the ECM-substrate interactions, the pulling forces of the metabolic active cells exceed the tensile stress of the ECM, which leads to cell rounding and detachment from the surface. This mechanism is even more drastic for cell sheets, as the intact cell-to-cell-junctions

and the therefore enhanced pulling force leads to a rolling and contraction of the cell sheet, even pulling the ECM from the surface. This allows harvest of intact cell sheets with their secreted ECM[22,160,161]. This is exceptionally promising for tissue engineering applications, since the sheets maintain growth and secretion activities, and substrate adhesiveness nearly comparable to primary cells[162]. The only drawback is the lower environmental temperature. Surfaces should allow a cell harvest at room temperature, because with lower temperatures and even to long exposure to room temperatures, the cells are exposed to cold stress, limiting their metabolic activity and hence the ability to detach from the substrate. Short exposure at not to low temperatures should be aimed for[120].

The former section introduces surface coating techniques. The synthetic PNIPAm has seen several developments concerning surface grafting. As mentioned before, they were initially prepared by electron beam (EB) irradiation of a monomer solution on polystyrene (PS) substrates. Other chemical surface modification techniques were developed that achieved similar results, such as UV irradiation, visible light irradiation, and plasma vapor deposition. In recent years, the fabrication of PNIPAm brush surfaces has been achieved by to surface-initiated methods, namely atom transfer radical polymerization (ATRP) and reversible addition fragmentation chain transfer (RAFT). The detailed explanation of these methods would go beyond the scope of this work, hence the comprehensive reviews of other authors are recommended[22,163]. Even though these methods are well established and used for the fabrication of PNIPAm-modified surfaces for cell sheet engineering (grafting PNIPAm on PS substrates using EB irradiation has resulted in commercially available products), they present some drawbacks or optimization potential, respectively. These difficulties include the use of metal-ions (e.g., copper ions in ATRP), photo imitators and other cytotoxic chemical compounds, the harmful process conditions (radiations, high temperatures), and the expensive machinery. Especially the harmful process conditions limit the potential use of biomolecules and subsequently further bioactive modifications of PNIPAm surfaces. The aforementioned layer-by-layer (LbL) strategy presents a promising alternative. Even though PNIPAm might not be used directly, because its interactions with other polymers are limited, it could be co-polymerized with other, charged polymers. This might enable the combination of PNIPAm with biopolymers and the fabrication of bioactive surfaces for cell sheet engineering, better mimicking the natural ECM. The first research in that field has been performed by Serpe et al. (2003) by combining PNIPAm with acrylic acid and the formation of thin films using poly (allylamine hydrochloride) (PAH) as polycation[164]. Following that, similar approaches have been used, combining PNIPAm with different, in these cases synthetic, polymers[165,166]. It has been shown, that PNIPAm can also be grafted to charged

biopolymers, e.g., cellulose derivatives (except cellulose sulphate) and chitosan[167]. This is encouraging to use newly synthesized PNIPAm-grafted biopolymers for the fabrication of potentially thermoresponsive polyelectrolyte multilayers. So far, research efforts in this direction are sparse, but hold great potential. The benefits are not only the use of the versatile and inexpensive LbL technique, but the potential to fabricate thermoresponsive surface coatings, that present biological cues to the cells promoting their interaction with the surface.

While the combination of PNIPAm with biopolymers might hold great potential, extensive research has been done in other direction and resulted already in diverse application possibilities. Foremost, the aforementioned thermoresponsive surface coatings of PNIPAm grafted to PS for cell sheet engineering. It resulted in the fabrication of commercially available thermoresponsive cell culture dishes (TRCD) are the by now the "gold standard" using cell sheets in clinical applications. Conventionally, cells for TE applications were used as cell suspension and either incorporated into the scaffold, e.g., in hydrogels or capsules, or seeded on top of them. However, incorporation often led to a lack in nutrition and oxygen supply for the cells and seeding onto the scaffolds was accompanied by loss of cells that do not attach. This caused the need for high cell numbers, which are not always easy to produce, especially when host cells are used. Primary or stem cells from a patient are difficult to retrieve and therefore quite valuable and should be used with optimal seeding efficiency. The use of cell sheets could enhance the seeding efficiency. Not only does the thermoresponsive surface allow for a non-harmful harvest (contrary to enzymes) of the cells, but they maintain cell-to-cell junctions and often most of their secreted ECM: Less cells die and the cell sheets maintain a certain adhesiveness, since remaining ECM is acting like a "glue"[21]. This allows easy surface re-attachment and stacking, for high seeding efficiency or fabrication of thick and dense tissues for scaffold-free applications[20,168]. The presence of glycoproteins, especially fibronectin (FN), enables cell sheets to cover wounds without the need of sutures or tissue sealants. This is due to the ability of FN to bind a large number of biomolecules, among them several ECM, signalling and adhesion (e.g., proteoglycans, growth factors and integrins) molecules[169]. This has inspired a multitude of research efforts aiming for the in vitro fabrication of cell sheets, used for transplantation to enable or facilitate host tissue regeneration. Due to the research efforts over the past 15 years, several cell sheets, homotypic or heterotypic, have been fabricated from different cells and used for different tissues. Some are already in clinical use, other in preclinical studies and further still in research. Nagase et al. (2018) reviewed the current clinical applications of PNIPAm coated thermoresponsive surfaces[20].

2.3. Aim of the study

Considering the recent increasing popularity of cell sheet engineering for the replacement and regeneration of tissue by the harvest of intact cell sheets, the aim of this study is the development of a biomimetic, thermoresponsive surface coating which can mimic the natural environment of cells and has the potential to influence cell growth and differentiation by further modification, e.g., by increasing its bioactivity. able to allow harm-free cultivation and harvest of single cells and cell sheets.

The aim was to use the layer-by-layer technique as simple and affordable method to fabricate surface coatings based on PNIPAm-grafted-cellulose sulphate (PCS) and different polycations. Not only for the possibility to precisely deposit a certain number of layers and control the film thickness, but also because it allows the integration of bioactive components, such as growth factors. For this, polyelectrolyte of opposite charge were necessary and cellulose sulphate and chitosan as abundant, well-known, and chemically modifiable biopolymers were chosen. PNIPAm does not allow for the use in layer-by-layer technique as it is rather uncharged, as such was newly synthesized and characterized. Followed by the characterization of potential polyelectrolyte multilayers, their biocompatibility, and the extent of thermoresponsivity the surface coating possesses.

The fabrication of thermoresponsive surface coatings by combining PNIPAm with bioactive polyelectrolytes has not been described as such before. Hence, the development and characterization and fine tuning of materials and methods was a central part of this work. The benefits would not only by the use of the versatile and inexpensive LbL technique, but the potential to fabricate thermoresponsive and bioactive surface coatings, that present biological cues to the cells promoting cell surface interaction and the possibility to integrate other bioactive components such as growth factors to control cell fate. Additionally, the thermoresponsivity would in best case allow for the harm-free harvest of intact cell layers for potential cell sheet engineering applications. Figure 6 is a graphical abstract and overview of the aim of this study and the guideline to what has been done.
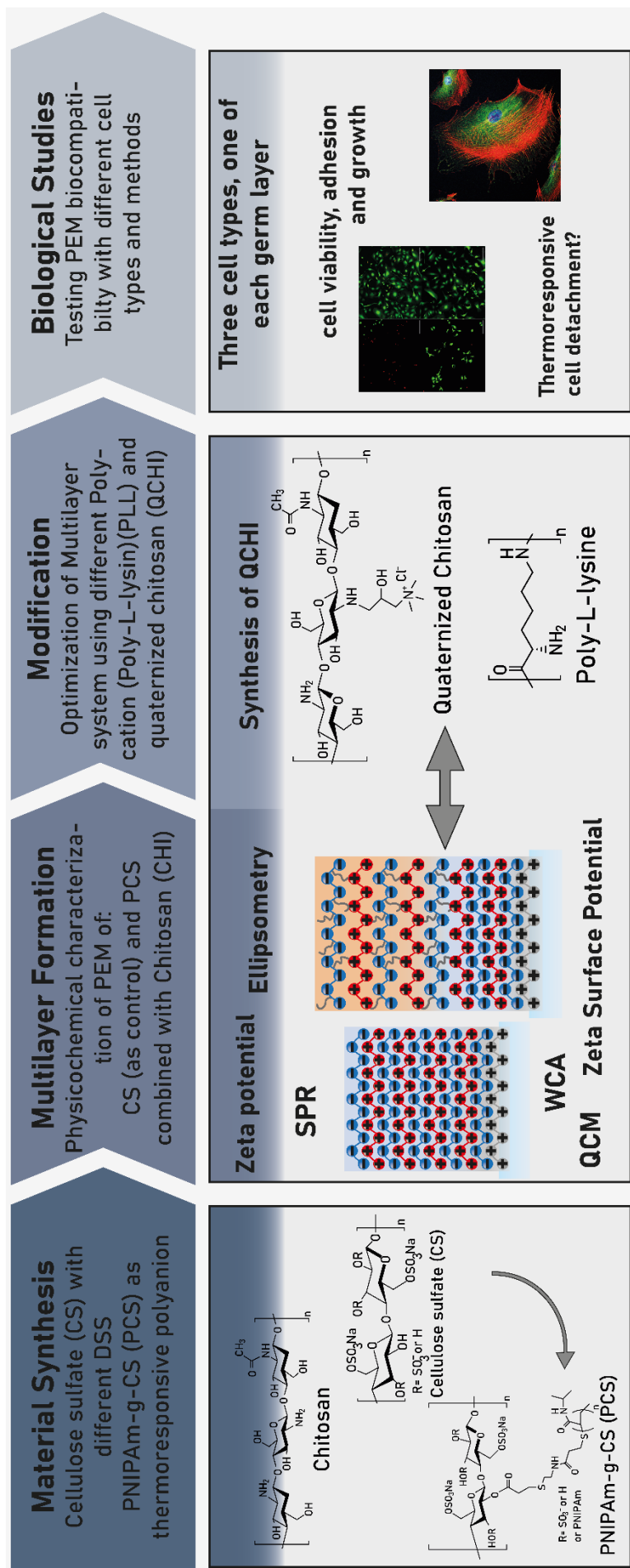
Figure 6: Schematic visualization of the objective and workflow of this thesis

3. Materials & Methods

3.1. Materials

Table 3: Detailed overview of all materials

AgNO₃	Silver nitrate solution 0.1 N; Art.: 931.1; Carl Roth GmbH & Co., Karlsruhe, Germany
Albumin Fraction V	Bovine Serum Albumin (BSA), 50 g, Art.-Nr.: 8076.2, Charge: 067254757; Carl Roth GmbH & Co., Karlsruhe, Germany
Ammonia solution 25%	Art.: 2672.2511; Th. Geyer GmbH & Co. KG, Renningen, Germany
Aquatex®	aqueous mounting agent for microscopy, Merck KGaA, Darmstadt, Germany
Cell culture well plates	Sterile, with lid, different sizes (6-, 12-, 24-, 48-wells), Cellstar ®, Greiner Bio-One GmbH, Frickenhausen, Germany
Cellulose acetate filter circles	0.2 µm pore size; Sartorius Stedim Biotech GmbH, Goettingen, Germany
Chitosan (CHI)	Chitosan 95/500, Chitoceuticals CAS 9012-76-4; MW: 200 – 400 kDa; Heppe Medical Chitosan GmbH, Halle (Saale), Germany
Deep Blue Cell Viability™ Kit	100 ml, Cat: 424702, BioLegend, San Diego, CA, USA
Dimethyl sulfoxide (DMSO)	≥ 99,5 %, Art.-Nr.: A994.1, Carl Roth GmbH & Co. KG, Karlsruhe, Germany
Dulbeccos's Modified Eagle Medium (DMEM)	500 ml, sterile filtered, with 4.5 g/l glucose and with L-glutamine (Catalogue Nr.: 12-604F), Lonza, Walkersville, MD, USA
Dulbeccos's Modified Eagle Medium (DMEM), low glucose, without Phenol Red	500 ml, sterile filtered, with 1 g/l glucose, L-glutamine, sodium bicarbonate, sodium pyruvate (AL183A-500ML), HIMedia Laboratories Pvt. Ltd., Mumbai- India
Dulbeccos's Modified Eagle Medium (DMEM), without Phenol Red	500 ml, sterile filtered, with 4.5 g/l glucose and without L-glutamine (Catalogue Nr.: 12-917F), Lonza, Walkersville, MD, USA

Eagle's Minimum Essential Medium (EMEM)	500 ml, sterile filtered, with EBSS (Earle's balanced salt solution), NEAA (Non-essential amino acids) and Sodium pyruvate, without L-glutamine (Catalog Nr.: 12-662F), Lonza, Walkersville, MD, USA
F-actin staining	Phalloidin CruzFluor™ 555 Conjugate (sc-363794), Santa Cruz Biotechnology, Inc., Heidelberg, Germany
FBS Superior	Foetal bovine serum, 500 ml, standardized, for cell culture, Biochrom GmbH, Berlin, Germany
Filter circles	MN 615, $\varnothing$ 70 mm, Macherey-Nagel; Carl Roth GmbH & Co., Karlsruhe, Germany
Glycidyl trimethylammonium chloride (GTMAC)	80% in water, CAS 3033-77-0, Tokyo Chemical Industries, Eschborn, Germany
HCl	Hydrochloric acid, ROTIPURAN® $\geq$ 32%, Art. Nr.: P074.1, Carl Roth GmbH & Co., Karlsruhe, Germany
KCl	Potassium chloride p. a., Art.: 678.1; Carl Roth GmbH & Co., Karlsruhe, Germany
KH_2PO_4	Potassium dihydrogen phosphate p.a.; Merck KGaA, Darmstadt, Germany
Microscope cover glasses (rectangle)	10x20 mm, as substrate for surface potential measurements, Paul Marienfeld GmbH & Co. KG, Lauda-Köngishofen, Germany
Microscope cover glasses (round)	Different diameters (10 to 15 mm), VWR International GmbH, Darmstadt, Germany
$Na_2HPO_4 \cdot 2\,H_2O$	di-Sodium hydrogen phosphate dihydrate p. a.; Art.: 8622.0500; Th. Geyer GmbH & Co. KG, Renningen, Germany
NaCl	Sodium chloride p.a., CAS 7647-14-5; Th. Geyer GmbH & Co. KG, Renningen, Germany
NaOH	Sodium-hydroxide, Art. Nr.: 9356.1, Carl Roth GmbH & Co., Karlsruhe, Germany
Nuclei staining	TWO-PRO™ 3 (equivalent to TO-PRO®-3), CAS: 157199-63-8, AAT Bioquest, Inc., Sunnyvale, CA, USA

Parafilm	Bemis™ Curwood Parafilm™ M, Th. Geyer GmbH & Co. KG, Renningen, Germany
PBS buffer	0.4 g KCl, 16 g NaCl, 0.38 g KH2PO4, 1.53 g Na2HPO4
PEI	Poly(ethyleneimine) solution, 50 wt. % H2O; MW ~ 750 kDa; Sigma-Aldrich Chemie GmbH, Taufkirchen, Germany
Pen/Strep	100 ml, sterile filtered, 10000 UI/ml Penicillin, 10000 UI/ml Streptomycin, Lonza, Walkersville, MD, USA
Pen/Strep/Amph	100 ml, sterile filtered, 10000 UI/ml Penicillin, 10 mg/ml Streptomycin, 25 mg/ml Amphotericin B, Lonza, Walkersville, MD, USA
Pipette tips (10, 100, 1000 µl)	Brand GmbH & Co. KG, Wertheim, Germany
Pipette tips (2500, 5000 µl)	epT.I.P.S., Eppendorf SE, Hamburg, Germany
PNIPAm-COOH	Poly(N-isopropylacrylamide), carboxylic acid terminated, Art.: 724815-5G; Sigma-Aldrich Chemie GmbH, Taufkirchen, Germany
Poly-L-lysine (PLL)	Poly-L-lysine hydrobromide, MW = 52 kDa, 1g, CAS 25988-63-0, Alamanda Polymers Inc., Huntsville, AL, USA
Primary antibody	Monoclonal Anti-Vinculin antibody produced in mouse (V9131), Sigma-Aldrich Chemie GmbH, Taufkirchen, Germany
Quartz chip Au (QCM sensor)	Art. Nr. 711.05.Ti/Au, quartz chip coated with Ti and surface coated with Au, 3T analytik GmbH & Co. KG, Tuttlingen, Germany
Rabbit serum	Gibco™ 16120099 Rabbit Serum, Fisher Scientific GmbH, Schwerte, Germany
ROTI® Histofix 4%	4% Formaldehyde, pH 7, acid free, Art.: P087.6; Carl Roth GmbH & Co., Karlsruhe, Germany
Roti®-Mount FluorCare	15 ml, aqueous mounting agent for fluorescence microscopy, Art. Nr.: HP19.1, Carl Roth GmbH & Co., Karlsruhe, Germany
Secondary antibody	Rabbit anti mouse IgG1 antibody Cy2 conjugated (ABIN6699052), antibodies-online GmbH, Aachen, Germany

Serological pipettes	Sterile, different sizes (5, 10, 25 ml), Cellstar ®, Greiner Bio-One GmbH, Frickenhausen, Germany
Silicon (Si) wafer	100 mm diameter (cut to 10x10 mm size), Siegert Wafer GmbH, Aachen, Deutschland
SPR Sensor	Glass squares, coated with 50 nm Au (16 x 16 1 mm); Ssens bv, Enschede, The Netherlands
Syringe filters	Cellulose acetate filter, Whatman® FP30/0.2 CA-S; Sigma-Aldrich Chemie GmbH, Taufkirchen, Germany
T75 Cell culture flasks	Sterile, Cellstar ®, Greiner Bio-One GmbH, Frickenhausen, Germany
Trypsin/EDTA 0.25%/0.02 % (w/v)	In PBS, w/o Ca2+/Mg2+, Biochrom GmbH, Berlin, Germany and Biowest, Nuaillé, France
Tubes	Cellstar ® tubes, 15 and 50 ml, sterile, blue screw cap, conical bottom, Greiner Bio-One GmbH, Frickenhausen, Germany
Viability/Cytotoxicity Assay Kit for Animal	Live & Dead Cells (Calcein-AM and Ethidium Homodimer 1), Biotium Inc., Fremont, CA, USA

3.2. Synthesis of quaternized chitosan

Quaternized chitosan (QCHI) was prepared following the protocol from Mi et al. (2014) with some minor modifications, adapting the process to laboratory equipment[170]. 6 g Chitosan (CHI, details see Table 3) were dispersed in 240 ml micropure water in a 500 ml three-neck round-bottom flask. After dispersion, 16.82 g (21.3 ml) GTMAC were added in three portions in 2 h intervals, while the mixture was stirred at 85°C in an oil bath overnight (10 h). Afterwards, the reaction solution was dialyzed for 3 days in regenerated cellulose dialysis tubes with 3.5 kDa MWCO against distilled water (changing water in regular intervals) to remove unreacted GTMAC. Using micropure water, the dialyzed solution was diluted and divided into 50 ml centrifuging tubes. Tubes were centrifuged at 3000 rpm to precipitate unreacted CHI at the bottom. Solution of the tubes was decanted and subsequently vacuum filtered with a fine porosity fritted disc covered with round filter paper, to finally remove all solids from the solution. The clear, diluted solution was concentrated under vacuum using a rotary evaporator Rotavapor R-114 with a water bath B-480 (Büchi Labortechnik GmbH, Essen, Germany) at 70 °C. The concentrated solution was lyophilized in vacuum at -48 °C using a Christ Alpha 1-2 LO Plus freeze dryer (Martin Christ Gefriertrocknungsanlagen GmbH, Osterode am Harz, Germany). Dry, final product was stored in tubes inside a

desiccator at room temperature. Final product was characterized using 1H-NMR and chloride titration using silver nitrate. For 1H-NMR analysis, 20 mg of final product were dissolved in 1 mL of deuterated water (D_2O) and filled in analysis tubes. 1H-NMR was performed by the Institute of Chemistry of the Martin-Luther-Universität Halle-Wittenberg. For chloride titration using silver nitrate and potassium chromate as color indicator, a 1 wt % silver nitrate solution was placed in a 25 ml burette and 25 ml of a 1 wt % QCHI solution was mixed with 5 ml of 1 wt % potassium chromate solution in a 100 ml Erlenmeyer flask. Dropwise addition of silver nitrate resulted finally in a color change from yellow and clear to an orange-red and turbid solution. The amount of used silver nitrate solution was recorded, titration was repeated 3 times.

3.3. Substrate cleaning

Glass cover slips (12 mm diameter) or slides (VWR, Germany), and silicon wafers (cut to a size of 10x10 mm², Siegert Wafer GmbH, Aachen, Germany), were cleaned following the RCA-1 protocol for the removal of organic residues on the surface[171]. The procedure uses a mixture of ammonium hydroxide (Chem Solute, Th. Geyer, Renningen, Germany), hydrogen peroxide (Carl Roth GmbH + Co. KG, Karlsruhe, Germany) and micro-pure water (Milli-Q-plus system, Millipore) at a ratio of 1:1:5. Initially, micro-pure water and ammonium hydroxide were heated to 80°C, at which point hydrogen peroxide was added to the mixture and temperature should not drop below 70°C. The substrates (Si wafer or glass) were placed in a Teflon rack and immersed in cleaning solution for 15 min. Subsequently, substrates were extensively washed in micro-pure water and dried in a stream of compressed nitrogen gas. New gold-coated glass sensors, used for SPR measurements, were purchased from Ssens E.V. (Netherlands). They were rinsed with 99.8% ethanol and micro-pure water and immediately used for the SPR measurement.

3.4. Preparation of polyelectrolyte solutions and multilayers

The multilayers in this study were prepared using the Layer-by-layer technique, combining the polycations chitosan (CHI), poly-L-lysin (PLL) and quaternized chitosan (QCHI) with polyanions cellulose sulphate (CS) or PNIPAm-grafted-cellulose sulphate (PCS). All polyelectrolytes were dissolved in deionized water containing 0.15 M NaCl at a concentration of 1 mg/ml. Chitosan (95/500) was solubilized at 50°C for 3h (in water bath) and then stirred overnight in 0.15M NaCl containing 0.05M acetic acid. All polyelectrolyte and washing solutions were adjusted to pH 4.0 and filtered through a 0.2 μm pore sterile filter. PEI used as an anchoring layer on the substrate, was prepared at a concentration of 5 mg/ml. PEM assembly follows the simple alteration of polycation/polyanion-deposition on different

substrates, according to the requirement of the experiment (Si-Wafer, tissue culture polystyrene wells). LbL coating was achieved using a pipet approach, whereby a certain volume of polymer solution, depending on the well size (100 μl in 96 well plate; 500 μl in 24 well plate) was deposited directly onto the substrate. Polymer adsorption was carried out for 15 min. In between each polymer adsorption step, 0.15 M NaCl buffer was used for washing of unbound polymers from the surface for 3x1 min. The polymer deposition and washing were performed at room temperature and under mild shaking. For all multilayer compositions, the first anchoring layer was always PEI, to provide an evenly positive charged surface. The subsequent layer sequence was different for samples containing only CS or samples containing functionalized PCS derivatives.

Polyanionic CSs were simply alternated with polycation (CHI, PLL or QCHI) until the 10th layer, where CS was used for even, and polycations were used for uneven layers (e.g., PEI[CHI/CS2]$_4$CS2, see Figure 7, left side). These are the control groups, as the PEM did not contain PNIPAm. For the PCS derivatives, the approach of a basal layer was used. After the anchoring layer PEI, CS 2 was used for the 2nd and 4th layer, and PCS 1 or PCS 2 were used for the final layers, namely the 6th, 8th, and 10th. Uneven layers were polycations (CHI, PLL or QCHI, e.g., PEI[CHI/CS2]$_2$[CHI/PCS1]$_2$PCS1; see Figure 7, right side). The basal layer (1st to 5th layer) is not functionalized, the functional layer (6th to 10th layer) contains PCS. Phosphate buffered saline (PBS) with pH 7.4 was applied for 20 minutes after layer build up to test the multilayer's stability under physiological conditions.

The abbreviations for CS and PCS (CS 1, CS 2, PCS 1, or PCS 2) are explained in detail in in Table 4 in chapter 4.1.
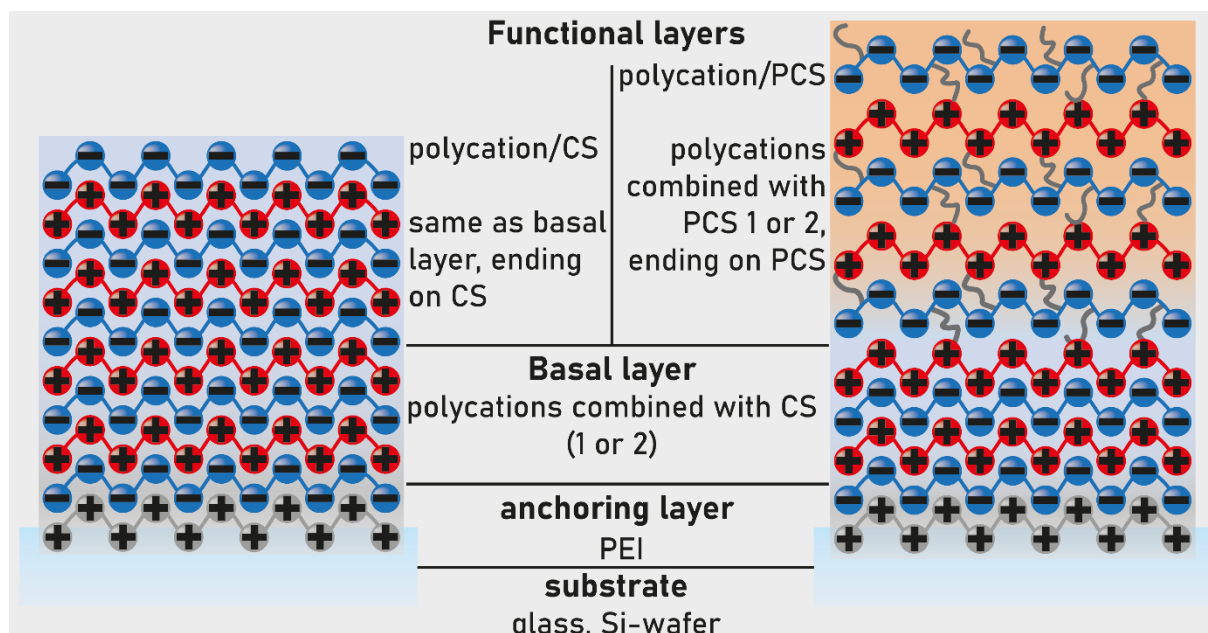
Figure 7: Scheme representing the polyelectrolyte multilayer structure, visualizing the anchoring, basal and functional layer, and the differences between samples for control without PNIPAm, polycation/CS 1 or CS 2, and the functionalized films with PNIPAm: polycation/PCS1 or PCS 2 (colored in orange).

3.5. Physicochemical characterization

3.5.1. Zeta potential of polyelectrolytes

The zeta potential provides information on the charge of the polyelectrolytes in solution. Since the LbL technique is in great parts based in electrostatic interactions, the predetermination of the polyelectrolyte charge helps to determine the interaction between polyanionic and polycationic molecules. Furthermore, the method provides information on how weak or strong the polyelectrolytes are, respectively.

Polyelectrolyte zeta potential was studied by measuring zeta potential via electrophoretic light scattering with a Zetasizer ZS (Malvern Panalytical, Malvern, UK). Polyelectrolytes were prepared at 2 mg/ml in a 20 mM NaCl solution (reduced salt concentration to preserve gold electrodes of folded capillary cell DTS1070) at pH 4. Samples were diluted to 0.5 mg/ml with 20 mM NaCl buffer before measurement and were measured at 25 °C with an applied voltage of 60 V. The measured electrophoretic mobilities were transformed into zeta potential using Smoluchowski's formula.[172,173] This method allows to initially access the polyelectrolyte charge and to estimate their electrostatic interactions during multilayer formation.

3.5.2. Surface plasmon resonance measurements

Surface Plasmon Resonance (SPR) experiments were performed using IBIS-iSPR equipment (IBIS Technologies B.V., Hengelo, Netherlands). SPR as an optical-based, analytical tool for real-time monitor of molecular adsorption kinetics[2]. SPR measurements give insight into the adsorption of the single layers of a multilayer system and allows assessment of the adsorption quality and the multilayer growth. This light-based method relies on the excitation of surface plasmon and changes in the optical properties, namely the refractive index, of the measured system. To exploit this physical phenomenon, polarized light travels through a prism towards a metal (mostly gold) coated sensor. The light hits the sensor from below, being reflected from the sensor surface. At a certain angle of incidence, the light intensity reaches a minimum, the point at which surface plasmon are excited and inducing surface plasmon resonance. The angle at which the maximum reduction of reflected light due to the interaction of p-polarized light with the metal electrons occurs is called resonance or SPR angle. It depends on the refractive index on both sides of the metal interface. However, one side has constant optical properties (prism side) while the adsorption of molecules leads to changes in the refractive index (RI) on the top side of the metal surface. These changes lead to a shift of the SPR angle (which is the measured value), providing information on the kinetics of biomolecule adsorption onto surfaces. The basic setup consists of mainly three components: the optical unit (dry), liquid handling unit (wet) and the sensor surface (interface between dry and wet). The optical unit comprises a light source and a glass prism, on top of which the gold-coated glass sensor is placed. The sensor, as mentioned before, is the barrier between the dry optical unit and the wet liquid handling system. The liquid unit consists of syringe (pumps) and tubes, allowing the controlled liquid flow across the sensor surface, whereas the liquid contains the molecules that ought to adsorb. This setup is known as Kretschmann configuration[174,175].

For the assessment of the PEM formation using SPR, the experimental protocol was similar to the fabrication of PEM using LbL. The gold-coated glass sensor was rinsed with 70% ethanol and micro-pure water and subsequently dried using N_2 stream. Completely dry, the sensor was mounted onto the SPR prism using oil (having the same RI as the glass), to avoid changes in RI on this side of the gold layer. Mounted inside the SPR; a measuring cell is mounted tightly on top of the gold surface, with in- and outlet for the liquid handling. Firstly, the NaCl buffer solution was introduced to the sensor surface and a SPR angle baseline is determined. Thereafter, the measurement begins and polyanionic and polycationic solutions were alternately introduced to the surface for 10 min using 150 µl solution that is run back

and forth over the surface at a flow rate of 4 µl/s⁻¹. In between the polyelectrolyte solutions, 1000 µl buffer solution is introduced for 15 min, rinsing loosely bound molecules. The experiment follows the earlier explained multilayer formation, with PEI as anchoring layer, basal layers containing polycation and cellulose sulphate and thereafter the functional layers with PCS as polyanion. Each step had to reach an equilibrium in angle shift, which basically determined the time used for each adsorption step. The experimental data presented are mean values of triplicate measurements with SD, which is however quite small and not visible due to the symbol size.

The IBIS iSPR used was not multiparametric, which limits the experimental data to SPR angle shifts and a purely qualitative interpretation. The thickness, refractive indices and other quantitative data of the formed PEMs was not accessible.

3.5.3. Quartz crystal microbalance

For the further characterization of the PEM films, quartz crystal microbalance with dissipation monitoring (QCM-D) was used in addition to SPR. It enables the *in situ* real-time monitoring of layer formation and growth, including bound water. The QCM-D technique was previously described by Rodahl et al. (1995)[176]. In contrast to the light-based SPR method, QCM-D is an acoustic method. An AT-cut piezoelectric quartz crystal (hence the name) coated with gold on both sides (functioning as electrodes) is excited at its fundamental frequency (10 MHz). This frequency is monitored in real-time and any deposited mass onto the gold surface causes a decrease of the resonant frequency, Δf. For thin and rigid films adsorbing in air, this frequency change is proportional to a mass change Δm following the Sauerbrey equation (Eq. 1):

$$\Delta m = \frac{-C\Delta f}{n} \ (Eq. 1)$$

C is the mass sensitivity constant given for the QCM-D setup used and n the overtone number. In this study, a QCM-D device from 3T analytik GmbH & Co. KG (Tuttlingen, Germany) was used which only allows measurements at the fundamental frequency, hence n = 1 and can be neglected in the Sauerbrey equation. At 10 MHz, C = 0.23 ng/cm²Hz for this QCM-D machine.

However, PEM systems mostly form more viscoelastic layers, for which the mass does not fully couple to the quartz crystal oscillation and subsequently dampens the oscillation. This dampening is measured after the driving voltage of the quartz crystal oscillation is shut off and real-time measured as positive frequency change ΔD (dissipation factor). The calculation for Δm was performed by the QCM-D software qGraph viewer (3T analytik GmbH & Co. KG, Tuttlingen, Germany). However, it presented some drawbacks, as the mass calculations are only based on the Sauerbrey equation, which underestimates the adsorbed

mass for viscoelastic films. Hence, these values are not presented in this work. On the other hand, using the software, calculation of thickness of viscoelastic layers were possible using a Voigt based model. This setup is defined as a spring and dashpot in parallel under no slip conditions. Under the assumption that the film homogenously covered the entire sensor area with uniform thickness and the liquid in which the sensor resonated is a bulk Newtonian fluid, Voinova et al. (1999) published the mathematical formula for the changes of Δf (Eq. 2) and ΔD (Eq. 3) as[177]:

$$\Delta f \approx \frac{1}{2\pi\rho_0 h_0}\left\{\frac{\eta_B}{\delta_B} + h_L\rho_L\omega - 2h_L\left(\frac{\eta_B}{\delta_B}\right)^2 \frac{\eta_L\omega^2}{\mu_L^2 + \omega^{2}\eta_L^2}\right\} \quad (Eq.2)$$

and

$$\Delta D \approx \frac{1}{\pi f \rho_0 h_0}\left\{\frac{\eta_B}{\delta_B} + 2h_L\left(\frac{\eta_B}{\delta_B}\right)^2 \frac{\mu_L\omega}{\mu_L^2 + \omega^{2}\eta_L^2}\right\} \quad (Eq.3)$$

where ω is the angular frequency of the oscillation, ρ_0 is the density and h_0 is the thickness of the quartz crystal. For the bulk liquid, η_B defines the viscosity, $\delta_B \left(= \sqrt{(2\eta_B/\rho_B\omega)}\right) (Eq.4)$ is the viscous penetration depth of the shear wave and ρ_B is the liquid's density. For the adsorbed layer, h_L, ρ_L, η_L and μ_L represent the thickness, density, viscosity, and elastic shear modulus, respectively.

For the experimental measurement, different polyelectrolyte solutions were pumped into the system at a constant flow rate of 100μl/min and allowed to adsorb to equilibrium state for 10 minutes. Followed by injection of 0.15M sodium chloride buffer (NaCl) pH 4.0 for another 15min to remove weakly bound molecules. After the 10th layer, the QCM-D chamber was injected with PBS with pH = 7.4 at the same flow rate until resonance frequency and dissipation signal reach an equilibrium. PEM films have been prepared *in situ* as described in the previous section concerning multilayer formation. Based on the aforementioned model from Voinova et al. (1999) (see Eq. 1 and Eq. 2), approximation of the wet thickness based on the Voigt-model was calculated using the frequency and dissipation change of QCM-D measurement[177] by the software. The machine software needs the input of layer density, buffer density and buffer viscosity and automatically calculates an approximation of layer thickness. Based on previous work[178], layer density of $\rho_{PEM} = 1400$ kg·m^{-3}, buffer density ($\rho_B = 1000$ kg·m^{-3}) and viscosity ($\eta_B = 1$ mPa·s) were chosen and approximate values for wet thickness of PEM systems were calculated. However, it should be mentioned that the QCM-D software used does not present any quality indications of the modulation, as other QCM machines (especially with overtone measurements) would be able to. This should be kept in mind when interpreting the results.

3.5.4. Ellipsometry

Spectroscopic ellipsometry was used to determine the dry thickness of polyelectrolyte multilayer films. Ellipsometry is an optical method measuring changes in the polarization of light that is reflected from a material surface. These changes are represented by two values, amplitude ratio Psi (Ψ) and phase difference Delta (Δ), which depend on the material's optical properties and thickness, hence enabling the determination of film thickness.

Using a polarizer, light from a light source is linearly polarized (with p- and s-components describing the light wave). The incident polarized light arrives at the sample surface and is reflected (and partially refracted) becoming elliptically polarized (hence the name ellipsometry) and travels through the analyzer and towards a detector, converting light into and electromagnetic signal. Comparing the information received from the detector to the input light polarization, the polarization changes caused by the samples are measured in form of Ψ and Δ. The film thickness (and other optical constants) is determined using a regression model. In case of polymeric multilayers, the Cauchy Model is a fitting representation of materials properties. The model components are compared to the measured values, adjusting the optical constants of the model until the Mean Squared Error (MSE), an estimator for the quality of the fit, reaches a minimum. At this MSE minimum, the fit is most accurate and that corresponds to the actual film thickness.

The measurements were performed using the VASE ellipsometer (J.A Woollam Co., Inc. Nebraska U.S.A) with affiliated software VWASE32, with incident light in wavelength range 400 to 1200nm. The spectroscopic angle scan was performed from 55° to 70° of incident light by six steps of 3°. Using the software, the beam position and intensity was manually optimized. Therefore, the ellipsometer table (on which the sample was placed) was adjusted until the sample was well aligned, giving highest intensity at the double position-sensitive (x and y) detector visible in the software. This ensures highest accuracy and reproducibility of measurements. After the measurement of Ψ and Δ, the software is further used to mathematically fit the measured data to the Cauchy model, looking for MSE minimum. The resulting values was used to determine the thickness (and RI) for our polyelectrolyte films. The samples were scanned at two different positions to examine if the film is evenly spread over the whole sample surface. Measurements were performed in triplicates.

3.5.5. Water contact angle measurements

One important property of surfaces, predetermining many possible interactions with liquids, molecules, cells and more, is the wettability. Hence, the determination of a surface wettability and subsequently the characterization as more hydrophilic or hydrophobic is very important. One simple method which allows surface wettability characterization is the water

contact angle (WCA) measurement. Using a defined droplet of water, a diffuse light source and a camera for imaging, calculation of contact angles and following that the determination of surface wettability is possible. Luckily, calculations are by now carried out in the corresponding WCA software.

The wettability characterization of PEM coated silicon wafer substrates was performed with an OCA 15+ machine (Dataphysics GmbH, Filderstadt, Germany) at room temperature. Using the sessile drop method, 3 drops of the testing liquid (micropure water) were dispensed through a micro-syringe (0.26 μm inner diameter) onto a horizontally arranged PEM coated Si-wafer. Using the software, the motor-controlled dosing volume of 3 μl per drop at a dosing rate of 0.5 μl/s was selected. For the sessile drop method, the drop is placed on the substrate from above, the needle is retracted. Using a diffuse light source, a camera takes images of the high contrast images, on which the drop (absorbing the diffuse light) is black in front of a bright background. Images of the drops were immediately taken after drop placement. Using the SCA20 software (Dataphysics GmbH, Filderstadt, Germany) the contact angle was calculated. Due to the well visible drop silhouette, the software automatically draws the baseline (contact of the drop to the substrate) and outline (border between black drop and white background). With these lines automatically placed, the static contact angle values were obtained from at least 6 independent measurements by curve fitting the drop profile using Ellipse fitting. Values obtained from the independent measurements are represented as mean values with standard deviation.

3.5.6. Streaming potential measurement

The measurement of zeta surface potential basically measures the surface charge and hence provides information on surface functionality, stability and interaction with dissolved compounds or molecules. Especially in biomaterial research, this information is vital to predetermine the possible interaction with blood, proteins and subsequently cells. For polyelectrolyte multilayers, it further gives insight into the multilayer composition, structure, and stability. Measuring at different pH values enables the observation of the dominant functional groups related to the polyanionic or polycationic compounds in the multilayer and which component is dominant towards the PEM film surface.

The surface zeta-potential was determined using the SurPASS electrokinetic analyzer (Anton Paar, Graz, Austria). The software the equipment calculates the surface zeta potential using the following equation (Eq. 5):

$$\zeta = \frac{dU}{d\Delta p} \frac{\eta k_B}{\epsilon_r \epsilon_0} \ (Eq.\,5)$$

Where dU is the streaming potential, $d\Delta p$ is the pressure difference across the sample, ϵ_r is the dielectric constant, ϵ_0 is the vacuum permittivity, k_B is the electrolyte conductivity, and η the electrolyte viscosity.

Therefore, PEM systems were prepared on special glass slides (10 x 20 mm²) followed by streaming potential measurements. Two glass slides modified with the identical PEM were inserted into the machine, creating a small gap through which the electrolyte (1 mM KCl in water) was flown. A flow rate of 100-150 ml/min was achieved at a maximum pressure of 300 mbar, which was adjusted through changing the width of the gap between the glass slides. Before starting the measurement, 0.1 M Hydrochloric acid (HCl) was used to adjust to pH 2.5. During the measurement, automated titration with 0.1 M sodium hydroxide (NaOH) adjusted the pH towards the predefined end point at pH 9.5. Zeta potential was calculated by the provided software. Each test was done in triplicates.

3.6. Biological characterization

For the comprehensive biological characterization of the different PEM surfaces, especially with regard to their biocompatibility, diverse experiments were carried out. Focusing on the viability and growth of cells, Live/Dead and Deep Blue cell growth assays were executed. Since the newly developed surface coatings ought to be applicable over a wide range of potential tissue engineering purposes, biocompatibility with different cell types would be beneficial. With this in mind, cell experiments were carried out using cell types originating from different germ layers. These are the primary cell layers in embryonic development, namely endoderm (inner layer), ectoderm (outer layer) and mesoderm (middle layer). During embryonic development, cells originating from these germ layers give rise to certain tissue types in the human organism, all different regarding the cell adhesion behaviour[179]. As representative cell types for the three different germ layers, mouse fibroblast originating from the mesoderm, humane keratinocytes originating from the ectoderm, and humane epithelial-like hepatocellular carcinoma cells originating from the endoderm were selected. For all cell types, well-known and standardized cell lines were utilized, as primary cells are not only expensive and difficult to purchase, they also normally show donor to donor variability.

3.6.1. Culture of 3T3 mouse fibroblast cells

Fibroblasts are cells of the connective tissue of mesodermal origin. In this study, the NIH3T3 mouse embryonic fibroblast cell line (ATCC, Manassas, VA, USA) was used for

several experiments. It is one of the most commonly used cell lines and was applied in a wide range of experimental studies[180]. They are immortalized, adherent and rather easy to grow.

3T3 cells were cultured in T75 flasks, seeded at a density between 5.000-6.000 cells/cm². Dulbecco's modified Eagle's serum containing 4.5 g/L glucose and 4 mM glutamine, supplemented with 10% fetal bovine serum (FBS) and 1% penicillin, streptomycin, and amphotericin B (Pen/Strep/Amp). Cultured cells were grown at 37°C in a humidified incubator (5% CO_2/95% air atmosphere). Medium was changed twice in 7 days. At 70-90% confluency of the cells, splitting was performed by washing the cells with sterile PBS once and adding 3 mL 0.25% trypsin/0.02% ethylenediaminetetraacetic acid (EDTA) solution and incubate for 5 min at 37°C. Addition of 5 ml serum-containing DMEM inactivates trypsin. Cell suspension was centrifuged for 5 min at 500 rpm, resulting in a cell palette. Supernatant (w/ trypsin) was removed, and cells resuspended in 1 ml fresh cell culture medium. Cells were counted using a Neubauer chamber and seeded in new culture flask or at certain cell densities (specified in the corresponding experimental section) in well plates.

3.6.2. Culture of HepG2 human hepatocellular carcinoma cells

The liver hepatocellular carcinoma cell line named HepG2 has been used as representative cell type from endodermal origin. This immortalized cell line was originally derived from the liver tissue of a 15-year-old male patient with a well-differentiated hepatocellular carcinoma. This cell line is commonly used in biomedical research. HEpG2 cells are adherent and healthily grow in small aggregates[181,182].

HepG2 cells, obtained from ATCC (Manassas, VA, USA), were cultured in T75 flasks, seeded at a density of 20.000 – 25.000 cells/cm². Eagle's Minimum Essential Medium (MEM) containing Earle's balanced salt solution (EBSS), non-essential amino acids (NEAA), supplemented with 2 mM L-glutamine and 10% FBS was used as culture medium. Additionally, antibiotics in form of 1% penicillin/streptomycin (Pen/Strep) solutions was added. The subculture protocol was similar to that of 3T3 cells. Cells were grown to 75-90 % confluency, before they were split using trypsin/EDTA, with a reduced trypsin concentration of 0.05 %. HepG2 cells are sensitive to dissociation agents and exposure should be kept to a minimum. Cell detachment was checked after 3 min and as soon as cells visibly detached (examined under phase contrast microscope), inactivation of trypsin was done by adding EMEM with 10% FBS. The centrifugation to gain a cell palette and remove the medium containing trypsin residues was performed at reduced speed of 250 rpm for 5 min, to prevent cell clumping. After counting using a Neubauer chamber, cells were seeded for further culture in T75 flasks or at specific concentrations for biocompatibility experiments.

3.6.3. Culture of HaCaT human keratinocyte cells

As representative for cells of ectodermal origin, the HaCaT cell line was employed. This immortalized human keratinocyte cell line has been widely used for diverse biomedical studies. They are suitable for long-term growth and exhibits normal morphogenesis and functional activities similar to primary keratinocytes. HaCaT cells are adherent and proliferate from small cell aggregates[183,184].

HaCaT cells, purchased from CLS (Cell Line Service GmbH, Eppelheim, Germany), were seeded in T75 cell culture flasks at a density of 15.000 cells/cm² and cultivated until 70-80 % confluency. As cell culture medium DMEM containing 4.5 g/L glucose and 4 mM L-glutamine, supplemented with 10 % FBS and antibiotics in form of 1% Pen/Strep solution. The culture and passaging protocol were basically the same as for HepG2 cells. Reduced trypsin concentration of 0.05 % and reduced centrifugation speed of 250 rpm for 5 min was applied. After counting in a Neubauer chamber, cells were again seeded in T75 cell culture flask for further cultivation or at specific densities in well plates for viability and growth experiments.

3.6.4. Cell viability assay using live/dead-staining-Kit

Viability of adherent 3T3 mouse fibroblasts cells and subsequent biocompatibility of PEM films was assessed using a live/dead assay. A cell viability/cytotoxicity assay kit consisting of two probes. namely Calcein AM and ethidium homodimer III, was used to fluorescently stain cells seeded in PEM coated wells of a well plate. Ethidium homodimer III is a cell membrane impermeant nucleic acid dye, only staining the nucleus of dead cells with a damaged cell membrane. On the other hand, in living cells the nonfluorescent Calcein AM is converted to green fluorescent Calcein, after acetoxymethyl ester hydrolysis by intercellular esterase. All aforementioned cell types were examined using the live/dead assay.

Using the LbL technique, the wells of a 24-well plate were coated with different PEM compositions (see section for multilayer fabrication for details). The well plate was sterilized using a UV chamber for 60 min at 2.5 kJ at a wavelength of 254 nm. After sterilization, cells were seeded on differently PEM-coated wells of a 24-well plate at a density of 10000 cells/cm² and cultivated for 24 h. The staining was conducted according to the manufacturer's protocol. Cells were seeded in uncoated tissue culture polystyrene wells as control. Images were taken using a confocal laser scanning microscope (CLSM, LSM 710, Carl Zeiss, Oberkochen, Germany). ImageJ software was used for further calculations and image characterization. During the imaging process, the well plate was placed in a heated (37 °C) and with a 5 % CO_2 atmosphere supplied microscope stage inlay, to accommodate the living cells under culture conditions.

3.6.5. Cell growth assay

Cell growth/proliferation was quantified using a Deep Blue assay. This assay is based on the resazurin reagent. The typical blue resazurin, hence the name of the assay, is converted to fluorescence by the action of metabolic enzymes. Thereby, resazurin is reduced to the pink-colored and highly fluorescent resorufin. The reduction of resazurin and production of resorufin is proportional to the number of metabolic active cells, allowing to correlate the fluorescence intensity to the number of living cells in the examined culture. This assay was conducted for all aforementioned cell types.

Using the LbL technique, the wells of a 48-well plate were coated with different PEM compositions (see section for multilayer fabrication for details). Quintuplicates per PEM system were prepared. The well plate was sterilized using a UV chamber for 60 min at 2.5 kJ at a wavelength of 254 nm. Cells were seeded into precoated 48 well plates at a density of 13500 cells/cm², marking day 0. After 1, 4 and 7 days of cell culture, cells on this well plate were washed with colorless DMEM and images were taken with a phase contrast microscope (Eclipse Ti2-U, Nikon, Tokyo, Japan). Subsequently, 300 µl of a 10% Deep Blue solution (100% Deep Blue diluted in colorless DMEM, w/o FBS) were added to the well, followed by 2 h incubation at 37°C. After incubation, 100 µl of the supernatant has been collected in a black 96-well plate. The plate was excited at 540 nm wavelength in a fluorescence plate reader (Fluostar Optima™, BMG Labtech, Ortenberg, Germany). Each well was washed once more with colorless DMEM, afterwards culture medium was added for further culture. This process was repeated at the other time points. The mean values of the excitation measured by the plate reader with SD are presented and directly proportional to cell activity.

3.6.6. Immunofluorescence staining of 3T3 mouse fibroblasts

The staining of specific protein using corresponding antibodies is known as immunofluorescent staining. Certain antibodies that bind exclusively to specific proteins are labelled with fluorescent elements, allowing to visualize the targeted proteins and subsequently specific cell components using fluorescence microscopy. It allows the qualitative interpretation of cell adhesion and morphology on different PEM systems subsequently relating to the biocompatibility of these surfaces.

Firstly, RCA-1 cleaned glass cover slips (12 mm diameter) have been coated using LbL technique with different multilayer compositions. Surfaces that showed good biocompatibility behavior in the cell viability and growth tests performed before, have been selected. Hence, glass cover slips have been coated with CS derivatives (CS 2 and PCS 2) in combination with the polycations PLL and QCHI. The PEM structure/composition is as

described earlier, with PEI as anchoring layer, the basal layers, and the functional layers. Terminal layers are polyanionic, which means CS or PCS. Prior to cell seeding, the coated glass cover slips (and uncoated glass as control) were sterilized in a UV chamber for 60 min at 2.5 kJ (λ = 254 nm). 3T3 mouse fibroblasts, cultivated as mentioned before, were seeded onto the sterilized glass cover slips in a 12-well plate, at a density of 5000 cells/cm². After 24 h of cultivation in DMEM with 10% FBS at 37 °C, immunostaining commenced.

The staining was performed under room temperature conditions. The adherent cells were carefully washed with DPBS and subsequently fixed upon their substrates using Roti®-Histofix™ solution for 15 min, followed by rinsing with PBS. After cell fixation, they were permeabilized using 0,1 % v/v Triton-X100 in PBS for 10 min followed by three times rinsing with PBS. To block unspecific binding sites, samples were incubated in 1% bovine serum albumin (BSA) + glycine in PBS for 30 min. After rinsing three times with PBS, cells were ready for triple staining of focal adhesion complexes (vinculin), actin fibers and cell nucleus. The antibody and staining solutions were economically used, resulting in a meticulous staining procedure. The lid of a well plate was covered in parafilm and using a pipette, a 50 μl droplet of staining/antibody solutions was placed on top (one drop for each sample). Using 2 pairs of tweezers, the samples were transferred from the well and placed upside down on the droplet of staining solution. After incubation for 30 mins, they samples were transferred into their wells again and three times for 10 min washed in PBS on low-speed shaker, to rinse unbound staining/antibody residues. This process was repeated for all staining/antibody dilutions. The dilution of each antibody or staining solution was done directly before their application. Directly before their application, the dilutions were centrifuged at 4°C and 13.000 rpm for 5 min. The order of staining is very important. So firstly, primary mouse monoclonal antibodies against vinculin diluted 1:25 in 1% BSA solution were used. Following, the secondary anti-mouse Cy2-conjugated antibody diluted 1:1500 in 1% rabbit serum (to block unspecific staining) as fluorescent marker targeting the primary antibody was applied. In the last two cycles, Santa Cruz Phalloidin (F-actin staining, diluted 1:1000) and TWO-PRO3 (nuclei staining, diluted 1:200) were applied. After the last cycle, the stained samples were dipped in MilliQ water and immediately mounted upon objective slides using Roti-Mount Fluor care or Aquatex™ and stored for at least 24 h to dry. The samples were investigated using a confocal laser scanning microscope (LSM 710, Carl Zeiss Microimaging GmbH, Jena, Germany) using a 40x immersion oil objective. The acquired images were process using open-source FIJI software[185].

4. Results & Discussion

4.1. Synthesis of cellulose sulphate derivatives

The following section presents a short but comprehensive overview on the preparation of PNIPAm-grafted-cellulose sulphates (PCS)[103]. Cellulose sulphates of different sulfation degrees and their modification with PNIPAm and the necessary characterization of these newly synthesized polymers are presented. These results enable the comprehensive discussion of the multilayer and biological characterization that stands in the center of this study.

For the grafting of PNIPAm-CS (PCS) a multi-step synthesis method was designed (Figure 8). Beginning from a commercially available cellulose, in the first step CSs were synthesized and thereafter, PNIPAm chains were introduced onto the CS backbone, leading to PCS. Concurring to the protocol established by Zhang et al.[186], CS 1 with a low degree of sulfation (DSs= 0.67) and CS 2 with a high degree of sulfation (DSs= 1.17) were obtained via quasi-homogeneous nucleophilic substitution. Further reactions, necessary for the PNIPAm-modification, are causing the desulfation of CS[187], hence two strategies were designed to adjust the DSs in the final products.
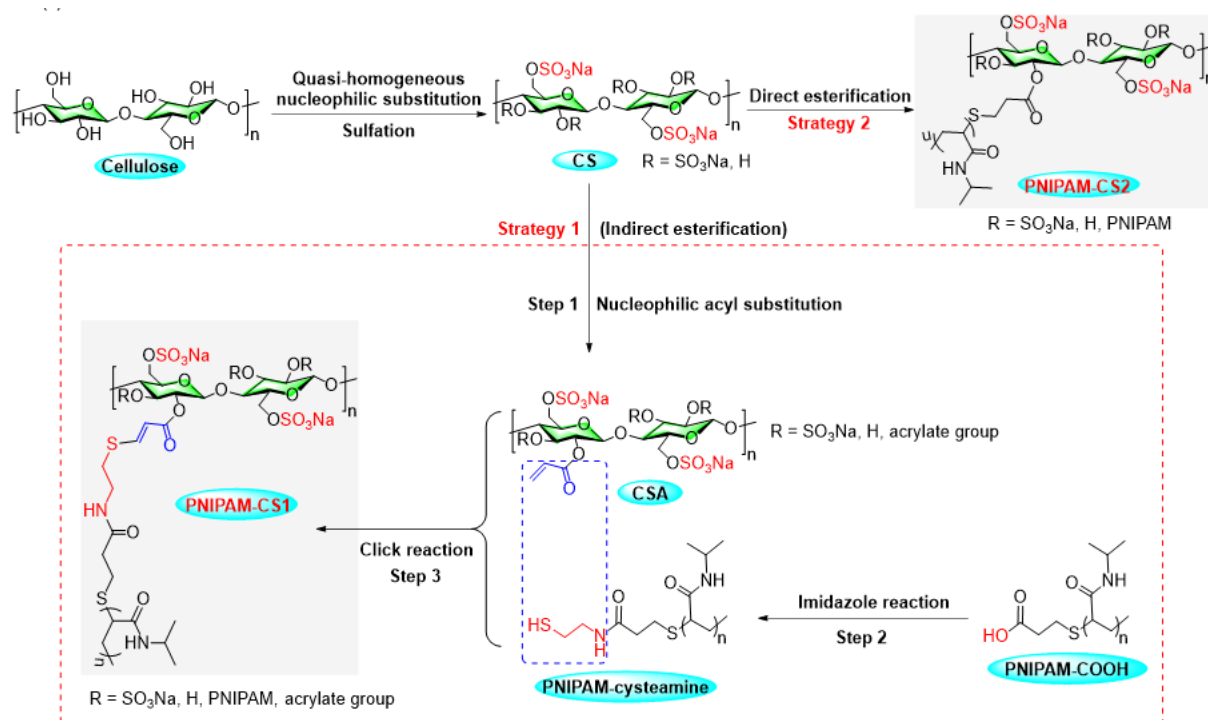
Figure 8: Schematic illustration for the general synthesis of PCSs. Two synthesis routes: (1) Strategy 1 for indirect esterification including step 1-3; (2) Strategy 2 as the direct esterification.

For strategy 1, cellulose sulphate acrylate (CSA) was synthesized from CS 1 with acryloyl chloride via nucleophilic acyl substitution reaction[188]. Subsequently, PNIPAm-cysteamine was synthesized using cysteamine hydrochloride with commercial terminal carboxyl PNIPAm

(PNIPAm-COOH) via the imidazole reaction (Figure 8, Strategy 1, step 2)[189,190]. Finally, PCS 1 was first time synthesized via click reaction of PNIPAm-cysteamine with CSA under UV light and catalyst 4-dimethylaminopyridine (DMAP) (Figure 8, Strategy 1, step 3). As the second strategy, the direct esterification of CS 2 with the PNIPAm-COOH via EDC/NHS-catalyzed reaction (Figure 8, Strategy 2) was used, resulting in the synthesis of PCS 2.

After the application of these two synthesizing strategies, the final product needed thorough examination using Fourier-transform infrared (FT-IR) and carbon-13 nuclear magnetic resonance (^{13}C-NMR) spectroscopy to confirm the successful synthesis. The spectroscopy methods show the presence of specific chemical compounds or functional groups. For the examined synthesis products, both methods showed the presence of important moieties that distinctively indicate the successful synthesize of PCS 1 and PCS 2 using the two different strategies. Sulfation of cellulose and subsequent modification with PNIPAm of the cellulose sulphates was thereby confirmed.

The ^{13}C-NMR and elemental analysis were additionally used to determine the degree of sulfation (DS_S) and degree of substitution of PNIPAm (DS_{PNIPAm}) of the PCS products. The signal integral of the "substituted" (C6s) and the "non-substituted" carbon (C6) at the sixth position were compared to determine the DS_S of PCS 1 and revealed a DS_S of 0.41. For PCS 2, the higher DS_S of 0.93 was calculated via the same route, but beside the comparison of the C6 signal integrals, the "substituted" (C1s) and "non-substituted" (C1) carbon at the first position were compared. Using elemental analysis, it was revealed that the DS_{PNIPAm} of PCS 1 was 0.14 and for PCS 2 DS_{PNIPAm} = 0.11, and therefore only slightly different. The results for all samples are summarized in Table 4.

Table 4: DS values of PNIPAm-CS1 and PNIPAm-CS2

	Starting CS	Intermediate	DS_S	DS_{PNIPAm}
PNIPAm-CS1 (PCS 1)	CS 1	CSA	0.41	0.14
PNIPAm-CS2 (PCS 2)	CS 2	---	0.93	0.11

Following the successful synthesis of the PNIPAm-modified cellulose sulphates, there thermoresponsive potential was examined using dynamic light scattering analysis.

PCSs did not show distinct thermoresponsive behavior between 25 °C and 32 °C (Figure 9a-left side). The cloudy phenomenon indicating thermoresponsive behavior first appeared when the PCS solution was heated above 33 °C. Cooling below 33 °C and fading of the turbidity showed the reversibility of the cloudy phenomenon. The visible cloud point well matched with the DLS analysis (Figure 9, right side), as DLS curves exhibited multiple peaks below but only one peak above 33 °C. Additionally, the Z-average diameters increased with

(c)	pH	Z-average d (nm) / PDI	Temp. (°C)
PNIPAM-CS1	7	226.5 ± 0.1 / 0.23 ± 0.01	32 (LCST)
		469.4 ± 0.1 / 0.16 ± 0.01	37
	4	193.1 ± 0.1 / 0.20 ± 0.01	32 (LCST)
		478.3 ± 0.1 / 0.18 ± 0.01	37
PNIPAM-CS1 in 0.15 M NaCl	7	271.1 ± 0.1 / 0.24 ± 0.01	30 (LCST)
		2170.3 ± 0.1 / 0.16 ± 0.01	37
	4	398.3 ± 0.1 / 0.23 ± 0.01	30 (LCST)
		1988.7 ± 0.1 / 0.17 ± 0.01	37
PNIPAM-CS2	7	190.0 ± 0.1 / 0.23 ± 0.01	33 (LCST)
		264.3 ± 0.1 / 0.12 ± 0.01	37
	4	517.7 ± 0.1 / 0.23 ± 0.01	34 (LCST)
		793.4 ± 0.1 / 0.11 ± 0.01	37
PNIPAM-CS2 in 0.15 M NaCl	7	384.3 ± 0.1 / 0.37 ± 0.01	32 (LCST)
		785.1 ± 0.1 / 0.11 ± 0.01	37
	4	503.4 ± 0.1 / 0.16 ± 0.01	32 (LCST)
		1140.0 ± 0.1 / 0.16 ± 0.01	37

Figure 9 a) DLS curves for the measurement of the LCST and cloud point of PNIPAm-CS by analyzing the Z-average diameters. Aqueous solutions of PNIPAm-CS with the concentrations of 1.2 mg / mL at pH 7 were used. b) Schematic illustration for the thermoresponsive behaviors of PNIPAm-CS in solution. c) The Z-average diameters and PDI were tested at LCST and 37 °C.

increasing temperature from 32 °C to 37 °C (Figure 9 c), and decreased during cooling down. The multiple factors in summary indicated a reversible LCST behavior between 30 and 33 °C.

Below the LCST, PCS chain swelling occurred in aqueous phase due to intermolecular hydrogen bonding between hydrophobic chains (isopropyl groups) of PNIPAm and water molecules. Additionally, there are polar interactions between sulphate groups of the CS backbone and water molecules (Figure 9 b). These interactions lead to a complete dissolution of PCS in aqueous solution and resulted in a clear PCS solution and the multiple peaks visible in DLS analysis. When the solution temperature was elevated above the LCST, the hydrogen bonding between polymer chains and water is energetically preferred, leading to exposure of hydrophobic PNIPAm chains. These chains gradually associated with one another, which resulted in a heat-induced aggregation of molecules. Consequently, PCS aggregates precipitated from the aqueous solvent and the solution became cloudy. The DLS analysis only represented one single peak, corresponding to the PCS aggregates.

Moreover, the thermoresponsive properties of PCS 1 and PCS 2 were examined depending on environmental factors, e.g., the presence of ions and different pH values. Hence, PCSs were diluted in water and 150 mM NaCl solution (LbL multilayer formation condition). The solution pH was adjusted to pH 4 (LbL multilayer formation condition) and pH 7 (physiological conditions). The Z-averages, corresponding to molecular size were measured at the LCST and at 37 °C, which gave insight into the swelling behavior and the size of the PCS aggregates depending on the environmental conditions. This enabled the comparison of the two different PCS derivatives, PCS 1, and PCS 2, as they differ in DS_S and DS_{PNIPAm}.

The summary of the results, presented in Figure 9 c revealed that the pH value of the PCS solution has only minor influence on the aggregation and Z-averages of the molecules. Only for PCS 2, the Z-averages measured at the LCST are at pH 4 higher (> 500 nm) than at pH 7 (< 390 nm). Generally speaking, PCS 1 aggregates to bigger Z-averages than PCS 2. While PCS 1 dissolved in water doubles in size from LCST to 37 °C, while the Z-averages for PCS 2 only slightly increases at pH 4 and growth about 50% at pH 7.

The salt content of the solvent has a visible impact on the PCS aggregation. The Z-averages are significantly different from those measured when PCS was dissolved in water. For PCS 2, the initial Z-average at pH 7 at the LCST doubles compared to the one measured in water and the Z-average increment towards 37°C was noticeably higher when dissolved in NaCl. At pH 7, aggregation results in the doubling of Z-averages, at pH 4 it increased to even slightly more than double the size. This latter effect was more distinct for PCS 1. While the initial size at LCST was not different for PCS 1 dissolved in NaCl compared to water, the size increment towards 37 °C was astonishingly high. PCS 1 dissolved in NaCl at pH 4 increased

52

to the sevenfold size, while at pH 7 by fivefold. For both, PCS 1, and PCS 2, when dissolved in NaCl solution, additionally to the changes in aggregation, the LCST decreased by circa 2 °C.

PCS 1 generally showed higher Z-average increments than PCS 2 when heated from LCST towards body temperature (37 °C). The reason could be the lower DS_{PNIPAm} of PCS2, which causes the weaker chain association and heat-induced aggregation. Moreover, in the presence of NaCl, the LCST of PCSs decreased and larger Z-average diameters of PCSs formed, especially for PCS 1 at 37 °C. Kosmotropic anions, such as Cl^- ions, are more hydrophilic. These ions compete with PCS for water molecules and cause polymer dehydration, which promotes the decrease in the LCST[191,192]. Additionally, larger Z-average diameters of PCS formed at pH 4. The reason can be the hydrophobic chains of PCS that are more inclined to associate at pH 4 to avoid hydrophilic solvent and the concentration of Cl^- ions is increasing when adjusting pH from 7 to 4, resulting in larger Z-average diameters than that at pH 7[193].

The size differences between PCS 1 and PCS 2 and higher Z-averages of PCS 1 aggregates might also be explained by the lower DS_S of PCS 1. The sulfation process often causes chain scission, which results in lower MW of cellulose sulphates with higher DS_S[194]. Shorter chains subsequently result in smaller Z-average diameters of aggregated molecule chains.

In summary, CS with a lower and higher sulfation degree could be synthesized successfully. Furthermore, modification with PNIPAm was achieved, even though only with low degree of substitution. But the newly developed PNIPAm-g-cellulose sulphate polyelectrolyte not only showed thermoresponsive properties with an LCST in the range of 30-32 °C, but furthermore are polyanions that can be used for PEM fabrication using LbL technique.

4.2. Fabrication and characterization of multilayers made of chitosan and cellulose derivatives

4.2.1. Application of PNIPAm-CS for formation of multilayers

4.2.1.1. Measurement of zeta potential of polysaccharides

The potential application of PNIPAm-CS as polyanion for multilayer formation requires their ability to form complexes with polycations. Since, the grafting of PNIPAm to CS introduces bulky polymer side chains along the CS backbone, the ability to form multilayers might be hampered. Therefore, the effect on the formation of PEM was studied, with regard to degree of substitution of PNIPAm and the sulfation degree, using CHI as polycations in previous studies[102,195].
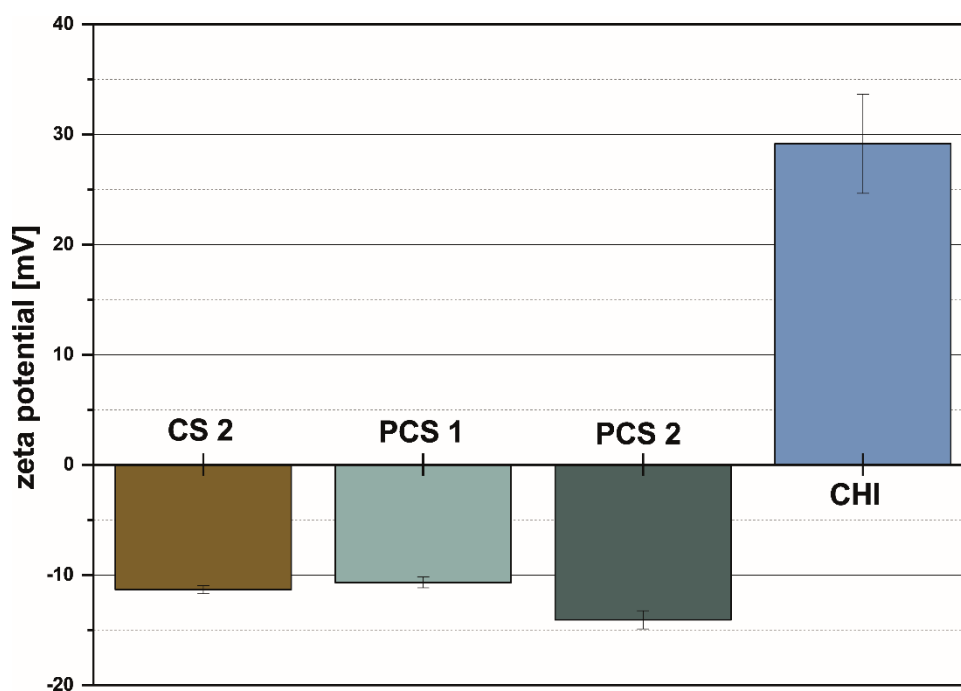
Figure 10: Bar graph shows zeta potential of polyelectrolytes solutions measured at pH 4. The bars represent the mean value and corresponding standard deviation (error bars) [n=6].

Since the fabrication of multilayers via layer-by-layer technique is partially driven by electrostatic interactions and ion pairing of the polyelectrolytes[82], CS derivatives and CHI were characterized using zeta potential measurement. The results shown in Figure 10, demonstrate that CHI is positively charged at pH 4 in the region of 29 mV. CHI has a pK_a value of 6.3 which means that the amino groups are protonated[196] as NH_3^+. CS derivatives possessed all negative zeta potentials in the range of -10 to -15 mV as expected due to the presence of negatively charged sulphate groups. This in mind, negative charge was expected to be related to the degree of sulfation (DS_S). However, PCS 1 having the lowest DS_S (DS_S = 0.4) showed a similar potential as CS 2 and PCS 2, which possessed a higher degree of sulfation (DS_S = 1.0 and DS_S = 0.9, respectively). It is possible that the different molecular weights lead to different mobility of the molecules that affects the calculated zeta potentials. PCS1 has a lower degree of sulfation of 0.41, which is related to a higher molecular weight because the more harsh the sulfation process the more chain scissions are observed[194]. Additionally, the grafting of bulky PNIPAm as a side chain on PCS samples increases the molecular weight and will lead to differences in measured charge when compared to the CS samples, since it might influence electrophoretic mobility. It has been shown that the molecular weight alone is not influencing the electrophoretic mobility of polyelectrolytes. However, the phenomenon is more complex, as the charge density and with that the interaction with counterions (present in salt solutions) influence the mobility as well[197]. Furthermore, with increasing sulfation the amount of charge moieties in the polyelectrolyte is increasing, leading to increased intrachain

54

repulsion and an increase in hydrodynamic radii due to elongation, which seems applicable for CS 2. The bigger radii lead to decreased mobility which results in increased zeta potential. PCS 2 is a rather small molecule (due to intensive chemical processing) but still possesses a high charge density. Hence, the combination of high charge density and small hydrodynamic radius leads to the lowest measured potential. This could explain why CS 2 was measured with a less negative potential compared to PCS 2. Even though the results for CS derivatives are not necessarily in agreement with the expectation regarding degree of sulfation and hence the amount of charged moieties, the charge difference between CHI and CS derivatives suggests that a multilayer build-up driven by electrostatic attraction and ion pairing is possible.

4.2.1.2. *Characterization of multilayer growth and thickness*

Following the zeta potential measurements that theoretically showed the possible interaction between the polyelectrolytes, Surface Plasmon Resonance (SPR) and Quartz crystal microbalance (QCM) measurements were used to study whether grafting of PNIPAm as bulky polymer with a MW of 2000 Da to CS is affecting the ability of the polyanions to form polyelectrolyte multilayers with chitosan. Additionally, it enables insight into the layer formation and PEM growth.
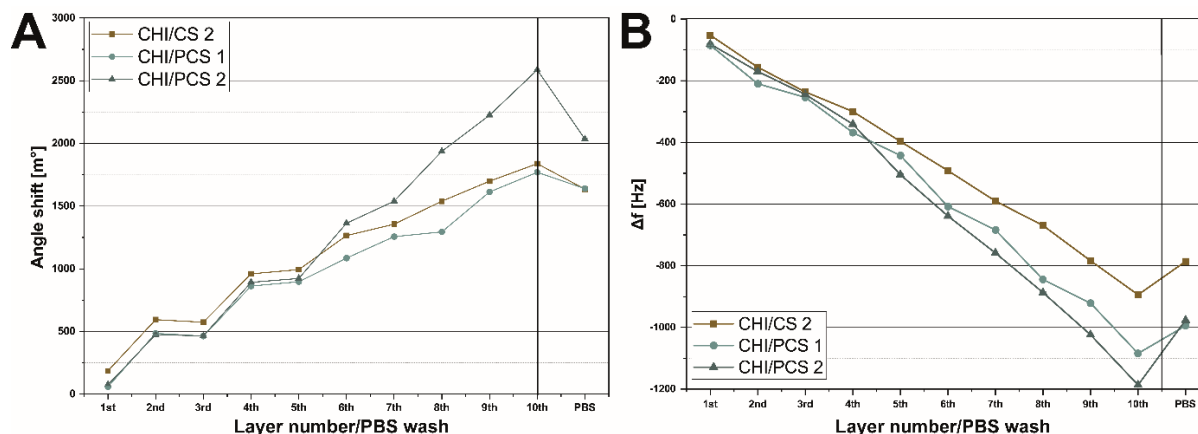
Figure 11: Surface plasmon resonance (A) and Quartz crystal microbalance (B) measurements, showing the angle shift and frequency change, respectively. Positive angle shift in SPR is proportional to mass adsorption onto sensor surface. Negative frequency change in QCM is proportional to material adsorbing to gold coated quartz crystal. Odd numbers represent polyanion adsorption, with 2nd and 4th layer being CS 2 and depending on sample name with 6th, 8th and 10th layer being CS 2, PCS 1, or PCS 2. Even numbers correspond to polycation adsorption, with 1st anchoring layer of PEI and subsequently 3rd – 9th layer of CHI (see *Materials & Methods* for conclusive layer formation information). Measurements were performed in triplicates and data points represent mean values (SD was calculated and is shown, but not visible due to symbols at data points).

Therefore, CS 2, PCS 1 and PCS 2 were used for the *in situ* formation of PEM on the sensor surface to investigate the dry mass adsorption during multilayer deposition using SPR[198]. The multilayer formation was done at room temperature when PCS 1 and PCS 2 were

still well solubilized. The aggregation of PCS above LCST eliminates the possibility of multilayer formation as we observed during preliminary studies.

Figure 11 A shows SPR angle shifts of CS 2 and PCS 1 and 2 as polyanions and CHI as polycation during multilayer formation. For all combinations, an increasing angle shift was observed, which suggests multilayer formation. CHI/CS 2 and CHI/PCS 1 show similar results ending at around 1750 to 1800° angle shift. CHI/PCS 2 shows much higher angle shift after 10 layers, around 2600°, indicating adsorption of more material. PCS 2 (DS_S 0.9; DS_{PNIPAm} 0.1) with apparent higher charge density and smaller size made a more significant contribution to the layer growth than PCS 1 (DS_S 0.4; DS_{PNIPAm} 0.1) with lower charge density. The zeta potential measurements associated with the charge density support these measurements. It would explain the similar growth behavior of multilayers prepared with either PCS 1 or CS 2, as they were measured at comparable zeta potentials. However, the size of the molecules should influence the layer formation. PCS 1 was less sulphated and should therefore be bigger than CS 2 with a higher DS_S, since sulfation leads to chain scission, as explained before[194]. But the difference in size could be compensated by the adsorption of more CS 2 due to the higher charge density. PCS 2 showed the highest angle shifts, which makes sense when looking at the highest zeta potential and therefore possibly charge density compared to the other CS derivatives.

QCM-D measurements were performed to quantify the total amount of material adsorbed, including the solvent water (Figure 11 B). At a constant pH of 4.0 and with 0.15 M NaCl buffer solution, the multilayer formation showed a linear growth behavior like the findings of SPR studies. Interestingly, PCS 1 (DS_S 0.4; DS_{PNIPAm} 0.1) and PCS2 (DS_S 0.9; DS_{PNIPAm} 0.1) show similar results regarding frequency shifts (Δf for PCS 1 after 10th layer around 1100 Hz^{-1}, for PCS 2 around 1200 Hz^{-1}), despite their differences in charge density related to the degree of sulfation (DS_S). On the other hand, CS 2 (DS_S 1.0), chemically comparably to PCS 2, showed noticeably lower frequency changes with only around 900 Hz^{-1}. Compared to SPR, QCM provides comparable results, with PCS 1 being the exception since frequency shifts suggest higher mass adsorption than in SPR. However, as stated before, QCM measurements include the amount of couple water in the films and results can differ from SPR. One reason for that might be the presence of PNIPAm. Since PNIPAm at room temperature is rather elongated and more hydrophilic[125], PCS samples are probably more hydrated during the QCM studies done at RT, explaining the differences to CS 2. Additionally, charge density based on the DS_S might have a supporting effect. The lower charge density of PCS 1 may be related to a less extended conformation of the polysaccharide. This occupies more space and possibly entraps more water inside the chains. PCS 2, with a higher DS_S,

56

should be more elongated due to stronger intramolecular electrostatic repulsion. Hence less water might be included in these layers. The high charge density of PCS 2 still causes high frequency change, similar to high angle shift in SPR, and therefore high material adsorption.

Beside the charge density, molecular size influences the layer growth. As explained before, PCS 1, based on the DS_S, should have the largest molecular size. Regarding the measured size using DLS (see Figure 9c), PCS 1 and PCS 2 have a similar size measured Z-average molecular size. This might explain, why QCM measurement did not reveal large differences between the PEM containing PCS 1 or PCS 2. Moreover, it must be noted that the examined multilayers had the same composition until the 5th layer, as explained in section 3.4. However, the examined systems showed differences in Δf even before the fifth layer. This limits the possible interpretations of QCM results for the comparison between the different multilayer compositions. This might be linked to problems regarding reproducibility. It is quite difficult with the device to make sure that the process works without any interruption, especially air bubbles that are built in the tubing and subsequently in the measurement chamber. Several factors made the process of QCM somewhat unreliable.

During the washing step with PBS, all PEM systems showed an angle shift reduction during SPR and positive frequency changes during QCM studies, which is normally related to material desorption, but also to structural changes in the multilayer[199,200]. This can most likely be attributed to the change in pH, from pH 4.0 to 7.4 of the PBS solution. The effect of changes in pH was mostly examined during multilayer build-up. However, Halthur et al. discussed in their study the influence of alternating pH values on PEM films after they have been built[201]. They observed a deswelling behavior when the pH was increased towards pH 7.4 of 10-20 %. They correlated that to the decreasing charge density of one of the polyelectrolytes, affecting the secondary structure of the polyelectrolyte, the intramolecular repulsion, the intermolecular connections, and the concentrations of counterions within the PEM film. This effect has been observed for chitosan before[202]. For the here examined PEM films, CHI with a pK$_a$ value of 6.3 will deprotonate with increasing pH and hence charge density decreases. Which would mean, that the observation made in SPR and QCM measurements were less related to loss of material and subsequently multilayer stability problems but might rather be explained by the deswelling of the PEM films. Additionally, the Z-average diameters of PCS 1 and PCS 2 were measured at pH 4 and pH 7. Results showed the Z-average decreased with increasing pH value, which might add to the deswelling effect of the multilayers.

The multilayer growth can be characterized as linear. SPR and QCM showed that with increasing layer number, the angle shift and Δf are not exponentially changing. For PEM films

exhibiting linear growth mechanism, the diffusion of polyelectrolytes within the film is limited. Each polyelectrolyte is only penetrating its adjacent layer and the films have a more stratified structure. The last oppositely charged polyelectrolyte forms the outer layer of the film. It should be addressed that SPR measurements revealed a stair-case pattern for the multilayer growth for the CHI/CS basal layers (2nd - 5th layer). Previous studies have shown that this could be due to charge compensation with chitosan and the formation of a quasi-soluble complex with CS, causing it to be stripped off the surface[99]. This may explain why there was almost no increase in the mass adsorption when CHI was deposited and could result in thinner film formation as demonstrated before[203]. However, this could not be observed in the QCM measurements.

Overall, SPR and QCM measurements demonstrate that the formation of multilayers is possible when using PCS as polyanion and CHI as polycation, which means that the low DS$_{PNIPAm}$ is not disturbing the process of ion pairing. However, the reduction of angle shift reduction in SPR and increasing frequency change in QCM after washing the multilayers with PBS pH 7.4 might indicate a limited stability at physiological conditions. However, it might not be solely stability issues, as it has been shown before, that increasing pH value towards 7.4 causes deswelling of PEM films.
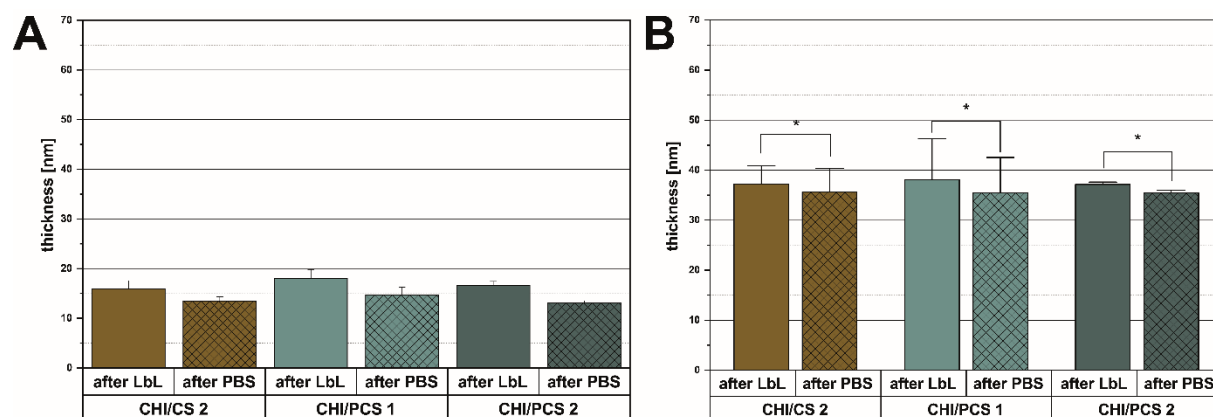
Figure 12: Bar graphs show thickness of PEM films measured by ellipsometry on Si wafers in dry conditions (A) or calculated from frequency shift in QCM-D using the Voigt-model (B), respectively. Mean values are represented with error bars showing standard deviation for n = 4 (ellipsometry) and n = 3 (QCM).

Ellipsometry was used to measure the PEMs thickness in dry state after formation of multilayers and subsequent washing with PBS (pH 7.4) (Figure 12 A). We discovered a film thickness range of 12-19nm using the Cauchy model, which is consistent with Sui et al. observation for linearly growing film[203]. The influence of the different CS derivatives on dry multilayer thickness was comparatively low, which means thickness was not significantly different for the different polyanions. Interestingly, the results are somewhat in contrast to the SPR measurements. SPR revealed the highest angle shifts, correlated to material

adsorption, for the multilayer system CHI/PCS 2. The thickness measured with ellipsometry does not reflect that. The differences could be due to the underlying principle that uses the refractive index (RI) for the calculation of angle shift and thickness, respectively. While SPR measurement was performed *in situ*, under the presence of NaCl solution and unfortunately gives no insight into the RI of the deposited multilayer, ellipsometry was performed after the multilayer system was dried in air in a desiccator, changing the hydration state. Hence, the RI of the PEM film during ellipsometry will probably be different from the one during SPR measurement[201]. Since we cannot compare the approximated RI from ellipsometry to the one in SPR, differences can occur. This might explain, why the in the SPR measurement observed differences between the PEM films are not visible in dry thickness calculated from ellipsometry measurements.

Moreover, the wet thickness based on the Voigt-model was calculated using the frequency and dissipation changes of QCM-D measurements[204] (Figure 12 A). In general, films are about 35 to 40 nm thick which is more than double compared to dry thickness measured with ellipsometry and is obviously contributed to the water content. The same trend as for dry thickness was observed, as CHI/PCS 1 formed thicker layers than CHI/PCS 2 and CHI/CS 2 films. The measured thickness of 35 – 40 nm for the PEM films in wet state is in a reasonable window for biomedical applications, as other groups have shown[195,205]. The ellipsometry measurement of the dried films supported the results from SPR and QCM concerning the effect of changing pH value upon the built films. After washing with PBS buffer at pH 7.4, the thickness of the films was reduced. As explained before, it is probably caused by the change in pH value and the decrease in CHI charge density, leading to deswelling of the PEM films. However, to this point the limited stability of the films cannot be excluded.

4.2.1.3. *Characterization of multilayer wetting properties*

Protein adsorption and cell adhesion are dependent on wettability of substrata [206,207]. Hence static water contact angle measurements were performed. All PEM systems were prepared with the polyanion as final layer, which means the cellulose sulphate should predominantly influence this surface property which was also related to the thought that CS can bind adhesive proteins like vitronectin present in serum or fibronectin secreted from cells[99,208].
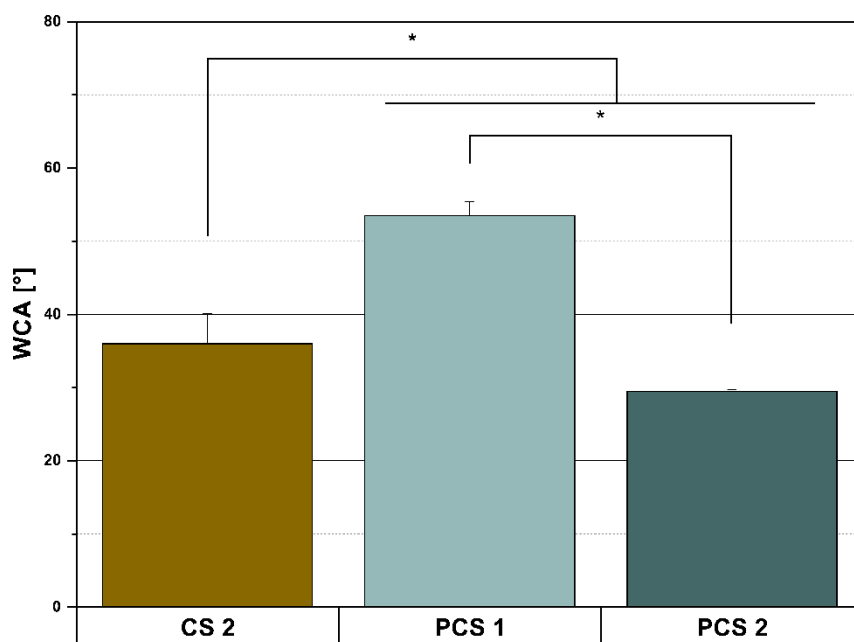
Figure 13: Bar graph shows contact angle of PEM with terminal (10th) layer being the polyanion (CS 2, PCS 1, or PCS 2). For each sample (n=3), three drops of deionized water were placed on the PEM coated surfaces. The PEM coated Si wafer have been washed in PBS before measurement and dipped in water to remove salt residues. Bar graphs represent mean value with SD (*: $p < 0.05$).

The measured water contact angles of PEM terminated by CS derivatives are presented in Figure 13. The CHI/PCS 1 multilayer films, possessing an outer layer of PCS 1 (DS_S 0.4; DS_{PNIPAm} 0.1) showed contact angles of around 57°. Both PEM ending in cellulose sulphate derivatives with higher DS_S 1.0 (CHI/CS 2) and 0.9 (CHI/PCS 2), respectively, showed significantly lower contact angles of around 37° for CS 2 and 35 ° for PCS 2. The two prominent groups for the PEM films in this study are, as mentioned before, OSO_3^- (sulphate) groups for CS and PCS and NH_2^+ (amine) groups for CHI. Sulphate groups are known to be hydrophilic, while amine groups are rather hydrophobic. In previous studies, the contact angles for different functional groups were characterized[209]. Interestingly, surfaces functionalized with amine groups showed contact angles of slightly above 60°. Surfaces modified by SO_3^- moieties, more wettable surfaces with contact angles of about 30° were observed. This would allow to deduce how the functional groups of the polyelectrolytes used in PEM formation influence the contact angle. Hence, PEM ending on CS 2 and PCS 2, the lower contact angle close to 30° lead to the conclusion that the more hydrophilic sulphate groups of the polyanions are indeed present and predominant in the interfacial area. The higher contact angles of PEM films ending with a layer of PCS 1 might be explained by the lower degree of sulfation (DS_S = 0.4). On the other hand, the higher contact angle also suggests an influence of the CHI and its amine groups. Fu et al. (2004) could show for PEM systems of CHI and Heparin (HEP) that the contact angle was influenced not only by the outermost layer[210]. Depending on the pH

during multilayer formation, the underlying layers influence the contact angle. For pH = 3.8 (close to pH 4.0 in this study), they presented contact angles for layers ending in heparin of above 45°. This is comparable to the results of PCS 1 ending PEM films. This is explained by the deposition of a thinner polyanionic layer, enabling more chain segments of the underlying chitosan layer to penetrate this thinner layer. This phenomenon could be happening for PEM films with PCS 1 and present another explanation for the higher contact angles. In summary, the contact angle measurements suggested, that CHI/CS 2 and CHI/PCS 2 with CS derivatives of higher DS_S around 1 are more hydrophilic with the sulphate groups being dominant in the interfacial region of the films. For CHI/PCS 1 multilayer films, the outermost polyanionic layer seems to be penetrated by some segments of CHI, making them less hydrophilic.

4.2.2. Conclusion

The in the first chapter of this section described CS derivatives, in particular CS 2 (DS_S = 1.04), PCS 1 (DS_S = 0.41, DS_{PNIPAm} = 0.14) and PCS 2 (DS_S = 0.93, DS_{PNIPAm} = 0.11) have been used as polyelectrolytes for the fabrication of multilayer films using LbL technique. Several experiments to determine multilayer formation kinetics and the physicochemical characterization of multilayers have been performed. These experiments showed the successful PEM fabrication via LbL with the use of CHI as polycation. PEM with 5 bilayers were successfully fabricated and showed a linear growth behavior resulting in PEM films of common thickness for application as coating in tissue engineering. The combination of CS derivatives with CHI interestingly revealed one issue: stability at physiological pH. Washing in pH 7.4 PBS resulted in thickness reduction of the multilayer systems, either due to deswelling or material desorption. This issue should be addressed in further experiments and is most likely attributed to CHI and its deprotonation at physiological pH. Any crosslinking of the multilayers to increase stability would not have been feasible due to the missing carboxylic groups of the cellulose sulphates. At this point, no cell experiments were performed due to the stability issues of the PEM. For cell experiments, the multilayers are exposed to pH 7.4 cell culture medium, which might lead to desorption of final PCS layers. As these are most relevant for experiments with regard to biocompatibility and especially thermoresponsive detachment, cell experiments were not deemed sensible at this point. Subsequent studies consider the stability issue and examine biocompatibility.

4.3. Fabrication of multilayer with poly-L-lysin and quaternized chitosan as polycations.

4.3.1. Synthesis of quaternized chitosan

To address stability issues of the multilayers with CHI as polycation, two other biopolymers, namely poly-L-lysin (PLL) and quaternized chitosan (QCHI) were used as polycations[107,211–213]. While PLL was commercially available, but expensive, QCHI was synthesized following established synthesis routes (see chapter 3 section 3.2) and presents a further development from chitosan. Compared to CHI, QCHI possesses a higher charge density and both, PLL and QCHI, show positive zeta potentials at physiological pH values.
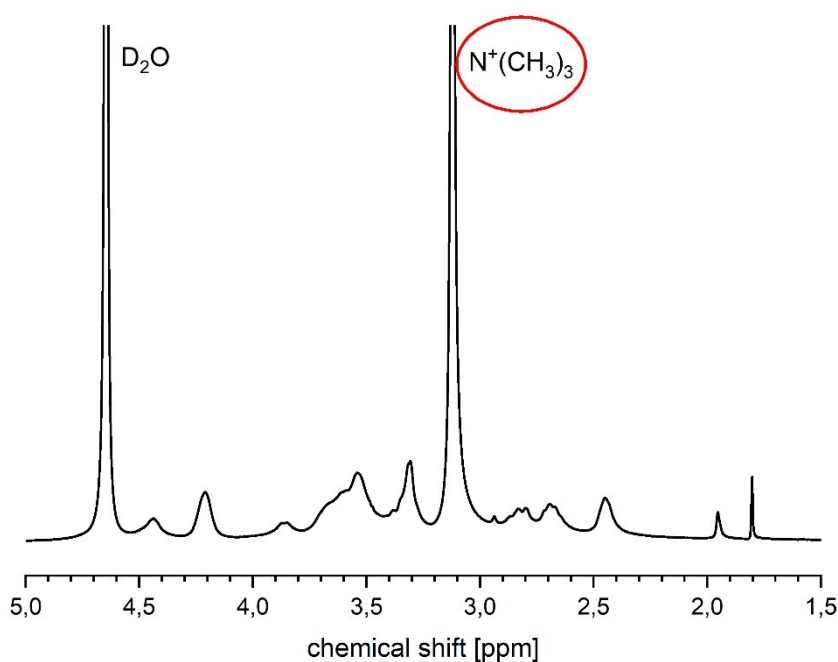
Figure 14: 1H-NMR spectrum of quaternized chitosan. Indicated by the red circle is the increased signal of the quaternized ammonium group.

Quaternized chitosan was synthesized as described above. The lyophilized final product was characterized using 1H-NMR to assess the successful quaternization. Additionally, the degree of quaternization (DQ) was measured by chloride titration using silver nitrate and potassium chromate as color indicator. The 1H-NMR spectrograms showed a high peak corresponding to quaternized ammonium group located at the C3 position of chitosan (see Figure 14). This indicated a successful synthesis of QCHI. To determine the degree of quaternization, relevant to gain information on the amount of quaternized ammonium groups present, the aforementioned titration using silver nitrate was used. Following Wu et al. (2007), the DQ was calculated at 80.6 ± 1.9[214] for the applied synthetization route. Slightly over 80% of all ammino groups of the chitosan were substituted by quaternized ammonium groups. As this resulted in the water-solubility of QCHI and could be reproduced for several synthesis, this material

was deemed appropriate for the formation of polyelectrolyte multilayers and used for further physicochemical characterization.

4.3.2. Physicochemical characterization of polyelectrolytes and polyelectrolyte multilayers

4.3.2.1. Zeta potential measurement of polyelectrolyte solutions

Before examining the multilayer formation, measurements of zeta potential were done with the polyelectrolytes. Charge density related to zeta potentials is an important factor for PEM growth related to the interaction between polyanions and -cations[82]. Here, the measurements were performed for CS derivatives and polycations PLL and QCHI at two different pH values. Multilayer formation was carried out at pH 4, being one of the pH regimes examined. The other pH value of interest was pH 7.4, being the physiological pH during biological studies using cells.
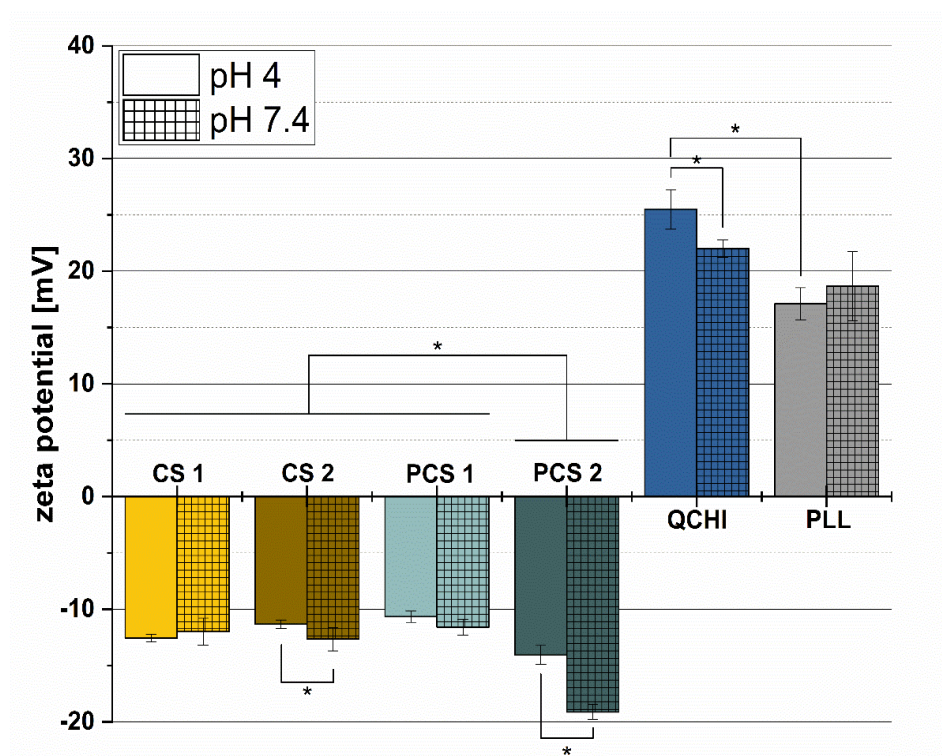
Figure 15: Bar graph shows zeta potential of PEL in solution at pH 4 and physiological pH 7.4. It shows negative potential for cellulose derivatives, only PCS 2 showing higher charge density than other CS derivatives, especially at physiological conditions (pH 7.4). PLL shows lower, but more pH independent positive charge than QCHI.

The zeta potential measurements revealed (see Figure 15), that as expected, all CS derivatives showed negative zeta potential values in the range of -11 to 19 mV, with slightly lower values at pH 7.4 than at pH 4. QCHI had the highest zeta potential of more than 25 mV

at pH 4 that was slightly reduced to 22 mV at pH 7.4. For PLL, the zeta potential at pH 4 was measured with 17 mV, increasing at pH 7.4 to 18.5 mV. The measurement revealed, as theoretically expected, the opposing charges of CS derivatives and PLL/QCHI, hence the chosen PEL should be able to form multilayers at pH 4 driven by electrostatic interactions. Except for PCS 2 and QCHI, the zeta potential changed only slightly from pH 4 to pH 7.4.

For the fabrication of PEM films via LbL technique, oppositely charged polyelectrolytes are predominantly used. For the estimation of the charge density of the polyelectrolytes, the zeta potential of polyelectrolyte solutions was determined at pH 4 (pH value during layer formation) and pH 7.4 (physiological pH for biological applications). The polycations, namely QCHI and PLL, show high positive charge at both pH values. Alone the ability to measure QCHI in aqueous solution at pH 7.4 furthermore proved the successful quaternization of CHI because Chitosan has a pKa-value of 6.3 and would therefore be insoluble above pH 7[196]. However, quaternized ammonium groups were still protonated with increasing pH, explaining the slightly reduced zeta potential of QCHI at pH 7.4 as the remaining amine groups on the QCHI backbone became uncharged[215]. PLL also contains amine groups, so with increasing pH (7.4), the amine groups are deprotonated. However, zeta potential increased for pH 7.4. The increase is not significant and might be related to effects regarding hydrodynamic radius. It has been shown that hydrodynamic radius of PLL decreases with increasing pH[216]. Hence, as the measurement is influenced by electrophoretic mobility, smaller molecules move faster leading to the slight increase in measured zeta potential of PLL. Concerning the CS derivatives, the net charge is theoretically related to the DS_S, due to the presence of more charged sulphate moieties. CS 1 (DS_S=0.6) and PCS 1 (DS_S=0.4) with lower sulfation degrees would be expected to have lower zeta potentials as CS 2 (DS_S=1.0) and PCS 2 (DS_S=0.9) having higher sulfation degrees. With regard to the theoretical background, it is surprising that CS 2 was measured with the same potential as CS 1 and PCS 1, since the sulfation degree suggest higher amount of negatively charged moieties. PCS 2 shows higher zetapotential, corresponding to higher degree of sulfation. As sulphates are the residues of the strong sulfuric acid, their protonation occurs only at very low pH values. Hence, with increasing pH, the zeta potential is only slightly changing. Therefore, it was somewhat surprising that PCS 2 was observed with distinctly lower zeta potential at pH 7.4. On one hand, the zeta potential is probably related to the sulfation pattern and not predominantly depends on sulfation degree[217,218]. On the other hand, the zeta potential measurements relied on electrophoretic mobility, which is influenced by a multitude of factors, including molecule size and presence of counter ions, which could lead to differences unrelated to the presence of charged moieties. As explained earlier for the measurements of CS derivatives and CHI, the electrophoretic

mobility, which is dependent of the hydrodynamic radii of the molecules, influences the measured potential. A less mobile molecule is measured with a lower (more positive) potential. Elongated molecules due to, e.g., steric repulsion of charged groups, have a higher hydrodynamic radius, and are therefore measured with a lower potential. This might explain that CS 2, elongated due to steric repulsion of the charged groups, is measured with a potential similar CS 1 and PCS 1 with a lower degree of sulfation. PCS 2 is thought to be generally smaller due to the intensive chemical processing during synthesis. The incorporation of PNIPAm side chains might influence the measured potential, as it possesses secondary amines. At pH 4, these are protonated and result in a higher (more positive) potential for PCS, countering the negative sulphate groups. With increasing pH, some of these secondary amines deprotonate, and the zeta potential decreases, especially observed for PCS 2[219]. Beside the charge stability of all polyelectrolytes at both pH regimes, the zeta potential measurements allowed to deduce that the charge difference at pH 4 should be high enough for the formation of multilayer systems based on electrostatic interactions. Only slight changes of the potential at pH 7.4 would also suggest the stability of the polyelectrolyte combinations under physiological conditions.

.

4.3.2.2.   *Characterization of multilayer formation and thickness*

Following the zeta potential measurements, Surface plasmon resonance (SPR) measurements were performed to assess layer growth and PEM stability after washing with PBS (Figure 16). In conformity with the results of zeta potential measurements, layer growth for all PEL combinations was observed, as an increasing angle shift correlates to the adsorption of material onto the surface. As positive angle shift was detected for all multilayer systems, successful PEM fabrication could be deduced. For PLL and QCHI containing

multilayers, the SPR angle shifts showed similar behavior with increasing layer deposition. For both, angle shift of samples built with CS 1 and PCS 2 showed highest angle shift. For QCHI/PCS 2, the highest angle shifts values of nearly 3500 m° were observed. Oppositely, the multilayers containing CS 2 and PCS 1 show distinctly lower angle shifts below 2000 m°. The angle shifts measured for the application of either PLL or QCHI showed similar courses. Only PCS 1 and CS 2 containing multilayers basically changed places. The washing with PBS after deposition of the 10th layer resulted caused the decrease of the angle shift. Reduction is similar for all different PEM films except, QCHI/PCS2 showed a particularly high angle shift reduction. Overall, PEM growth could be described as approximately linear for the PEL
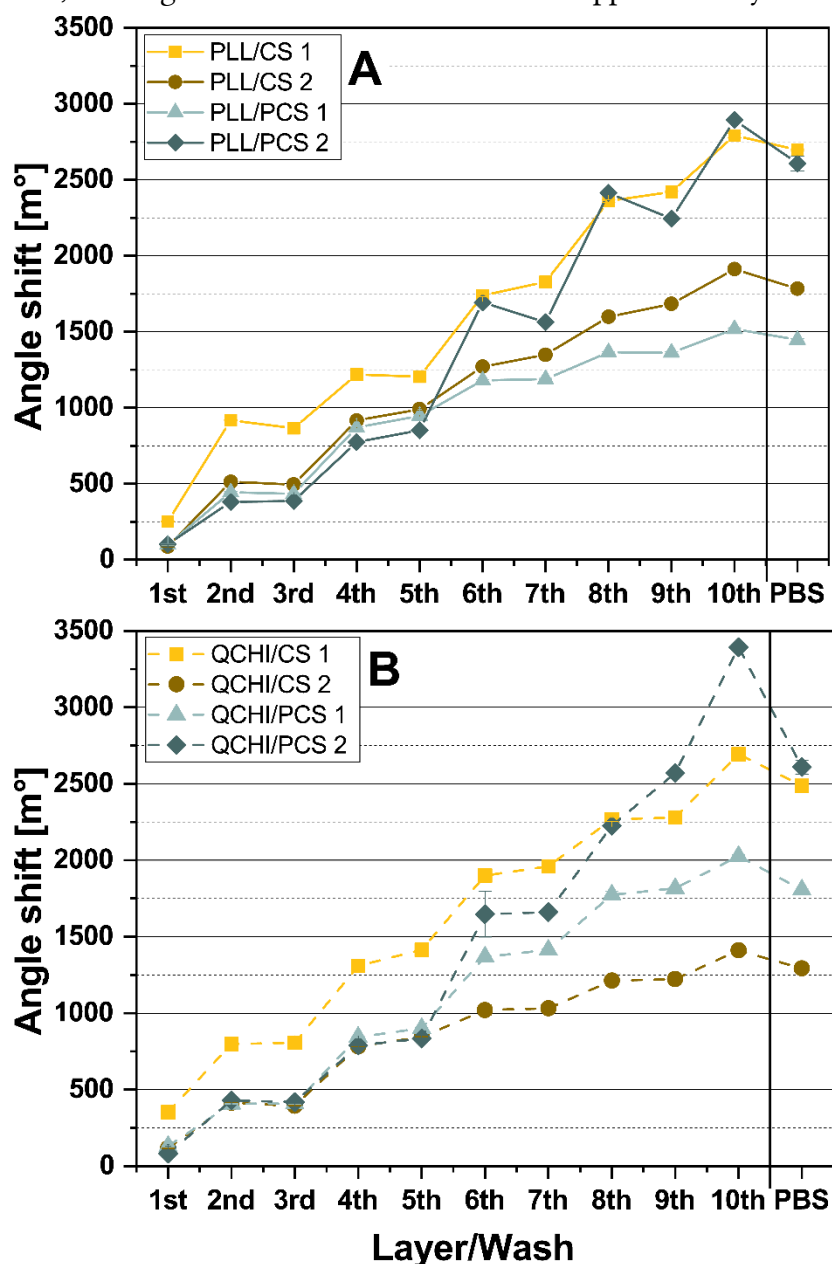
Figure 16: Surface Plasmon Resonance measurements show the angle shift of each layer. Positive angle shift corresponds to dry mass adhering to the substrate surface. Even layers are polyanions (CS 1/2: 2nd to 10th layer: CS 1 or 2; PCS1/2: basal: 2nd, 4th: CS 2; functional 6th, 8th, 10th: PCS 1 or 2) and uneven are polycations (1st: PEI, 3rd – 9th: (A) PLL and (B) QCHI).

combinations tested. Interestingly, as observed for the SPR curves in the previous section, polycations contributed only minor to the PEM growth, represented in Figure 16 as stair-case pattern.

Surface plasmon resonance was used to access the multilayer formation *in situ*. Since not only the charge of polyelectrolyte influence the successful layer formation, SPR aims to give more insight in the multilayer fabrication and composition. All multilayer systems show positive angle shifts in SPR over the course of 10 layers, which corresponds to material being adsorbed onto the gold sensor. All systems successfully form multilayers with a rather linear growth behavior. When changing the rinsing buffer, after the 10th layer, to PBS with pH 7.4, all systems show a negative angle shift, which could be related to desorbing material form the surface, or as explained in the previous section, caused by a deswelling of the multilayer. But, nevertheless, the pH change or the salt change influence the multilayer stability. PBS has the same salt concentration as the NaCl buffer used for washing (150 mM), which indicates that salt concentration would not be the influencing factor. However, a change in pH is connected to de-/protonation of polycation and polyanion, respectively. Electrostatic interaction between polyelectrolytes is weakened, which might cause the desorption of some material from the surface. The explanation given in the previous section that reduction of charge density leads to restructuring and deswelling of the multilayer might only be applicable to certain limits, as zeta potential measurement revealed that the charge only slightly or, as for PLL, did not change with pH alteration. Nevertheless, instability of multilayers with increased pH value was described before for PLL/HA multilayers[220], related to the deprotonation of PLLs amine groups. For QCHI on the other hand, the deswelling formerly described by Halthur et al. might be valid due to the slightly reduced zeta potential at pH 7.4[201]. It has been shown before that decreasing charge density leads to reduction of chains dimensions and collapse of the chitosan[202]. This might be the explanation for the decreasing angle shift during PBS wash.

Interestingly, systems with the CS 1 derivate show highest angle shifts. Since CS 2 and PCS 1 showed similar charge density in zeta potential measurement, the differences might be due to the size of the molecule. Results for PCS 1 are at least close to CS 2, rendering the size of CS 1 to be the influential factor. Due to the low DS_S it should be bigger, as further sulfation leads to chain scission and reduced molecule chain length[194]. The difference between PCS 1 and CS 2 might be explained by the additional PNIPAm side chain on the CS backbone of PCS 1, increasing molecular size. PCS 2 showed highest zeta potential, and highest angle shift for combination with PLL and QCHI after 10 layers. The quality of the measurements can be assessed by the first 5 layers for the systems with CS 2, PCS 1, and PCS 2, they all have 5 basal

layers consisting of polycation and CS 2. The influence of the polycations PLL or QCHI is nearly negligible. The biggest difference between PLL and QCHI, respectively, is the angle shift reduction for PLL/PCS 2 at layers 7 and 9, and that for QCHI systems, QCHI/CS 2 and QCHI/PCS 1 are directly opposite compared to the ones with PLL. This might be explained, that the rather big QCHI molecule in combination with the bigger PCS molecule (compared to CS 2) results in higher angle shifts. Sui et al. found that two polyelectrolytes that are rather big also result in thicker films[203]. This can be backed up by QCHI/PCS 2, where the shift for a single PCS 2 layer is also very high.

Noticeable was as well the staircase pattern for nearly all systems, however varying in intensity. These patterns were observed for other multilayer systems, were polycation adsorptions steps were observed to be distinctly higher than polyanion adsorption[202,221,222]. PLL/PCS 2 system shows even an angle shift reduction for the layers 7 and 9, in the range of the functional layers where PCS 2 was combined with PLL. This might mean that some material is stripped of the surface. This is due to polycations forming quasi-soluble complexes with the polyanion, thereby stripping it of the surface[99,203]. This explains the stair-case growth pattern for the PEM films, depending on the extent of the effect. Additionally for PLL, the diffusion of the polycation in and out of the multilayer might cause this pattern, as previously reported[105]. However, the non-exponential growth would suggest that the diffusion of the polyelectrolytes within the multilayer boundaries is minimal[82], suggesting that the formation of quasi-soluble complexes might be the more probable explanation. Adding to that, the mobility should be reduced by the present sulphate groups[106], meaning that the complexation is the main reason. Kumorek at el. found similar behavior when using QCHI as polycation[223].

The angle shift of SPR measurements is sometimes related to the layer thickness, especially if the refractive index (RI) of the build-up multilayer system is known. Since we cannot access the RI during SPR measurement, for a conclusive insight on dry layer thickness, the total PEM thickness of dried multilayers on Si wafers was determined with spectroscopic ellipsometry measurements (Figure 17). The samples were measured two times. Once after the LbL formation and subsequent drying in a desiccator for 24 h. Thereafter, samples were washed in PBS for 20 min, drying was repeated and measurement as well. This procedure should reveal the influence of washing with PBS on the dry multilayer thickness.

The measurements revealed that the dry thickness of the fabricated multilayers with polycation PLL is in the range of 10 to 15 nm, and with QCHI between 14 to 19 nm, depending on the polyanion (CS 1, CS 2, PCS 1 or 2). Comparing different CS derivatives, CS1 shows highest layer thickness. After washing with PBS, PEM films with PLL as polycation show no distinct thickness reduction. However, for multilayers with QCHI as polycation the washing at pH 7.4 results in loss of thickness, especially for QCHI/PCS2 multilayers (from 18.5 to 13 nm).
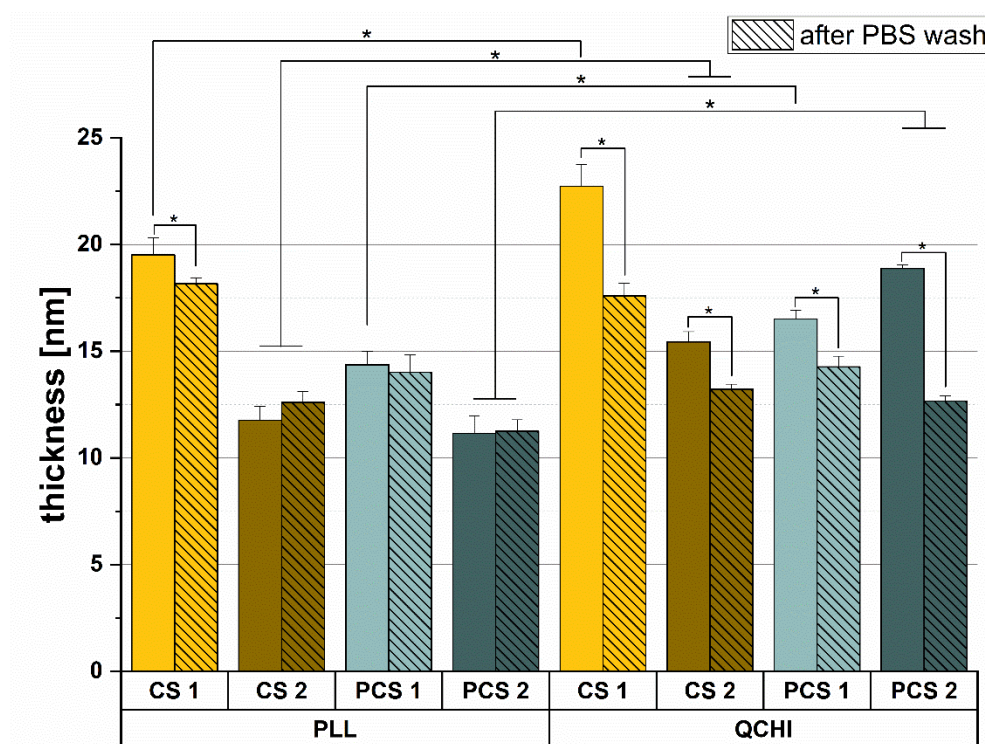
Figure 17: Fig. 2: Bar graph shows the thickness measured with spectroscopic ellipsometry, performed after LbL and after PBS wash at pH 7.4. Thickness was measured after complete PEM formation (10 layers) on Silicon wafers and at least 24 h after LbL and storage in desiccator. Measurements were performed in triplicates (n=3).

Generally, the measurements showed, that for all multilayer systems, thicknesses in the range of 11 up to 22.5 nm were obtained. Compared to previous work, this is in the range for biological applications of multilayer systems[206,224,225]. Compared to the multilayer prepared with CHI in the previous section, thickness was in similar dimensions. Washing with PBS confirmed the SPR measurements to some extent, as the dried films thickness was reduced after PBS wash. For PEM with PLL as polycation, thickness was reduced only slightly, meaning that these multilayers seem more stable under physiological conditions, coherent to the SPR results. For all PEM films using QCHI as polycation, thickness was reduced, especially for QCHI/CS 1 and QCHI/PCS 2. With regard to the zeta potential measurements of the

polyelectrolytes, the more pronounced thickness reduction of QCHI containing films compared to the once with PLL might be related to the decreasing potential with increasing pH. On the one hand, this could be caused by deswelling and build-up of more dense and compact layers after washing and subsequent drying. The pH and subsequent charge reduction of QCHI could lead, as explained before, to the reduction of chain dimensions and the structural collapse[202]. On the other hand, it could be related to the desorption of material. The measurement of surface zeta potential, giving insight into the electric charge in the interface region of the films might give more insight, if PCS as outermost layer was removed by PBS wash.

The PEM films that were built using PLL were generally thinner than the ones with QCHI, which is probably attributed to the lower MW of PLL (52 kDa) compared to QCHI (judging from the CHI used for fabrication: 200 – 400 kDa). Comparing the dry thickness with the adsorption of dry mass during SPR, some discrepancies are observable. Especially, the low thickness for PEM films with PCS 2 as polyanion. They showed highest angle shift in SPR before and after washing, but for PLL lowest thickness and for QCHI lowest thickness after washing with PBS. The PEM films with CS 2 as polyanions show the second lowest thickness of the measured systems. Koetse et al. observed in a multilayer formation of cellulose sulphate derivatives a general trend, that thickness of films increases, with a decrease of charge density[226]. This finding suits to the ellipsometry thickness measured here, since PCS 1 and CS 1 are thicker and have a lower degree of sulfation and a low measured zeta potential. This might be, as stated several times before, attributed to the longer chains due to the lower degree of sulfation. The observed differences to SPR results, especially for the PEM films containing PCS 2, might be explained by the different measurement method. For ellipsometry, samples are also shortly dipped in micro pure water to remove salt residues on the surface. This could lead to the removal of counterions, especially in less densely packed layers (which is probably the case for QCHI films). Furthermore, both measurements rely on the RI of the sample, which can differ, because in SPR, samples are constantly surrounded by liquid and for ellipsometry, they are completely dry, thus influencing the RI. This was explained in the previous section for multilayers with CHI as polycation.

4.3.2.3. *Characterization of polyelectrolyte multilayer surface properties*

The physicochemical surface properties of PEM are important for the response of the biological system. The zeta surface potential measurements reveal the surface charge of PEM films, relevant for the interactions with cells and proteins[209]. It might reveal, which polyelectrolyte is present in the interface region of the films, but it additionally allows to gain

information on the charge of the swollen and permeable layers underneath[227]. This might subsequently allow to deduce if pH increase leads to material desorption from the surface. Additionally, the interfacial energy, especially Coulomb interactions among other physical forces is a driving force of materials surface and cell/protein interactions[71]. The zeta surface potential, which is related to Coulomb interactions with charged proteins and cells, is an important factor to evaluate the interactions between biomaterial surfaces and cells/proteins[209].

The results presented in Figure 18 show, that with increasing pH all PEM films decrease to a negative zeta potential value. PLL and QCHI combined with PCS 2 start even at low pH with a zeta potential below 0, reaching its lowest point already at pH 6 at around -50 mV. For the other 6 samples, independent of PLL or QCHI as polycation, they show very similar values. Starting in the range of 30 to 50 mV, they rapidly decrease with increasing pH and have a point of zero charge in the area of pH 4 (PLL/CS 2 and PLL/PCS 1: PZC = 3.9; QCHI/CS1 and QCHI/CS2: PZC = 3.9 and PZC = 4). Deviating from PZC at pH 4 was QCHI/PCS 1 with the
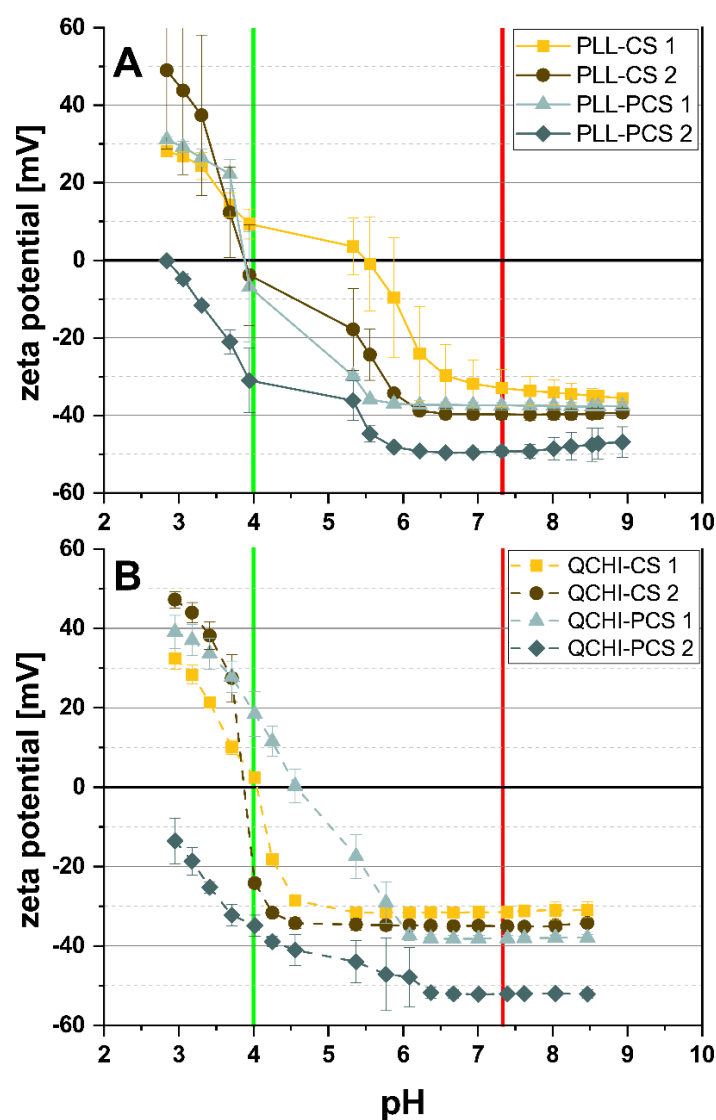
Figure 18: pH-dependent (acid-to-base pH titration) zeta surface potential measurements of the LbL multilayer films after complete assembly. (A) Comparison of different cellulose sulphate derivatives with PLL as polycation. (B) Comparison of different cellulose sulphate derivatives with QCHI as polycation. PEM film structure as described in previous section, meaning CS derivatives were the final layer. Additional lines highlight pH 4(green line in A, B), pH value during LbL multilayer assembly, and the physiological pH 7.4 (red line in A, B), the pH value at which films are applied in cell culture. PZC = point of zero charge.

point of zero charge at pH 4.6. Strongly deviating from the other samples were multilayers PLL/CS 1, gaining negative zeta potential at pH 5.5. However, near pH 6 all samples reach their minimum potential. At this point, all PEM films, except the ones with PCS 2, have comparable zeta potential values between 30 and 40 mV. For all multilayer systems, negative charge is predominant at pH 7.4, so under physiological conditions.

The streaming zeta surface potential results showed the high influence of deprotonated sulphate groups (OSO_3^-) of cellulose sulphate in the outer layers. For systems with PCS 2 as polyanion, negative zeta potential over the complete pH range indicates dominant influence of polyanion in the surface region. The other PEM films start at least with a positive potential at low pH, showing that protonated amine groups (NH_2^+) of Chitosan or PLL overcompensate the negative charge of sulphate groups in the interfacial region. But rapid reduction of zeta potential values suggested that the outermost layer is dominated by the polyanion, especially since the point of zero charge is mostly in the range of pH 4. At pH 7.4, all measured surface potentials have reached an equilibrium at a negative zeta potential. For PEM films with PCS 2 as polyanion, this value is lowest. All other samples are rather close to one another. It seems, similar to the measured zeta potential of the PEL solutions, that PCS 2 has the most exposed negatively charged groups. According to the sulfation degree, determining the amount of negatively charged sulphate groups, PEM films with CS 2 should be similar to PCS 2, but it is not, which is also somehow comparable to the zeta potential for PEL solutions. Overall, at the physiological relevant pH 7.4, all samples have a negative zeta surface potential, especially PLL and QCHI combined with PCS 2. Concerning the stability issues observed by angle shift and thickness reduction in SPR and ellipsometry, respectively, the zeta potential would at least lead to the assumption, that the outermost layer of the films was a CS derivative. That means, that washing with PBS might remove the 9th and 10th layer of the films, which would contradict SPR measurements, as angle shifts were not in that dimension. Thereafter, it might be more likely, that the multilayer films show deswelling behavior or the films somehow collapse towards a denser conformation.

The surface charge is one of the multilayer film properties that influences protein adsorption and subsequently cellular adhesion. It has been shown before, that fibronectin (FN) adsorbed better on positively charged surfaces[228]. FN facilitates the cellular adhesion, as there are specific integrins interacting with the FN. The negatively charged surface for the examined multilayer system is therefore less favorable for protein adsorption. However, in contrast to the protein adsorption, it was observed before, that cell adhesion was facilitated by negatively charged polyelectrolyte surfaces. According to Maroudas et al. (1975) the

density of surfaces charges might be even more important than the negative or positive character of the charges[229]. The presence of certain functional groups and the wettability are additional factors influencing cellular adhesion[230].

Following the zeta surface potential measurements, surface wettability, being another relevant factor to predetermine cell/surface interactions, has been examined. Wettability of different multilayer systems was determined using static contact angle measurements (Figure 19). The different PEM compositions composed of polycationic PLL or QCHI in combination with CS derivatives were examined. The final layer for each PEM system were as before the polyanions. The wettability was assessed after the surfaces have been washed once with PBS, as measurements were not possible beforehand due to inconsistent drop shapes.

Measured contact angles are similar for PLL and QCHI multilayer systems. They were
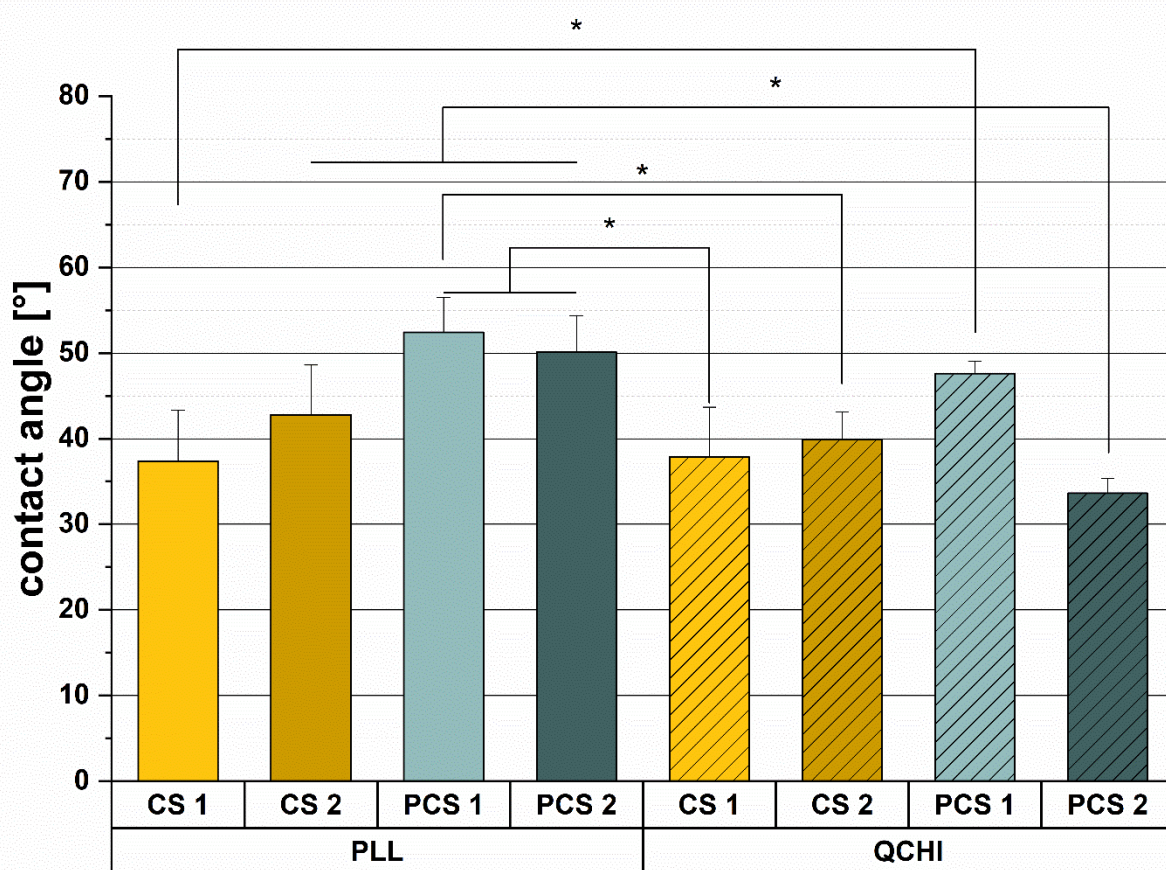
Figure 19: Bar graph shows Water Contact angle of Si wafers coated with different PEM compositions. Static Contact angles were determined using sessile drop method using ellipse fitting. Samples were washed with PBS before contact angle measurement. The final layer for each PEM is shown in the upper row of the x-axis, namely CS 1, CS2, PCS 1 and PCS 2. Measurements were done in triplicates.

lowest (37°) for CS 1 as final layer. Angles increase for CS 2 and PCS 1 containing multilayers, for both polycations. PLL/PCS 1 and QCHI/PCS 1 showed the highest contact angles compared to the other CS derivatives. The most distinct difference was observed between PLL/PCS 2

74

with 50° and QCHI/PCS 2 with 33°. Generally, multilayer containing PLL presented slightly higher contact angles than multilayers with QCHI.

In general, the contact angles for all PEM films did not differ much from one another and were in the range of 30 – 50 °. Similar contact angles were recorded for the combination of CHI or trimethyl-chitosan in combination with GAGs[221]. These results were comparable to the once of the precious section with PEM films with CHI as polycation. It is most likely, that the explanations for the effect are the same. CS derivatives are more hydrophilic due to the sulphate groups. For most of the PEM films, these sulphate groups are predominantly responsible for the low contact angles, as they were deposited as the outermost layer. Theoretically, the contact angle should be lowest for multilayers with CS derivatives CS 2 and PCS 2, as they possess higher DS_S and therefore more sulphate groups. But PLL/PCS 2 and the multilayers containing CS 1 showed contact angle that were not in agreement to this theoretical background. This could mean, that we do not have clearly separate layers of polycation and polyanion, but intermingling of both, which would allow the amine groups of PLL and QCHI to influence the contact angle. Altankov et al. (2003) determined the contact angle for surfaces coated with certain functional groups, among them SO_3^- (sulfonic) and $NH2^+$ (amine) [209]. The amine groups showed contact angles of around 60°. The influence of the amine groups of the polycation layers in the films might explain the higher contact angles for PLL/PCS 1 and PCS 2. The presence of negative charged SO_3^- functional groups of CS derivatives would explain the lower contact angles, as sulfonic groups of similar character were observed to have contact angles close to 30°[209]. However, for PLL/PCS 2, the influence of the underlying PLL layer is somewhat contradictory to the dominant negative surface charge determined via zeta surface potential measurements. The influence of PNIPAm side chains seems to play an underlying role. As measurements were performed at 25 °C, below the LCST, PNIPAm should have a hydrophilic character. However, PEM films with PCS1 or PCS 2 did not consequently show lower contact angles than PEM films with CS 1 or CS 2. Hence, the influence of PNIPAm chains on wettability were at least not observable.

4.3.3. Conclusion

In this section of this thesis, the newly synthesized CS derivatives, namely CS 1 (DS_S = 0.67), CS 2 (DS_S = 1.04), PCS 1 (DS_S = 0.41, DS_{PNIPAm} = 0.14) and PCS 2 (DS_S = 0.93, DS_{PNIPAm} = 0.11) have been used as polyelectrolytes for the fabrication of multilayer films using LbL technique. Building on the PEM films formed using CHI as polycation, PLL and QCHI were employed to overcome certain limitations. Several experiments to determine multilayer formation kinetics and the physicochemical characterization of multilayers have been

performed. These experiments showed the successful PEM fabrication via LbL was possible. PEM with 5 bilayers were successfully fabricated and showed a linear growth behavior resulting in PEM films of common thickness for application as coating in tissue engineering. The further examination in this chapter could not entirely resolve the issue if PBS wash causes some kind of desorption or deswelling/shrinking of the films. But from the conducted experiments, it is more likely that the PBS wash causes the multilayer to collapse than the removal of material from the surface, as surface potential and wettability indicate the presence of CS derivatives in the outermost layer. These multilayers were selected for the biological characterization using different cell types. In the following section, the results for cell viability and growth are presented. As the surfaces are moderately hydrophilic, they should enable cellular adhesion. The negatively charged surface is not necessarily facilitating protein or cell adhesion, but it has shown before that both events were happening on negatively charged substrates, depending on cell type and presence of functional groups[231].

4.4. Biological characterization of polyelectrolyte multilayers

4.4.1. Viability and growth studies for different germ layer cell types

After this comprehensive physicochemical characterization, the successful PEM film fabrication via LbL technique could be demonstrated. While for PEM using CHI as polycation we observed stability problems under physiological pH, the results for PEM, where QCHI and PLL were used, demonstrated stability at physiological pH and the final layer of CS derivatives seems to be prominent at the surface, following zeta surface potential and water contact angle measurements. With regard to the application of the multilayers as potentially thermoresponsive cell culture substrate, the biocompatibility of the different PEM films needed to be tested. In consequence of the low stability of PEM with CHI, the biological characterization was only performed for the more promising and stable PEM using the polycations QCHI and PLL in combination with the different CS derivatives. For the viability and growth studies, cell types originating from all three germ layers were seeded in PEM coated well plates and a live/dead assay after 24 h and a Deep Blue assay measuring metabolic activity over 7 days were carried out.

4.4.1.1. 3T3 mouse fibroblasts of mesodermal origin

The first biological characterization was conducted using 3T3 mouse fibroblast cells. Fibroblasts are cells originating from the mesodermal germ layers, being one of the prominent cell types in connective tissue and one of the most abundant cells in the human body. For the

PEM systems characterized in the last section, cells were seeded, and cell viability and cell growth were assessed using a live/dead and a Deep Blue assay, respectively.

The PEM films using CS1 combined with both QCHI and PLL as polycations showed the highest cell death as high as 100% and 80%, respectively (see Figure 20). For the PEMs combining QCHI and PLL with CS2, cell death percentage reached 25% and 15%, respectively. When PNIPAm-modified CS in form of PCS 1 or PCS 2 was incorporated into the PEMs, the percentage of dead cells was further reduced, reaching a dead cell percentage of 13% for PLL/PCS 1 and 5% for PLL/PCS2. The percentages were lower when QCHI was applied as polycation in the PEM, reaching 5% for QCHI/PCS 1 and only 2% for QCHI/PCS 2. Consequently, PCS1 and PCS2 in the combination with PLL resulted in a higher cell death percentage compared to lesser when QCHI was used as polycation. According to the findings of live/death assay, cell density and area were lower for PEM films containing CS1, particularly when QCHI was used as polycation as shown in Figure 20 B and C. Especially for QCHI/CS 1, cell density showed the lowest value (12.5%) and cells showed no spreading, with cell area being below 500 μm^2. For PLL-PEM systems, cell number was very similar for all CS derivatives, being slightly below 50 cells/mm² for PLL/CS1 and CS2, and slightly above 50 cells/mm² for PLL/PCS1 and PCS2. These values were lower compared to the TCPS positive control. Especially the cell area showed significant differences for PLL-PEMs compared to TCPS. Cells seeded on PLL/CS1 and CS2 showed low cell areas below 1000 μm^2, the cell area for PLL/PCS1 and PCS 2 increased to 1600 and 1800 μm^2, respectively. These values were still significantly lower than the 2800 μm^2 measured for TCPS. The multilayers made of QCHI with CS derivatives except CS1, as it was mentioned above, possessed a cell density on CS2 (60 cells/mm²) and PCS2 (80 cells/mm²) that was higher than on TCPS. For QCHI/PCS 1, cell number was comparably low at 43 cells/mm². Concerning the cell spreading, the measurements revealed substantially higher cell areas for QCHI-PEM multilayers compared to their PLL-based PEM (Figure 20 C). Cell area for QCHI/CS2 and PCS 2 were similar to TCPS around 2800 μm^2, while cells on QCHI/PCS 1 showed less spread morphology with cell areas below 2000 μm^2.
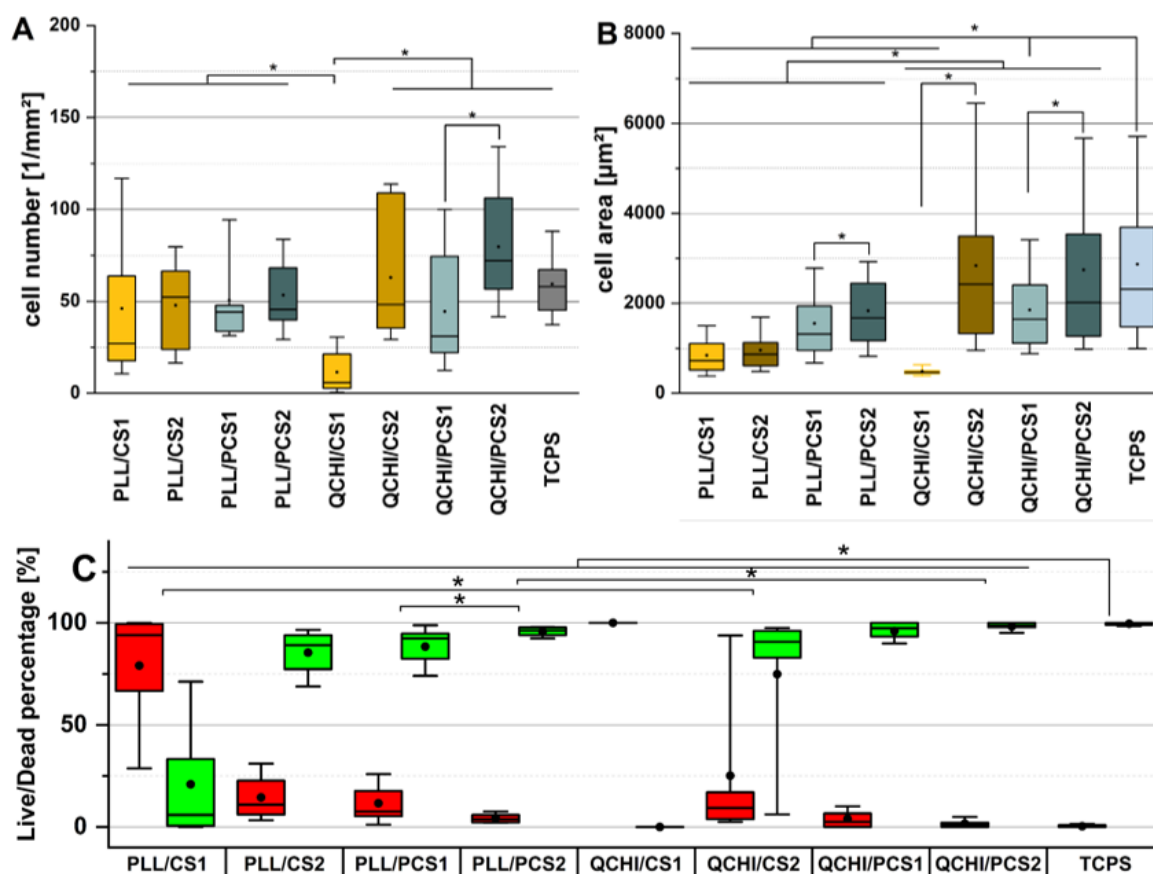
Figure 20: Quantification of cell number (A) and cell area (B) of 3T3 cells cultured for 24 h in different PEM coated wells. Images were analyzed using Fiji software using at least 10 images per condition. PLL and QCHI as polycations were combined with CS1, CS2, PCS 1 and PCS2 to form PEM coatings on TCPS, which was used as control. Polyanions were used as 10th and therefore outermost layer. The box corresponds to middle 50% of data, the band corresponds to the median and the square/point to the mean value. Whiskers represents middle 80% of all data. Complementary, Live/Dead percentage (C) of the cells seeded on the PEM surfaces, with TCPS as positive control, is presented, whereas the green bar represents living, and the red bar represents dead cells. Corresponding images are shown in supplementary (see Appendix A.1).

The Live/Dead cell assay provided results on cell number and spread, as well as cell viability after 24 h of cell culture on the coated surfaces (Figure 20). The cell numbers for PEMs with PLL as polycation are overall very similar after 24 h and lower than for cells seeded on TCPS (Figure 20, A). Cell numbers are distinctly lower for QCHI/CS 1. Cell density for QCHI/PCS 1 is in the range of PLL samples. QCHI/CS 2 and QCHI/PCS 2 show higher cell density than on TCPS. However, the data are more widely scattered. Additionally, information on the biocompatibility of PEM surfaces was provided by the measurement of cell area (Figure 20, B). These values showed that cells were not very spread on PLL/CS 1 and PLL/CS 2. The few cells on QCHI/CS 1 were not spread, too. Spreading of cells increased for PLL with PCS 1 and 2 and the QCHI/PCS 1. Cells seeded on QCHI/CS 2 and QCHI/PCS 2 were well spread and comparable to TCPS. After 24 h, nearly no cell death was evident for TCPS control (Figure 20, C). Samples with CS 1 as polyanion showed significantly higher cell death numbers (80%). Cell death was greatly reduced for samples with CS 2, following PCS 1. Most

living cells were counted for samples with polyanions PCS 1 and PCS 2, however still significantly different from TCPS. But overall, the number of death cells for QCHI/PCS 2 is very low at 2%. The corresponding fluorescent images are provided as a montage (Appendix Fig. 1) in the appendix.

The metabolic activity of the cells was measured using a Deep Blue assay. Cells were exposed to the staining solution on day 1, 4 and 7. Metabolic activity is proportional to the fluorescent intensity of the supernatant, collected from the cells after they were cultured in the Deep Blue staining solution for 2 h. Metabolic activity is correlating with cell number, which enables to track the cell growth over the course of 7 days. Additionally, to the staining, phase contrast images of the cultured cells were taken before the staining commenced at day 1, 4 and 7. This allowed to assess the phenotype of the cell, giving insight if the cells look healthy. Montages for the different cell types on TCPS control and for the 3T3 cells on PEM films are presented in the appendix in Appendix Fig. 4 and Appendix Fig. 5, respectively.
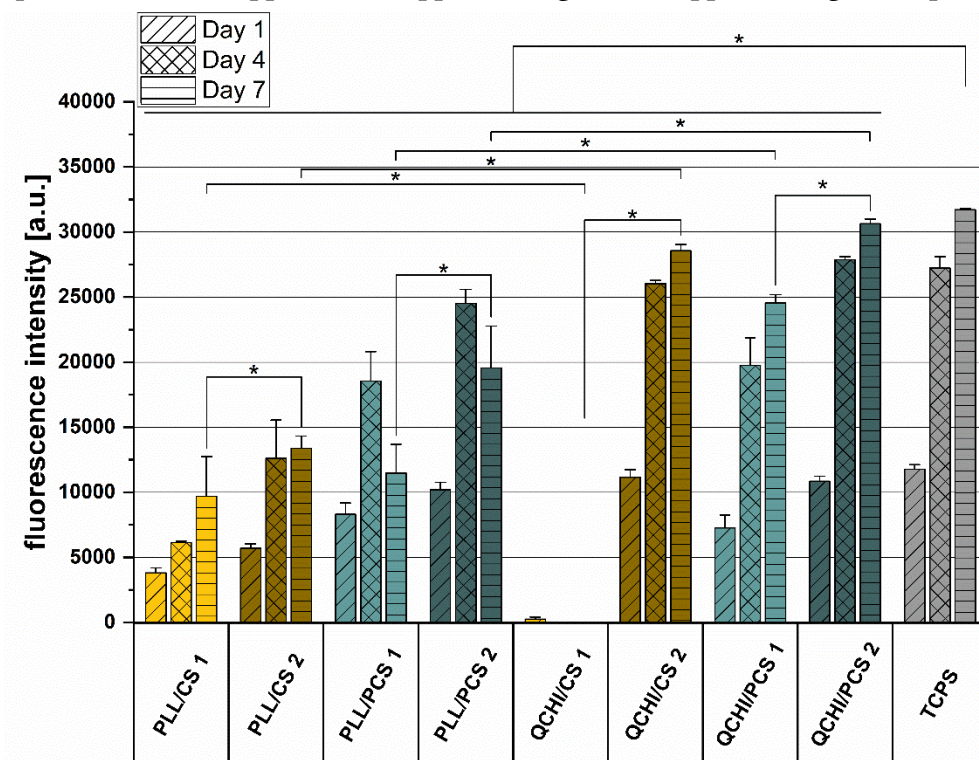
Figure 21: Deep Blue cell viability test over the course of 7 days for the study of cell activity on PEM coated surfaces. Bar graphs show the excitation at add wavelength after cell cultivation of 1, 4 or 7 days. Higher excitation value corresponds to higher cell activity, meaning cells have proliferated and are viable over the course of time.

On day 1 of the Deep Blue cell metabolic activity test, FI could be measured for all samples, except for QCHI/CS 1 (for all measuring days) (Figure 21). TCPS control surface and QCHI combined with CS 2 and PCS 2 and PLL/PCS 2. Over the course of time, especially the aforementioned samples of QCHI/CS 2 and QCHI/PCS 2 show similar results to TCPS control.

All PLL samples show only a minor increase in excitation, for PLL combined with PNIPAm-grafted-cellulose sulphate even a loss at day 7 was detected. Overall, the bar graph shows for QCHI samples an increasing excitation, which corresponds to cell viability, over 7 days, comparable to TCPS.

The live/dead assay provided a first conclusive look on cytotoxicity of the different PEM films. After 24 h, 5 images per sample were taken and cell area, cell density and subsequently live/dead cell percentage were calculated after Fiji software was used for image analysis[185]. Cell density gave insight in the adhesion efficiency of 3T3 fibroblasts after 24 h on the different surfaces. A high cell density alone does not conclusively tell how well cells adhere to a certain surface. Therefore, cell area was measured as well. A wider spread cell generally has more contact points to the substrate for information exchange, therefore indicating a better biocompatibility of the surface[230]. Cell density is for all PLL-including PEM surfaces slightly lower than for TCPS, QCHI/CS 2 and QCHI/PCS 1 are also in this range. Only QCHI/CS 1 shows very low and QCHI/PCS 2 a higher cell density than TCPS. Now looking at the cell area, cells did not spread as well on PEM including PLL, with the best result for PCS derivatives. The best results, comparable to cell area on TCPS, are recorded for QCHI/CS 2 and QCHI/PCS 2. Generally, the presence of PNIPAm in the multilayer seems to benefit cell adhesion. It might be, that in accordance with literature, the surfaces are slightly more hydrophobic at 37°C at which cells are cultivated[125,163,206]. But also, the higher sulfation degree seems to benefit cell adhesion[96]. In fact, it was shown before that the presence of sulphate-groups in multilayer surfaces lead to increasing cell contact area and a more spread morphology[232].

Especially QCHI/CS 1 seems to be unattractive for cells, because nearly no cells adhered, and the few that are, are very rounded. more cells adhered and grew over the course of 7 days. However, the high number of dead cells and the low cell growth rate suggest a similar problem as QCHI/CS 1. The trend shows that increasing sulfation degree and presence of PNIPAm is beneficial for cell adhesion. This is explained by the capability of sulphated polysaccharides to bind adhesion proteins[99]. Additionally benefiting is the effect of PNIPAm on the water contact angle (except for QCHI/PCS 2, as contact angle decreased). Since the zeta surface potential revealed that PEM films are strongly negatively charged and cells are also generally negatively charged[233], repulsion on these surfaces would be expected[234]. But it seems, that negative surface charge is not the dominating factor, but the presence of adhesion molecule binding domains in CS that allow the adsorption of biological active molecules on the surface and facilitate cell adhesion[99]. The increasing contact angle for PCS samples is beneficial as well.

Live/dead staining revealed, as compared to control were nearly no cell death occurred, that especially on PEM films containing CS 1 a significant number of death cells (80% for PLL/CS 1 and QCHI/CS 1) was found. The combination of QCHI and PLL with CS derivatives of low charge density seem to be the determining factor. With regard to the physicochemical characterization, it is possible that due to this low charge density of some of the CS derivatives, especially CS 1, only a weak bond to the polycations establishes due to decreased ion pairing[103]. Especially under physiological pH this might lead to an increased release of polycations into solution, which are highly cytotoxic and lead to the observed cell death[235,236]. Lowest number of cell death occurred for PCS derivatives, especially PEMs with PCS 2, followed by PCS 1. When comparing with results for cell density and area, the QCHI/PCS 2 film showed the most promising results, with highest cell density, widespread cells and nearly no death cells comparable to TCPS surfaces. This is explained as mentioned earlier by the higher sulfation degree of the CS derivative in combination with PNIPAm. Higher DS_S means more sulfation and a higher number of functional groups that can interact with adhesion molecules. Additionally, PNIPAm can benefit cellular adhesion with regard to the increasing WCA. The combination of PCS 1 with polycations resulted in similar behavior as CS 2. It has a lower sulfation degree than CS 2 but includes PNIPAm. Hence, it is coherent to the theory that sulfation degree and PNIPAm are beneficial for cell attachment and survival.

For the insight of cell activity over a longer time, the Deep Blue cell viability assay was applied to track cell activity over the course of 7 days. Generally speaking, findings of the live/dead assay were confirmed, but it additionally showed a long-term influence of polycation PLL. Cell activity is significantly lower over the course of time and especially at day 7 on PEM films containing PLL. The poor cellular adhesion, spreading and growth that was observed for all PLL multilayer systems might be due to PLL mobility in the multilayer system. PLL tends to diffuse "in" and "out" of the multilayer system when not crosslinked[237]. As a result it is likely that PLL, which is highly cytotoxic when unbound and in solution[235,236] causes cell death. The unintended 3T3 cell detachment was visible on the phase contrast images. Even though cells fused to a connected layer, after a few days of culture, they started to detach and form aggregates or started to fold up (see Appendix Fig. 5). This is most likely attributed to the lower overall stability of the PLL containing PEM systems.

The poor biocompatibility of QCHI/CS 1 and PLL/CS 1 is observed once more. As stated earlier, this is most likely due to the lower stability of the films. CS 1 has a low DS_S and thereafter a lower charge density. In combination with the polycations, fewer ion pairing leads to an overall lower stability of the films. It is likely that some of the polycations are not

tightly bound and released into the solutions. In solution, they are highly cytotoxic and lead to the observed cell death or low survival rate[103,235,236]. This effect seems to be more prominent for PLL containing PEM, likely due to higher mobility of PLL in the multilayer (as explained above). All other PEMs with QCHI as polycation show cell proliferation and activity over 7 days, with QCHI/CS 2 and PCS 2, on which cells are as active as on TCPS. It seems that over the long term, especially the combination of QCHI, higher sulfation degree and presence of PNIPAm are facilitating cell growth and proliferation. Overall, the positive properties of QCHI seem to be a fitting polycationic counterpart to CS derivatives.

4.4.1.2. Viability and growth assays using cells of endodermal and ectodermal origin

The initial biological characterization of PEM surfaces composed of QCHI or PLL in combination with CS 1, CS 2, PCS 1, or PCS 2 using 3T3 mouse fibroblasts showed interesting results. Especially the combination of CS 2 and PCS 2 (higher DS_S) with QCHI showed promising results for cell viability and growth. Certain PEM compositions showed good biocompatibility similar to tissue culture polystyrene (TCPS) and thereafter would make promising surface coatings for further research. Beside the initial characterization using 3T3 cells of mesodermal origin, two more cell types originating from the other two germ layers were used for further biological characterization, because their adhesion behavior is different and it gives further interesting insight into the compatibility of the PEM system with different cell types[179]. One of these cell types were the HepG2 cells of endodermal origin (hepatocellular carcinoma cell line), while the other cells were the HaCaT cells of ectodermal origin (humane keratinocyte cell line). Both of them were seeded on the same PEM surfaces as 3T3 cells in the chapter before and cell viability and growth assays performed, their results are presented in Figure 22 and Figure 23.

HepG2 cells were seeded in PEM-coated 24-well plates and cultured for 24 h before staining with a Live/Dead cell viability kit for mammalian cells. The assay provided insight into cell number, especially of living and dead cells, enabling to assess the biocompatibility of the PEM surfaces. In contrast to the 3T3 cells, the morphology of the cells could not be assessed due to the natural aggregation of the HepG2 cells. Figure 22 A shows the cell density for HepG2 cells on the different PEM compositions. The outermost layer was the polyanion, so CS 1, CS 2, PCS 1, or PCS 2, combined with the polycations PLL or QCHI, respectively. For all PEM systems the low number of dead cells is striking. It does not exceed the 10 cells/mm². Additionally, the amount of living cells is fairly high, with densities surpassing 50 cells/mm² for all samples. In comparison, 3T3 cells on PEM surfaces distinctly surpassed this density
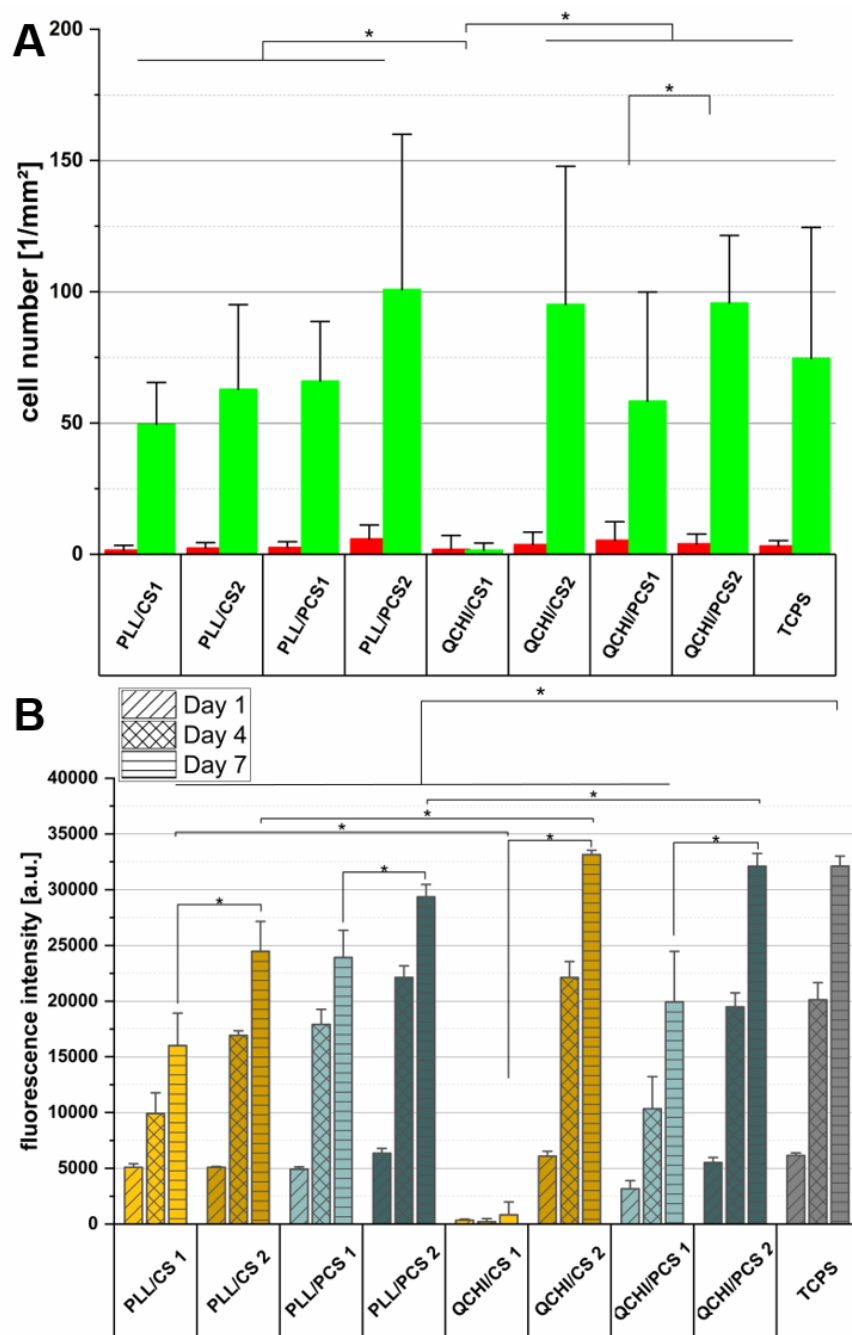
Figure 22: Cell viability (A) and growth (B) assay of HepG2 cells on PEM-coated surfaces. Bar graph (A) shows the cell density for living and dead cells on differently composed PEM surfaces. Fluorescent images from which cell density was calculated (using FIJI) were taken after 24 h of cell culture using laser scanning microscope. The cell growth assay (B) was performed using a Deep Blue assay. Excitation was measured at day 1, 4 and 7 of cultivation. High excitation is proportional to more cell activity.

only 2 times (QCHI/PCS 2 and TCPS, see Appendix Fig. 2 (L/D staining) and Appendix Fig. 6 (phase contrast microscopy images)). As HepG2 cells are a cancer cell line, a fast proliferation and growth is not surprising. The lowest number of cells, nearly none, were counted on QCHI/CS 1 surfaces (as seen for 3T3 cells, see Figure 20). The cell density showed similar values for most of the PEM systems examined, with PLL/PCS 2, QCHI/CS 2 and QCHI/PCS 2

being the exception and even exceeding the cell density of TCPS control. These three samples presented densities of HepG2 cells of nearly 100 cells/mm², exceeding the cell number of all other PEM samples noticeably. However, the standard deviation indicates high differences between the single samples, hence no significant differences were calculated. In addition to the cell viability assay after 24 h, the growth of HepG2 cells on the PEM surfaces was observed over the course of seven days and examined using a Deep Blue assay. The results, showing the fluorescence intensity, which is proportional to the amount of metabolic active cells, are presented in Figure 22 B. These results are perfectly in line with the cell viability assay. Cells seeded into QCHI/CS 1 coated wells showed no activity from day 1 to 7. On all other samples, activity was increasing over the course of these seven days. Initially, the activity measured on day 1 was more or less corresponding to the cell viability. The samples that showed highest cell density also presented the highest activity. Over the course of seven day, HepG2 cells on PLL/PCS 2, QCHI/CS 2 and QCHI/PCS 2 showed highest excitation values, corresponding to metabolically active cells, values comparable to cells growing on the TCPS positive control. While the cells on PLL containing multilayers showed maximum growth between day 1 and 4, cells on QCHI containing multilayers grew somewhat equally over the course of seven days. On each of the assay time points, phase contrast images of the cells on the samples were taken. These images revealed (see Appendix A.2) that HepG2 cells seeded on QCHI containing PEM films and TCPS grew normally, except for QCHI/CS 1 of course. Strikingly, HepG2 cells seeded on PLL containing surface coatings showed differences in the typical phenotype. Instead of growing in clusters of rather rounded cells, the cell morphology was more elongated and spread and showed less clustering.
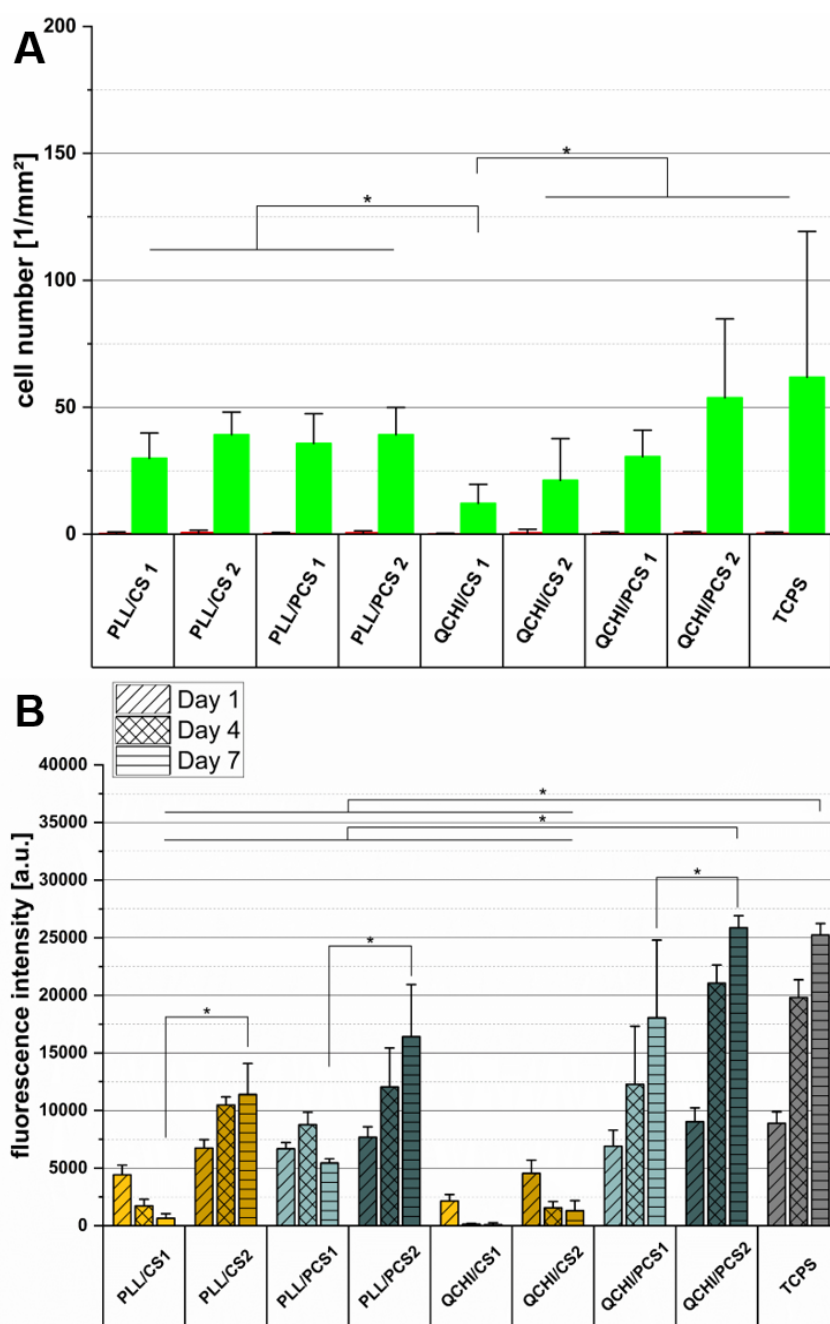
Figure 23: Cell viability (A) and growth (B) assay of HaCaT cells on PEM-coated surfaces. Bar graph (A) shows the cell density for living and dead cells on differently composed PEM surfaces. Fluorescent images from which cell density was calculated (using FIJI) were taken after 24 h of cell culture using laser scanning microscope. The cell growth assay (B) was performed using a Deep Blue assay. Excitation was measured at day 1, 4 and 7 of cultivation. High excitation is proportional to more cell activity.

Completing the cell biological characterization of the multilayers combining PLL or QCHI with CS derivatives, HaCaT cells were seeded in PEM coated wells. The cell viability assay was performed after 24 h of culture. The cell number was determined and subsequently cell density was calculated, split in dead and living cells. Surprisingly, almost no dead cells were visible in the fluorescent images, hence no dead cell density bars are visible in Figure 23

A. The cell density of living HaCaT cells seeded on show no significant differences. While cell densities calculated for PLL-containing multilayers show only minor differences, the densities for QCHI-containing multilayers showed quite low values for QCHI/CS 1 and increased towards QCHI/PCS 2. The density for QCHI/PCS 2 samples were the only ones, except for control TCPS, were the value exceeded 50 cells/mm². These cell numbers are quite low, but similar to the results achieved for 3T3 cells, even though the total amount of cells for all samples were lower.

The cell growth was also monitored for HaCaT cells on the differently composed PEM films over the course of seven days, with measuring time points at day 1, 4 and 7 of culture. At each day before the Deep Blue assay, phase-contrast images were taken to determine if cells looked healthy. The Deep Blue assay revealed the low cell activity over 7 days on PLL/CS 1, QCHI/CS 1, and QCHI/CS 2. Cells seeded on PLL/PCS 1 showed initial growth, but between day 4 and 7, cell activity was reduced. In general, the excitation was for all samples lower than observed in the assays for the other cell types. For HaCaT cells, only the ones seeded on QCHI/PCS 2 multilayers showed activities compared to TCPS positive control. This was somewhat contradictory to the other cell types, were also other surfaces showed good cell activity. However, these results were mostly in line with the findings for cell viability of the live/dead assay, were QCHI/PCS 2 showed good results comparable to TCPS.

The biological characterization of different PEM films using HepG2 and HaCaT cell lines presented the addition to the experiments performed before with 3T3 fibroblasts. Experiments with both cells suggested the high biocompatibility of QCHI/PCS 2 over the course of all experiments. In contrast to 3T3 and HaCaT cells, HepG2 cells showed a good viability and activity on most of the PLL surfaces. This has been shown in other works before, were hepatocarcinoma cells showed higher resistance towards multilayer surfaces composed of PLL among others[238]. As seen before, especially the multilayers containing CS derivatives with a lower sulfation degree, namely CS 1 and PCS 1, showed either lower cell viability and activity than on the TCPS control or even no viability or activity at all. As discussed for the 3T3 cells, it is likely that CS with lower sulfation degree formed fewer stable bonds with the polycations. Hence, the polycations might be present in unbound form in the solution where they are highly cytotoxic. It is also observed here that the presence of PNIPAm, related to its effect observed for WCA, is beneficial for the cell adhesion and growth. The highest biocompatibility could be observed for the combinations of CS with high sulfation degree and the presence of PNIPAm. These PEM present due to the high sulfation degree enough biological cues for adhesion proteins to adsorb and facilitate cell adhesion. Additionally, the PNIPAm allows for a wettability milieu from which cells benefit as well. The surface charge

measured via zeta surface potential was highly negative at physiological pH. In theory, this does not facilitate cell adhesion. But, for HepG2 cells the positively charged laminin is adhesion facilitating protein. The adsorption of laminin on negatively charged surfaces is electrostatically beneficial, which might explain the high cell density observed for HepG2 cells. Even though it has been shown in previous works that decreasing surface charge has negative impact on cell adhesion, it has limited effects for surface charges not lower than -50 mV[239]. The measured surface potential does not exceed these values (only QCHI/PCS 2 slightly), hence the effect of the surface charge on cell adhesion can be seen as limited.

Following these explanations, it is fitting that the combination of QCHI with CS 1 showed absolutely no biocompatibility with any of the cell types. It seems to inhibit cellular adhesion or results in necrosis of cells directly after attachment, as 24h after seeding none or only few cells remained on these surfaces. Overall, HaCaT and HepG2 cells, in accordance with the 3T3 results, seem to be most compatible with the QCHI/PCS 2 surface. QCHI containing surfaces in general (except for combination with CS 1 seems to be favorable for cell adhesion and growth, at least judging from the comparison to the positive control on TCPS, which is the gold standard for cell culture purposes. Especially the combination with the CS derivatives with higher DS_S, namely CS 2 and PCS 2, seemed biocompatible, judging from the recorded results. Only for HaCaT cells, the QCHI/CS 2 multilayers showed no biocompatibility, which might be due to other reasons or a low seeding efficiency, as it is contradictory to the findings for 3T3 and HepG2 cells. Generally, the findings that have been discussed for 3T3 fibroblast cells seem to be valid for the other two cell types as well.

In conclusion up to this point, multilayers containing CS derivatives with higher DS_S and polycations, especially QCHI, were biocompatible and allowed cellular adhesion and growth over the course of seven days. In most cases multilayers containing CS 1 and PCS 1, with lower degree of sulfation, showed cytotoxic tendencies, as did multilayers containing PLL. For 3T3 and HaCaT cells, no PLL containing multilayer reached comparable results to TCPS. While on the other hand, cells seem to thrive on most of the QCHI containing multilayers, especially for QCHI/PCS 2. This combination of polyelectrolytes resulted in a biocompatible multilayer with no observable cytotoxic effect, retaining the natural phenotype of the cells. For the completion of the biological characterization of the multilayers, immunofluorescence staining of focal adhesion complexes and the actin cytoskeleton of 3T3 cells was performed. This experiment allowed the assessment of the cellular adhesion quality on different multilayers.

4.4.2. Immunofluorescence staining of 3T3 mouse fibroblasts

Cell adhesion is the necessary prerequisite for subsequent cellular events such as proliferation and differentiation. The immunofluorescent staining of certain cellular proteins gave insight into the cellular adhesion on different PEM-coated surfaces. By staining proteins that are associated with the focal adhesion (FA) complexes or the cytoskeleton of cells, the compatibility of cells with their underlying surface can be evaluated. As conclusion from the cell viability and growth assays, the immunofluorescent staining with conjugated antibodies targeting specific cell proteins, namely vinculin (FA), actin (cytoskeleton fibers) and the nucleus, was performed on PLL/CS 2, PLL/PCS 2, QCHI/CS 2, and QCHI/PCS 2 multilayer systems. These showed promising biocompatibility for all cell types. 3T3 cells were chosen for this experiment, as they are not forming any cell clusters and showed in earlier experiments signs for good cellular adhesion on the chosen multilayer surfaces.
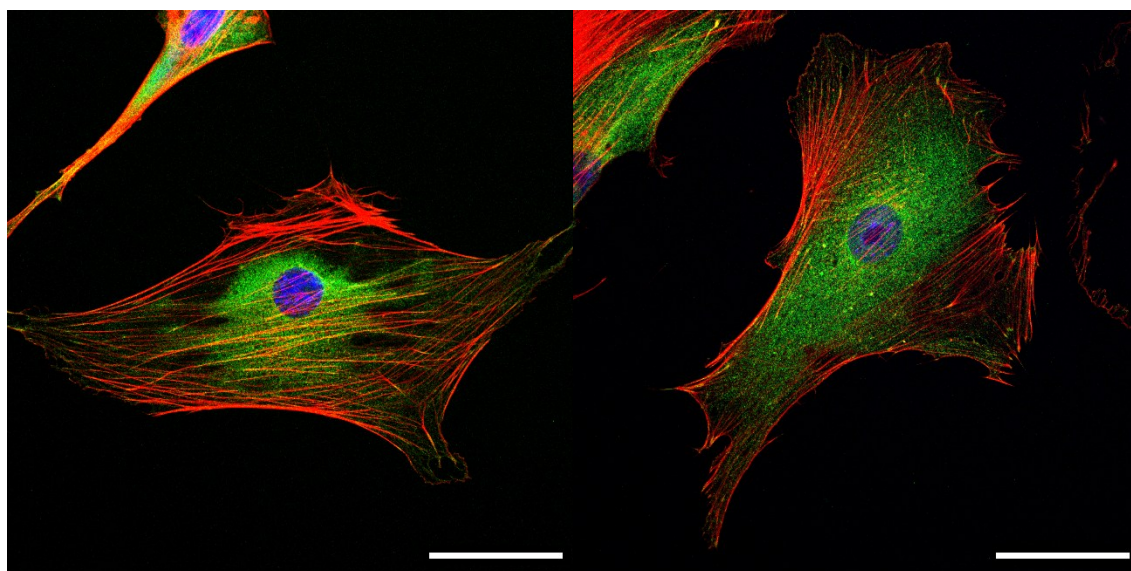
Figure 24: Immunofluorescence staining of 3T3 mouse fibroblasts. Vinculin (green), actin fibers (red) and nuclei (blue) have been stained to gain qualitative information of cell adhesion on clean glass substrates. The green, due to overlapping sometimes orange, spots at the end of the red actin fibers represent focal adhesions of the cells, connections to the substrate. Scale bar: 50 µm

Immunofluorescent staining was performed after the cultivation of 3T3 cells on PEM-coated glass cover slips for 24 h. Cells seeded on TCPS (Figure 24) and the multilayer systems PLL/CS 2 (Figure 25, A & B) and PCS 2 (Figure 25, C & D) and QCHI/CS 2 (Figure 26, A & B) and PCS 2 (Figure 26, C & D) were stained and the according images are presented.

All surfaces support cell adhesion, as all cells are spread, with pronounced actin fibers longitudinal stretching over the whole cell. On TCPS surfaces (Figure 24), cells showed an extended morphology, with actin fibers spreading covering most parts of the cell. However, the actin fibers were sometimes thin and short. At the end of most actin fibers, bride green,

or when overlapping with the red stained fibers, orange spots indicate the vinculin staining, representative of FA plaques.
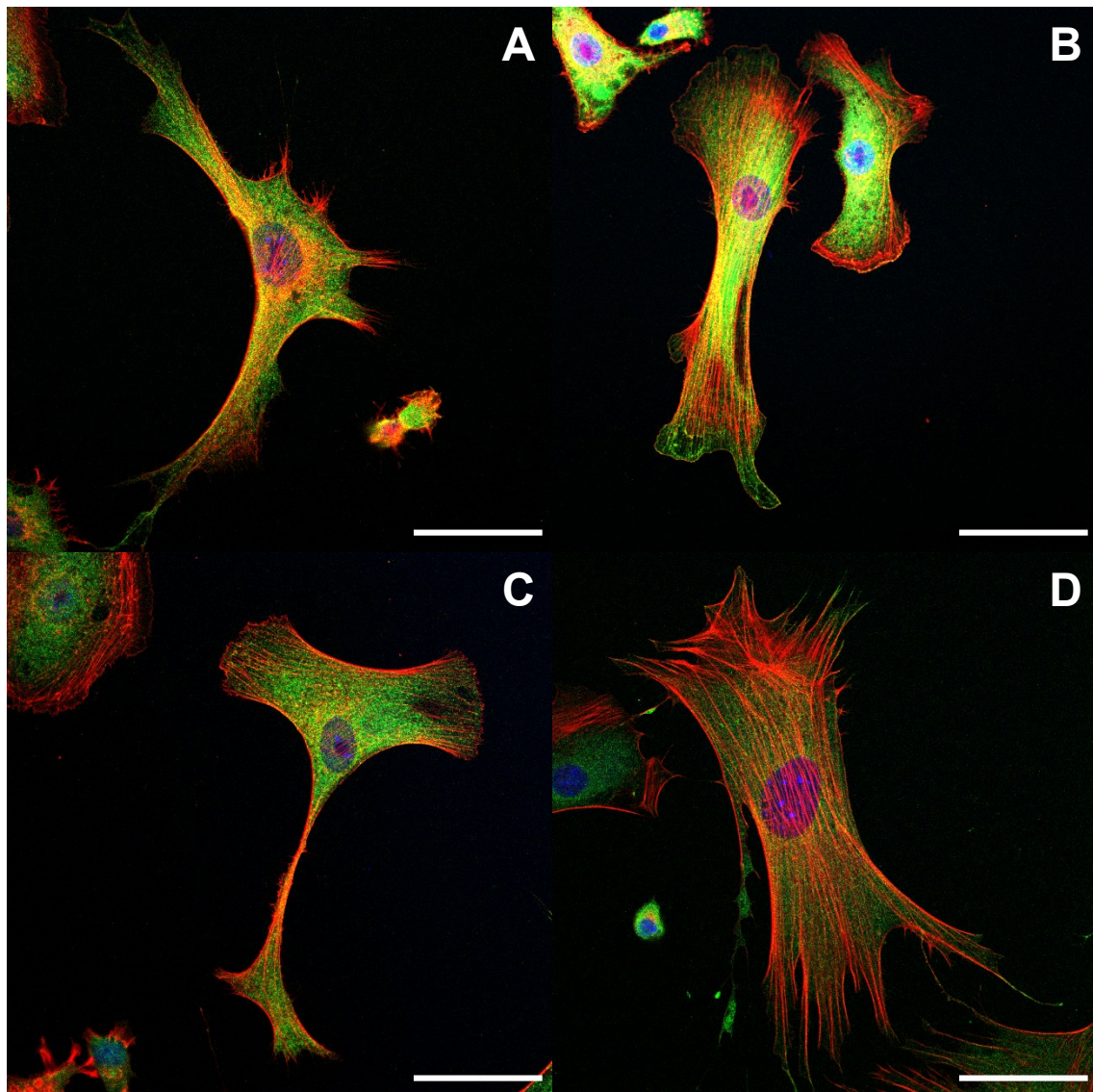
Figure 25: Immunofluorescence staining of 3T3 mouse fibroblasts. Vinculin (green), actin fibers (red) and nuclei (blue) have been stained to gain qualitative information of cell adhesion on PEMs with PLL as polycation. A and B show cells on PEM with CS 2 as polyanion (PLL/CS 2). C and D show the cells on PEM with PCS 2 as polyanion in the final three layers (PLL/PCS 2). At the end of some actin fibers, bigger green (due to overlapping sometimes orange) spots are focal adhesions of the cells. The low number of FAs indicate a rather weak cell adhesion and cells being … Scale bar: 50 µm.

The 3T3 cells adhering to PLL/CS 2 (Figure 25, A & B) were widely spread, with extending filopodia in especially in Figure 25 A. Actin fibers are extended over the whole cells, being long but thin. Only some of them were connected to FA plaques. Cells seeded onto PLL/PCS 2 PEM coatings showed similar behavior, but as visible in Figure 25 D, some of them have very pronounced longitudinal actin fibers. The formation of FAs is not enhanced, the vinculin staining revealed only few FA formations.
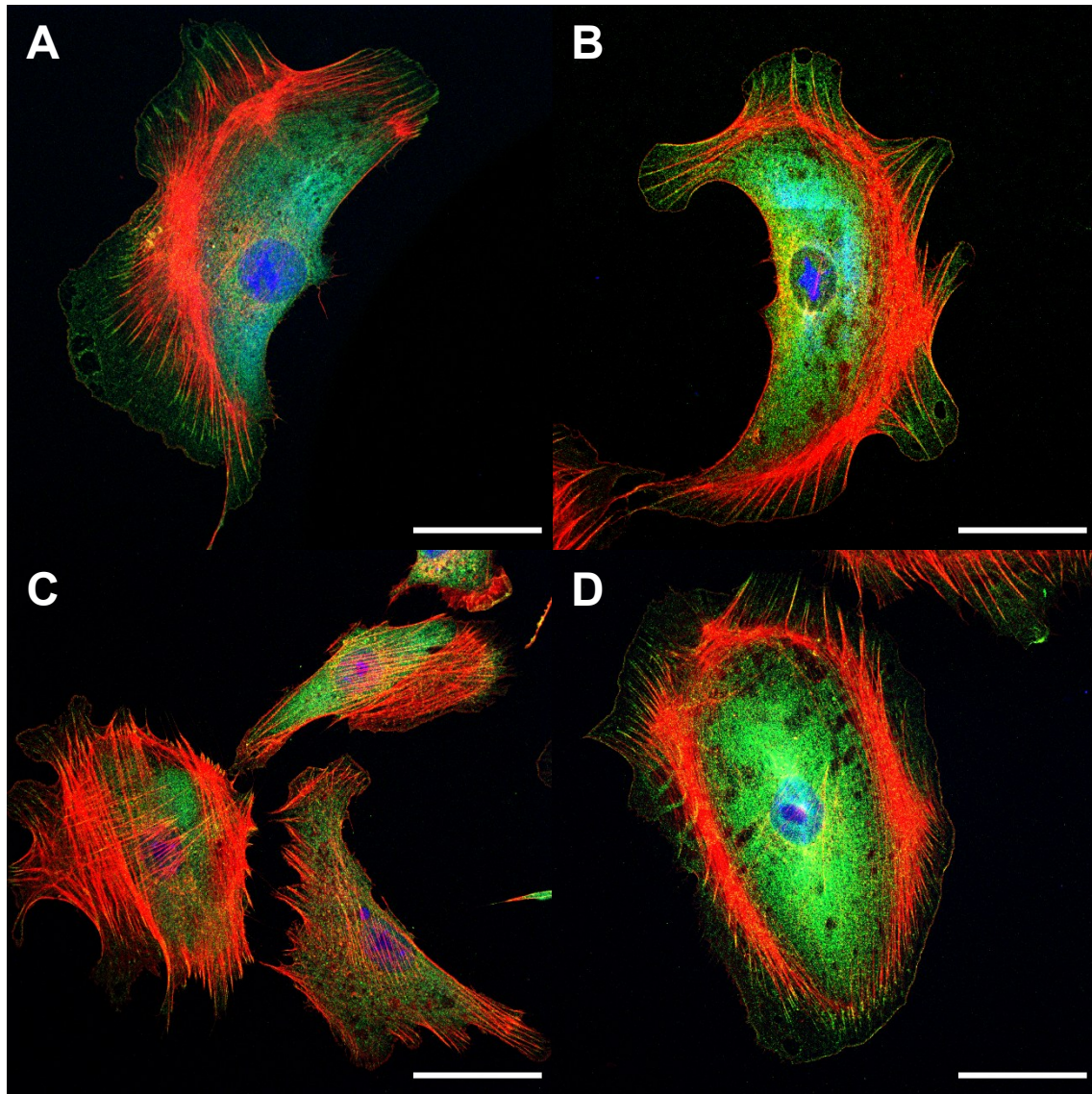
Figure 26: Immunofluorescence staining of 3T3 mouse fibroblasts. Vinculin (green), actin fibers (red) and nuclei (blue) have been stained to gain qualitative information of cell adhesion on PEMs with QCHI as polycation. A and B show cells on PEM with CS 2 as polyanion (QCHI/CS 2). C and D show the cells on PEM with PCS 2 as polyanion in the final three layers (QCHI/PCS 2). At the end of many actin fibers bigger green spots are visible. These are focal adhesions (FA) of the cells, their connection to the substrate. Scale bar: 50 µm

Cells on QCHI-containing surfaces showed similar characteristics (see Figure 26). They were somewhat more rounded and with less-to-non or only very short filopodia stretching out. However, the longitudinal action fibers were distinctly visible and thick, even though they were mostly limited to the circumference of the cells. The adhering cells on QCHI/CS 2 and QCHI/PCS 2 showed increased FA formation (see Figure 26, A/B and C/D, respectively). Many actin fibers are connected to bride and fairly elongated green spots, corresponding to vinculin accumulations at the FA plaques.

The 3T3 cells showed good adhesion qualities for all multilayer systems. As discussed before, multilayers containing sulphate groups, which all examined surfaces contained, lead to more spread morphology and bigger cell contact areas[232,240]. This might explain, why even

90

on the PLL containing multilayers, cells were spread and adherent. Only the thin actin fibers and formation of small focal complexes lead to the assumption that PEM films containing PLL, as stated for the viability and activity tests, related to the possible cytotoxic effect of PLL present unbound in solution[235,236]. This furthermore supports the conclusion that PLL containing PEM films possess a lower stiffness and maybe even stability. In contrary, on multilayers fabricated from QCHI with CS 2 or PCS 2, the pronounced, thick actin fibers and the formation of many and large focal adhesions suggested that these surfaces were attractive for cell adhesion[241]. The influence of the positive charge of quaternized chitosan could facilitate the adhesion of negatively charged ECM proteins (e.g., fibronectin) from the serum, leading to improved cellular adhesion[97,242]. Beside surface chemistry, mechanical properties of the surface influence the cellular adhesion. Stiffer surfaces promote cellular adhesion, while softer surfaces often lead to cell rounding, nucleus condensation and loss of focal adhesion[243]. This would suggest that the PEM substrates provide sufficient stiffness for cellular adhesion, as most of the cells possessed a spread morphology.

4.4.3. Summary biological characterization

The multilayers composed of the polycations PLL or QCHI in combination with different CS derivatives (CS 1, CS 2, PCS 1, and PCS 2) were tested if they were biocompatible. Therefore, cells originating from the three different germ layers, namely endoderm (HepG2), mesoderm (3T3) and ectoderm (HaCaT), were seeded on PEM coated substrates and viability and growth assays were conducted. These assays showed that in comparison of the polycation present in the PEM system, PLL possessed the less favorable properties for cellular interactions. Viability and growth of the cells, except for HepG2, was lower as for the TCPS positive control. Even though HepG2 cells showed better performance on PLL containing substrates, a change in their phenotype was observed. Regarding the CS derivatives, the cell assays revealed the clear preference towards CS 2 and PCS 2 with higher DS_S. For nearly all PEM coatings, they showed high values for viability and activity (except HaCaT cells seeded on QCHI/CS 2 surfaces). Especially QCHI/PCS 2 surfaces showed in all assays and for all types of cells comparable results to TCPS surfaces, hence should be entitled with high biocompatibility. To gain some more information, immunofluorescence assays using 3T3 fibroblasts were performed in the PEM systems using CS 2 and PCS 2 in combination with PLL and QCHI. The Immunofluorescence staining of 3T3 cells promotes the aforementioned statements for these surfaces, especially for QCHIS/PCS 2. Cells showed a spread morphology and pronounced actin fibers connected to FA plaques, indicating good cellular adhesion via integrins to the substrate and well-being of the cells. Generally, these results are very

promising to further develop these surfaces using QCHI in combination with PNIPAm-grafted-cellulose sulphates for biomedical applications.

4.5. Thermoresponsive properties of the multilayer systems – cellular detachment

At this point, the multilayer systems have been thoroughly investigated concerning their physicochemical and biological properties. The biocompatibility of certain PEM systems has been proven and further use and development as promising biomaterial coating suggested. The initial concept was to fabricate thermoresponsive surfaces from the newly synthesized cellulose sulphates by grafting PNIPAm side chains onto them. The thermoresponsive properties of PCS solutions has been proven. The formation, characterization, and biocompatibility of multilayers with these CS derivatives has been shown. The ultimate goal is the temperature-controlled cell detachment in form of cell layers from these surfaces. When the environmental temperature is decreased from 37 °C to below the LCST of PNIPAm, the surface hydrates and stiffness decreases, which is the basis for cell detachment[22]. Subsequently, the hydration and thereafter swelling of PNIPAm results in a more hydrophilic and softer surface, facilitating protein desorption and consequently leading to cell detachment. Unfortunately, it could not be shown in this study. Several experiments have been conducted using the thoroughly investigated multilayer systems based on the synthesized CS derivatives and 3T3 fibroblasts seeded on them. However, after different culturing time points (24h, 4 days, 7 days), cells were not able to detach from PEM coated surface, neither at room temperature nor at 4 °C. This could be due to multiple reasons. Most likely, the low DS_{PNIPAm} of PCSs and their inclusion into polyelectrolyte multilayers are responsible. Other works demonstrate thermoresponsive cell detachment with a different grafting technique, were PNIPAm chains with high MW and grafted in high density are applied[244]. On the other hand, the combination of low amount of PNIPAm inside a multilayer that due to a high degree of interpenetration reduces the degree of freedom of the PNIPAm chains due to steric hindrance[166,245], leading to the restricted conformational changes, subsequently resulting in insufficient change in surface properties and no thermoresponsive behavior. However, the possibility to finetune the DS_{PNIPAm} on the PCS derivatives and the properties of the PEM offers the potential for further development of the system with the goal to achieve thermoresponsive properties enough to achieve cell detachment.

5. Summary and Conclusion

The development of novel materials and their applications for biomedical purposes requires conscientious studies. Starting with the development and optimization of the synthesis process, continued by characterization of the product and subsequent utilization possibility need thorough experimental examination. This study focused on combining the abundance and beneficial properties of biopolymers with the thermoresponsive behavior of PNIPAm to fabricate surface for cell sheet engineering. Beginning with cellulose, the successful synthesis of cellulose sulphate with different DS_S and the subsequent grafting of PNIPAm onto the cellulose backbone has been shown. Additionally, the thermoresponsive behavior of the PCS in solution was presented. With regard for biomedical applications in tissue engineering, the aim was to fabricate surface coatings based on the CS and PCS polyelectrolytes using the established and cost-effective LbL method. With regard to the popularity and beneficial properties, CHI as polycation of biological origin was chosen as opposing material to the anionic CS derivatives. The initial examination of CHI-CS PEM films revealed that using these polymers, the formation of multilayers using the LbL technique is possible. Surface coatings in nanometer scale were successfully fabricated and characterized. However, the primary results indicated stability issues of the films at physiological conditions. Based on the insight from this initial study, the composition of the multilayer was adjusted and two polycations with increased charge stability at pH 7.4 were chosen: PLL, as one of the most used biological polycations in LbL fabrication research, and QCHI, a water-soluble modification of CHI that showed promising results in biomedical research. The examination with these two polymers presented basically comparable results to the preliminary studies with CHI. PEM films with nanometer scale thickness, negative surface charge and moderate hydrophilic wettability were fabricated. However, SPR and ellipsometry after exposing the films to physiological pH values in PBS solution still revealed decreasing angle shifts and thickness, respectively. After the further examination with zeta surface potential measurements and the confirmation of the negative surface potential, probably attributed to the CS derivatives as outermost layer, supported the thesis of structural changes of the polymer chains, leading to deswelling or collapsing of the polycations due to protonation at higher pH values and the subsequent weaker electrostatic charge.

Based on that conclusion, the combination of CS derivatives with PLL and QCHI, respectively, were subjected to biological characterization. As stated in the objective, cell types originated from each germ layer, endoderm, mesoderm, and ectoderm, were used and cell viability and growth, when seeded onto PEM coated surfaces, examined. 3T3 mouse

fibroblast, HepG2 hepatocellular carcinoma cells and HaCaT human keratinocytes were used for the examination. For all cell types, the PLL containing multilayers showed some problems, related to the cytotoxicity of the polycation[235,236]. Especially the combination of lower sulphated CS 1 and PCS 1 with reduce ion pairing resulted in a lower overall stability of the PEM, allowing for the exertion of the cytotoxic effect auf PLL. For 3T3 cells, the adhesion, and the unintentional detachment after a couple of days were noticeable shortcomings. The alteration of the HepG2 phenotype and the poor initial adhesion and growth for HaCaT cells added to the problematic biological interactions of PLL containing PEM. It should be mentioned that especially PLL/PCS 2 multilayers showed the best results for all cell types, but still not comparable to the viability and growth of the cells on TCPS. Under exclusion of the obviously cytotoxic QCHI/CS 1 PEM films, due to low sulfation degree of CS 1 and hence low PEM stability, the other QCHI-CS derivative-combinations showed promising cell viability and growth results comparable to TCPS. The cytotoxic effect of the polycation is more pronounced for PLL due to the presence in the surface region due to intermingling layers. Even though, QCHI/CS 2 showed low cell adhesion and growth for HaCaT cells and QCHI/PCS 1 showed for all types of cells lower cell viability and growth compared to TCPS. The highest biocompatibility is ascribed to QCHI/PCS 2 films. All cell types were viable and proliferated well, in the same manner as on TCPS. Additionally, the immunofluorescence images revealed formation of strong actin fibers and focal adhesion complexes on QCHI/PCS 2 coated glass, supporting the biocompatibility of this system.

With regard the gathered results up to this point, the fabrication of CS and PCS derivatives and the formation of multilayers with polycations was very successful, providing biocompatible surface coatings for biomedical applications. But the biggest drawback that could not be solved over the course of this study is the missing thermoresponsivity of the PEM films. Cell detachment after different days of culture could not be observed at different temperatures below 30 °C. Even though PCS showed thermoresponsive behavior when diluted in water, the amount of the material incorporated in the multilayers is not enough or the effect is somehow inhibited due to diverse interactions within the multilayer hindering the conformational and hydrational property changes of PCS.

Nevertheless, this study might be a promising guideline for further research and development towards the successful fabrication of thermoresponsive polyelectrolyte multilayers of biopolymers using LbL technique. The potential to easily modify the multilayer properties, the low-cost fabrication process, and the ability to incorporate proteins or growth factors make them promising biomedical surface coatings for tissue engineering purposes.

6. Literature

(1)   Hudecki, A.; Kiryczyński, G.; Łos, M. J. Chapter 7 - Biomaterials, Definition, Overview. In *Stem Cells and Biomaterials for Regenerative Medicine*; Łos, M. J., Hudecki, A., Wiecheć, E., Eds.; Academic Press, 2019; pp 85–98. https://doi.org/10.1016/B978-0-12-812258-7.00007-1.

(2)   *Biomaterials in Tissue Engineering and Regenerative Medicine: From Basic Concepts to State-of-the-Art Approaches*; Bhaskar, B., Sreenivasa Rao, P., Kasoju, N., Nagarjuna, V., Baadhe, R. R., Eds.; Springer Singapore: Singapore, 2021. https://doi.org/10.1007/978-981-16-0002-9.

(3)   Tathe, A.; Ghodke, M.; Nikalje, A. P. A BRIEF REVIEW: BIOMATERIALS AND THEIR APLLICATION. *2*.

(4)   Kuchinka, J.; Willems, C.; Telyshev, D. V.; Groth, T. Control of Blood Coagulation by Hemocompatible Material Surfaces—A Review. *Bioengineering* **2021**, *8* (12), 215. https://doi.org/10.3390/bioengineering8120215.

(5)   Navarro, M.; Michiardi, A.; Castaño, O.; Planell, J. a. Biomaterials in Orthopaedics. *J. R. Soc. Interface* **2008**, *5* (27), 1137–1158. https://doi.org/10.1098/rsif.2008.0151.

(6)   Anouz, R.; Groth, T. Chapter 13:Biomimetic Surface Modifications of Biomaterials Using a Layer-by-Layer Technique. In *Soft Matter for Biomedical Applications*; 2021; pp 326–362. https://doi.org/10.1039/9781839161124-00326.

(7)   Takahashi, H.; Okano, T. Thermally-Triggered Fabrication of Cell Sheets for Tissue Engineering and Regenerative Medicine. *Adv. Drug Deliv. Rev.* **2019**, *138*, 276–292. https://doi.org/10.1016/j.addr.2019.01.004.

(8)   Mason, C.; Dunnill, P. A Brief Definition of Regenerative Medicine. *Regen. Med.* **2008**, *3* (1), 1–5. https://doi.org/10.2217/17460751.3.1.1.

(9)   Matsuura, K.; Utoh, R.; Nagase, K.; Okano, T. Cell Sheet Approach for Tissue Engineering and Regenerative Medicine. *J. Controlled Release* **2014**, *190*, 228–239. https://doi.org/10.1016/j.jconrel.2014.05.024.

(10)   *Regenerative medicine - Latest research and news | Nature.* https://www.nature.com/subjects/regenerative-medicine (accessed 2021-12-27).

(11)   *Tissue Engineering and Regenerative Medicine.* https://www.nibib.nih.gov/science-education/science-topics/tissue-engineering-and-regenerative-medicine (accessed 2021-12-29).

(12)   Francis, M. E.; Uriel, S.; Brey, E. M. Endothelial Cell–Matrix Interactions in Neovascularization. *Tissue Eng. Part B Rev.* **2008**, *14* (1), 19–32. https://doi.org/10.1089/teb.2007.0115.

(13)   Kobayashi, J.; Kikuchi, A.; Aoyagi, T.; Okano, T. Cell Sheet Tissue Engineering: Cell Sheet Preparation, Harvesting/Manipulation, and Transplantation. *J. Biomed. Mater. Res. A* **2019**, *107* (5), 955–967. https://doi.org/10.1002/jbm.a.36627.

(14)   Yamato, M.; Okano, T. Cell Sheet Engineering. *Mater. Today* **2004**, *7* (5), 42–47. https://doi.org/10.1016/S1369-7021(04)00234-2.

(15)   Cooperstein, M. A.; Canavan, H. E. Assessment of Cytotoxicity of (*N* -Isopropyl Acrylamide) and Poly(*N* -Isopropyl Acrylamide)-Coated Surfaces. *Biointerphases* **2013**, *8* (1), 19. https://doi.org/10.1186/1559-4106-8-19.

(16)   da Silva, R. M. P.; Mano, J. F.; Reis, R. L. Smart Thermoresponsive Coatings and Surfaces for Tissue Engineering: Switching Cell-Material Boundaries. *Trends Biotechnol.* **2007**, *25* (12), 577–583. https://doi.org/10.1016/j.tibtech.2007.08.014.

(17)   Huang, H.-L.; Hsing, H.-W.; Lai, T.-C.; Chen, Y.-W.; Lee, T.-R.; Chan, H.-T.; Lyu, P.-C.; Wu, C.-L.; Lu, Y.-C.; Lin, S.-T.; Lin, C.-W.; Lai, C.-H.; Chang, H.-T.; Chou, H.-C.; Chan, H.-L. Trypsin-Induced Proteome Alteration during Cell Subculture in Mammalian Cells. *J. Biomed. Sci.* **2010**, *17* (1), 36. https://doi.org/10.1186/1423-0127-17-36.

(18)   CHEN, G.; QI, Y.; NIU, L.; DI, T.; ZHONG, J.; FANG, T.; YAN, W. Application of the Cell Sheet Technique in Tissue Engineering. *Biomed. Rep.* **2015**, *3* (6), 749–757. https://doi.org/10.3892/br.2015.522.

(19)   Moschouris, K.; Firoozi, N.; Kang, Y. The Application of Cell Sheet Engineering in the Vascularization of Tissue Regeneration. *Regen. Med.* **2016**, *11* (6), 559–570. https://doi.org/10.2217/rme-2016-0059.

(20)   Nagase, K.; Yamato, M.; Kanazawa, H.; Okano, T. Poly(N -Isopropylacrylamide)-Based Thermoresponsive Surfaces Provide New Types of Biomedical Applications. *Biomaterials* **2018**, *153*, 27–48. https://doi.org/10.1016/j.biomaterials.2017.10.026.

(21)   Kushida, A.; Yamato, M.; Konno, C.; Kikuchi, A.; Sakurai, Y.; Okano, T. Decrease in Culture Temperature Releases Monolayer Endothelial Cell Sheets Together with Deposited Fibronectin Matrix from Temperature-Responsive Culture Surfaces. *J. Biomed. Mater. Res.* **1999**, *45* (4), 355–362. https://doi.org/10.1002/(SICI)1097-4636(19990615)45:4<355::AID-JBM10>3.0.CO;2-7.

(22)   Doberenz, F.; Zeng, K.; Willems, C.; Zhang, K.; Groth, T. Thermoresponsive Polymers and Their Biomedical Application in Tissue Engineering – a Review. *J. Mater. Chem. B* **2020**, *8* (4), 607–628. https://doi.org/10.1039/C9TB02052G.

(23)   Kleinman, H. K.; Luckenbill-Edds, L.; Cannon, F. W.; Sephel, G. C. Use of Extracellular Matrix Components for Cell Culture. *Anal. Biochem.* **1987**, *166* (1), 1–13. https://doi.org/10.1016/0003-2697(87)90538-0.

(24)   Kleinman, H. K.; Klebe, R. J.; Martin, G. R. Role of Collagenous Matrices in the Adhesion and Growth of Cells. *J. Cell Biol.* **1981**, *88* (3), 473–485.

(25)   Hynes, R. O. Extracellular Matrix: Not Just Pretty Fibrils. *Science* **2009**, *326* (5957), 1216. https://doi.org/10.1126/science.1176009.

(26)   Alberts, B.; Johnson, A.; Lewis, J.; Raff, M.; Roberts, K.; Walter, P. Cell Junctions, Cell Adhesion, and the Extracellular Matrix. In *Molecular Biology of the Cell. 4th edition*; Garland Science, 2002.

(27)   Ekblom, P.; Vestweber, D.; Kemler, R. Cell-Matrix Interactions and Cell Adhesion During Development. *Annu. Rev. Cell Biol.* **1986**, *2* (1), 27–47. https://doi.org/10.1146/annurev.cb.02.110186.000331.

(28)   Köwitsch, A.; Zhou, G.; Groth, T. Medical Application of Glycosaminoglycans: A Review. *J. Tissue Eng. Regen. Med.* **2017**, *12* (1), e23–e41. https://doi.org/10.1002/term.2398.

(29)   Freeman, R.; Boekhoven, J.; Dickerson, M. B.; Naik, R. R.; Stupp, S. I. Biopolymers and Supramolecular Polymers as Biomaterials for Biomedical Applications. *MRS Bull.* **2015**, *40* (12), 1089–1101. https://doi.org/10.1557/mrs.2015.270.

(30)   Bosman, F. T.; Stamenkovic, I. Functional Structure and Composition of the Extracellular Matrix. *J. Pathol.* **2003**, *200* (4), 423–428. https://doi.org/10.1002/path.1437.

(31)   Yang, Y.; Lu, Y.-T.; Zeng, K.; Heinze, T.; Groth, T.; Zhang, K. Recent Progress on Cellulose-Based Ionic Compounds for Biomaterials. *Adv. Mater.* **2021**, *33* (28), 2000717. https://doi.org/10.1002/adma.202000717.

(32)   Guillame-Gentil, O.; Semenov, O.; Roca, A. S.; Groth, T.; Zahn, R.; Vörös, J.; Zenobi-Wong, M. Engineering the Extracellular Environment: Strategies for Building 2D and 3D Cellular Structures. *Adv. Mater. Deerfield Beach Fla* **2010**, *22* (48), 5443–5462. https://doi.org/10.1002/adma.201001747.

(33)   Schaefer, L.; Schaefer, R. M. Proteoglycans: From Structural Compounds to Signaling Molecules. *Cell Tissue Res.* **2010**, *339* (1), 237–246. https://doi.org/10.1007/s00441-009-0821-y.

(34)   Rnjak-Kovacina, J.; Tang, F.; Whitelock, J. M.; Lord, M. S. Glycosaminoglycan and Proteoglycan-Based Biomaterials: Current Trends and Future Perspectives. *Adv. Healthc. Mater.* **2018**, *7* (6), 1701042. https://doi.org/10.1002/adhm.201701042.

(35)   Iozzo, R. V.; Schaefer, L. Proteoglycan Form and Function: A Comprehensive Nomenclature of Proteoglycans. *Matrix Biol.* **2015**, *42*, 11–55. https://doi.org/10.1016/j.matbio.2015.02.003.

(36)   Gattazzo, F.; Urciuolo, A.; Bonaldo, P. Extracellular Matrix: A Dynamic Microenvironment for Stem Cell Niche. *Biochim. Biophys. Acta BBA - Gen. Subj.* **2014**, *1840* (8), 2506–2519. https://doi.org/10.1016/j.bbagen.2014.01.010.

(37)   Mammoto, T.; Ingber, D. E. Mechanical Control of Tissue and Organ Development. *Development* **2010**, *137* (9), 1407–1420. https://doi.org/10.1242/dev.024166.

(38)   Engler, A. J.; Sen, S.; Sweeney, H. L.; Discher, D. E. Matrix Elasticity Directs Stem Cell Lineage Specification. *Cell* **2006**, *126* (4), 677–689. https://doi.org/10.1016/j.cell.2006.06.044.

(39)   Park, J. S.; Chu, J. S.; Tsou, A. D.; Diop, R.; Tang, Z.; Wang, A.; Li, S. The Effect of Matrix Stiffness on the Differentiation of Mesenchymal Stem Cells in Response to TGF-β. *Biomaterials* **2011**, *32* (16), 3921–3930. https://doi.org/10.1016/j.biomaterials.2011.02.019.

(40)   Bafico, A.; Aaronson, S. A. Classification of Growth Factors and Their Receptors. In *Holland-Frei Cancer Medicine. 6th edition*; Kufe, D. W., Pollock, R. E., Weichselbaum, R. R., Bast, R. C., Gansler, T. S., Holland, J. F., Frei, E., Eds.; BC Decker, 2003.

(41)   Chen, D.; Zhao, M.; Mundy, G. R. Bone Morphogenetic Proteins. *Growth Factors* **2004**, *22* (4), 233–241. https://doi.org/10.1080/08977190412331279890.

(42)   Peschel, D. Steuerung des Wachstums und der Differenzierung von Zellen durch Kooperation regioseletiv-derivatisierter Polysaccharide mit Wachstumsfaktoren, Martin-Luther-Universität Halle-Wittenberg, Halle, 2012.

(43)   Chen, F.-M.; Zhang, M.; Wu, Z.-F. Toward Delivery of Multiple Growth Factors in Tissue Engineering. *Biomaterials* **2010**, *31* (24), 6279–6308. https://doi.org/10.1016/j.biomaterials.2010.04.053.

(44)   Ruoslahti, E. Structure and Biology of Proteoglycans. *Annu. Rev. Cell Biol.* **1988**, *4* (1), 229–255. https://doi.org/10.1146/annurev.cb.04.110188.001305.

(45)   Katz, B.-Z.; Zamir, E.; Bershadsky, A.; Kam, Z.; Yamada, K. M.; Geiger, B. Physical State of the Extracellular Matrix Regulates the Structure and Molecular Composition of Cell-Matrix Adhesions. *Mol. Biol. Cell* **2000**, *11* (3), 1047–1060.

(46)   Hynes, R. Integrins: A Family of Cell Surface Receptors. *Cell* **1987**, *48* (4), 549–554. https://doi.org/10.1016/0092-8674(87)90233-9.

(47)   Hynes, R. O. Integrins: Bidirectional, Allosteric Signaling Machines. *Cell* **2002**, *110* (6), 673–687. https://doi.org/10.1016/S0092-8674(02)00971-6.

(48)   Ruoslahti, E. Rgd and Other Recognition Sequences for Integrins. *Annu. Rev. Cell Dev. Biol.* **1996**, *12* (1), 697–715. https://doi.org/10.1146/annurev.cellbio.12.1.697.

(49)   Aplin, A. E.; Howe, A.; Alahari, S. K.; Juliano, R. L. Signal Transduction and Signal Modulation by Cell Adhesion Receptors: The Role of Integrins, Cadherins, Immunoglobulin-Cell Adhesion Molecules, and Selectins. *Pharmacol. Rev.* **1998**, *50* (2), 197–264.

(50)   Frisch, S. M.; Screaton, R. A. Anoikis Mechanisms. *Curr. Opin. Cell Biol.* **2001**, *13* (5), 555–562. https://doi.org/10.1016/s0955-0674(00)00251-9.

(51)   van Roy, F.; Berx, G. The Cell-Cell Adhesion Molecule E-Cadherin. *Cell. Mol. Life Sci.* **2008**, *65* (23), 3756–3788. https://doi.org/10.1007/s00018-008-8281-1.

(52)   Leckband, D.; Prakasam, A. Mechanism and Dynamics of Cadherin Adhesion. *Annu. Rev. Biomed. Eng.* **2006**, *8* (1), 259–287. https://doi.org/10.1146/annurev.bioeng.8.061505.095753.

(53)   Ekdahl, K. N.; Lambris, J. D.; Elwing, H.; Ricklin, D.; Nilsson, P. H.; Teramura, Y.; Nicholls, I. A.; Nilsson, B. Innate Immunity Activation on Biomaterial Surfaces: A Mechanistic Model and Coping Strategies. *Adv. Drug Deliv. Rev.* **2011**, *63* (12), 1042–1050. https://doi.org/10.1016/j.addr.2011.06.012.

(54)   Gumbiner, B. M. Cell Adhesion: The Molecular Basis of Tissue Architecture and Morphogenesis. *Cell* **1996**, *84* (3), 345–357. https://doi.org/10.1016/S0092-8674(00)81279-9.

(55)   Huang, S.; Ingber, D. E. The Structural and Mechanical Complexity of Cell-Growth Control. *Nat. Cell Biol.* **1999**, *1* (5), E131. https://doi.org/10.1038/13043.

(56)   Norde, W.; Lyklema, J. Why Proteins Prefer Interfaces. *J. Biomater. Sci. Polym. Ed.* **1991**, *2* (3), 183–202. https://doi.org/10.1080/09205063.1991.9756659.

(57)   Malmsten, M. *Biopolymers at Interfaces*; Marcel Dekker: New York, 2003.

(58)   Salloum, D. S.; Schlenoff, J. B. Protein Adsorption Modalities on Polyelectrolyte Multilayers. *Biomacromolecules* **2004**, *5* (3), 1089–1096. https://doi.org/10.1021/bm034522t.

(59)   Downes, S.; Mishra, A. A. Tissue-Biomaterial Interactions. In *Advanced Wound Repair Therapies*; Elsevier, 2011; pp 174–185. https://doi.org/10.1533/9780857093301.2.174.

(60)   Norde, W. Driving Forces for Protein Adsorption at Solid Surfaces. *Macromol. Symp.* **1996**, *103* (1), 5–18. https://doi.org/10.1002/masy.19961030104.

(61)   Israelachvili, J. N.; Pashley, R. M. Molecular Layering of Water at Surfaces and Origin of Repulsive Hydration Forces. *Nature* **1983**, *306* (5940), 249. https://doi.org/10.1038/306249a0.

(62)   Yuan, L.; Yu, Q.; Li, D.; Chen, H. Surface Modification to Control Protein/Surface Interactions. *Macromol. Biosci.* **2011**, *11* (8), 1031–1040. https://doi.org/10.1002/mabi.201000464.

(63)   Andrade, J. D.; Hlady, V. Protein Adsorption and Materials Biocompatibility: A Tutorial Review and Suggested Hypotheses. In *Biopolymers/Non-Exclusion HPLC*; Advances in Polymer Science; Springer Berlin Heidelberg, 1986; pp 1–63.

(64)   Ruoslahti, E.; Pierschbacher, M. D. New Perspectives in Cell Adhesion: RGD and Integrins. *Science* **1987**. https://doi.org/10.1126/science.2821619.

(65)   Bachmann, M.; Kukkurainen, S.; Hytönen, V. P.; Wehrle-Haller, B. Cell Adhesion by Integrins. *Physiol. Rev.* **2019**, *99* (4), 1655–1699. https://doi.org/10.1152/physrev.00036.2018.

(66)   Ahmad Khalili, A.; Ahmad, M. R. A Review of Cell Adhesion Studies for Biomedical and Biological Applications. *Int. J. Mol. Sci.* **2015**, *16* (8), 18149–18184. https://doi.org/10.3390/ijms160818149.

(67) Raynor, J. E.; Capadona, J. R.; Collard, D. M.; Petrie, T. A.; García, A. J. Polymer Brushes and Self-Assembled Monolayers: Versatile Platforms to Control Cell Adhesion to Biomaterials (Review). *Biointerphases* **2009**, *4* (2), FA3–FA16. https://doi.org/10.1116/1.3089252.

(68) Grinnell, F. Cellular Adhesiveness and Extracellular Substrata. *Int. Rev. Cytol.* **1978**, *53*, 65–144.

(69) Yamada, K. M.; Geiger, B. Molecular Interactions in Cell Adhesion Complexes. *Curr. Opin. Cell Biol.* **1997**, *9* (1), 76–85. https://doi.org/10.1016/S0955-0674(97)80155-X.

(70) Dubiel, E. A.; Martin, Y.; Vermette, P. Bridging the Gap Between Physicochemistry and Interpretation Prevalent in Cell–Surface Interactions. *Chem. Rev.* **2011**, *111* (4), 2900–2936. https://doi.org/10.1021/cr9002598.

(71) Bongrand, P.; Capo, C.; Depieds, R. Physics of Cell Adhesion. *Prog. Surf. Sci.* **1982**, *12* (3), 217–285. https://doi.org/10.1016/0079-6816(82)90007-7.

(72) Ma, Z.; Mao, Z.; Gao, C. Surface Modification and Property Analysis of Biomedical Polymers Used for Tissue Engineering. *Colloids Surf. B Biointerfaces* **2007**, *60* (2), 137–157. https://doi.org/10.1016/j.colsurfb.2007.06.019.

(73) Costa, R. R.; Mano, J. F. Polyelectrolyte Multilayered Assemblies in Biomedical Technologies. *Chem. Soc. Rev.* **2014**, *43* (10), 3453. https://doi.org/10.1039/c3cs60393h.

(74) Morra, M. Biomolecular Modification of Implant Surfaces. *Expert Rev. Med. Devices* **2007**, *4* (3), 361–372. https://doi.org/10.1586/17434440.4.3.361.

(75) Mas-Moruno, C. 3 - Surface Functionalization of Biomaterials for Bone Tissue Regeneration and Repair. In *Peptides and Proteins as Biomaterials for Tissue Regeneration and Repair*; Barbosa, M. A., Martins, M. C. L., Eds.; Woodhead Publishing, 2018; pp 73–100. https://doi.org/10.1016/B978-0-08-100803-4.00003-6.

(76) Morra, M. Biochemical Modification of Titanium Surfaces: Peptides and eCM Proteins. *Eur. Cell. Mater.* **2006**, *12*, 1–15. https://doi.org/10.22203/eCM.v012a01.

(77) Nouri, A.; Wen, C. Introduction to Surface Coating and Modification for Metallic Biomaterials. In *Surface Coating and Modification of Metallic Biomaterials*; Elsevier, 2015; pp 3–60. https://doi.org/10.1016/B978-1-78242-303-4.00001-6.

(78) Iler, R. K. Multilayers of Colloidal Particles. *J. Colloid Interface Sci.* **1966**, *21* (6), 569–594. https://doi.org/10.1016/0095-8522(66)90018-3.

(79) Decher, G.; Hong, J.-D. Buildup of Ultrathin Multilayer Films by a Self-Assembly Process, 1 Consecutive Adsorption of Anionic and Cationic Bipolar Amphiphiles on Charged Surfaces. *Makromol. Chem. Macromol. Symp.* **1991**, *46* (1), 321–327. https://doi.org/10.1002/masy.19910460145.

(80) Decher, G.; Hong, J. D.; Schmitt, J. Buildup of Ultrathin Multilayer Films by a Self-Assembly Process: III. Consecutively Alternating Adsorption of Anionic and Cationic Polyelectrolytes on Charged Surfaces. *Thin Solid Films* **1992**, *210–211*, 831–835. https://doi.org/10.1016/0040-6090(92)90417-A.

(81) Decher, G.; Eckle, M.; Schmitt, J.; Struth, B. Layer-by-Layer Assembled Multicomposite Films. *Curr. Opin. Colloid Interface Sci.* **1998**, *3* (1), 32–39. https://doi.org/10.1016/S1359-0294(98)80039-3.

(82) Borges, J.; Mano, J. F. Molecular Interactions Driving the Layer-by-Layer Assembly of Multilayers. *Chem. Rev.* **2014**, *114* (18), 8883–8942. https://doi.org/10.1021/cr400531v.

(83)   Asghari, F.; Samiei, M.; Adibkia, K.; Akbarzadeh, A.; Davaran, S. Biodegradable and Biocompatible Polymers for Tissue Engineering Application: A Review. *Artif. Cells Nanomedicine Biotechnol.* **2017**, *45* (2), 185–192. https://doi.org/10.3109/21691401.2016.1146731.

(84)   Reddy, M. S. B.; Ponnamma, D.; Choudhary, R.; Sadasivuni, K. K. A Comparative Review of Natural and Synthetic Biopolymer Composite Scaffolds. *Polymers* **2021**, *13* (7), 1105. https://doi.org/10.3390/polym13071105.

(85)   Malda, J.; Visser, J.; Melchels, F. P.; Jüngst, T.; Hennink, W. E.; Dhert, W. J. A.; Groll, J.; Hutmacher, D. W. 25th Anniversary Article: Engineering Hydrogels for Biofabrication. *Adv. Mater.* **2013**, *25* (36), 5011–5028. https://doi.org/10.1002/adma.201302042.

(86)   Van Vlierberghe, S.; Dubruel, P.; Schacht, E. Biopolymer-Based Hydrogels As Scaffolds for Tissue Engineering Applications: A Review. *Biomacromolecules* **2011**, *12* (5), 1387–1408. https://doi.org/10.1021/bm200083n.

(87)   Seddiqi, H.; Oliaei, E.; Honarkar, H.; Jin, J.; Geonzon, L. C.; Bacabac, R. G.; Klein-Nulend, J. Cellulose and Its Derivatives: Towards Biomedical Applications. *Cellulose* **2021**, *28* (4), 1893–1931. https://doi.org/10.1007/s10570-020-03674-w.

(88)   Russo, L.; Cipolla, L. Glycomics: New Challenges and Opportunities in Regenerative Medicine. *Chem. Weinh. Bergstr. Ger.* **2016**, *22* (38), 13380–13388. https://doi.org/10.1002/chem.201602156.

(89)   Tchobanian, A.; Van Oosterwyck, H.; Fardim, P. Polysaccharides for Tissue Engineering: Current Landscape and Future Prospects. *Carbohydr. Polym.* **2019**, *205*, 601–625. https://doi.org/10.1016/j.carbpol.2018.10.039.

(90)   Tiwari, S.; Patil, R.; Bahadur, P. Polysaccharide Based Scaffolds for Soft Tissue Engineering Applications. *Polymers* **2018**, *11* (1), 1. https://doi.org/10.3390/polym11010001.

(91)   Zhao, D.; Yu, S.; Sun, B.; Gao, S.; Guo, S.; Zhao, K. Biomedical Applications of Chitosan and Its Derivative Nanoparticles. *Polymers* **2018**, *10* (4), 462. https://doi.org/10.3390/polym10040462.

(92)   Chen, Q.; Xiao, S.; Shi, S. Q.; Cai, L. Synthesis, Characterization, and Antibacterial Activity of N-Substituted Quaternized Chitosan and Its Cellulose- Based Composite Film. **2020**, 14.

(93)   Piras, A. M.; Esin, S.; Benedetti, A.; Maisetta, G.; Fabiano, A.; Zambito, Y.; Batoni, G. Antibacterial, Antibiofilm, and Antiadhesive Properties of Different Quaternized Chitosan Derivatives. *Int. J. Mol. Sci.* **2019**, *20* (24), 6297. https://doi.org/10.3390/ijms20246297.

(94)   Chen, K.-Y.; Zeng, S.-Y. Preparation and Characterization of Quaternized Chitosan Coated Alginate Microspheres for Blue Dextran Delivery. *Polymers* **2017**, *9* (12), 210. https://doi.org/10.3390/polym9060210.

(95)   Siqueira, G.; Bras, J.; Dufresne, A. Cellulosic Bionanocomposites: A Review of Preparation, Properties and Applications. *Polymers* **2010**, *2* (4), 728–765. https://doi.org/10.3390/polym2040728.

(96)   Zhang, Q.; Lin, D.; Yao, S. Review on Biomedical and Bioengineering Applications of Cellulose Sulphate. *Carbohydr. Polym.* **2015**, *132*, 311–322. https://doi.org/10.1016/j.carbpol.2015.06.041.

(97)   Aggarwal, N.; Altgärde, N.; Svedhem, S.; Zhang, K.; Fischer, S.; Groth, T. Study on Multilayer Structures Prepared from Heparin and Semi-Synthetic Cellulose Sulfates as Polyanions and Their Influence on Cellular Response. *Colloids Surf. B Biointerfaces* **2014**, *116*, 93–103. https://doi.org/10.1016/j.colsurfb.2013.12.043.

(98)   Groth, T.; Willems, C.; Zhang, K.; Fischer, S. DEVELOPMENT OF BIOACTIVE CELLULOSE SULFATES FOR BIOMEDICAL APPLICATIONS. *Acta Medica Median.* **2020**, 12. https://doi.org/10.5633/amm.2020.0308.

(99)   Aggarwal, N.; Altgärde, N.; Svedhem, S.; Zhang, K.; Fischer, S.; Groth, T. Effect of Molecular Composition of Heparin and Cellulose Sulphate on Multilayer Formation and Cell Response. *Langmuir* **2013**, *29* (45), 13853–13864. https://doi.org/10.1021/la4028157.

(100)   Menezes, R.; Sherman, L.; Rameshwar, P.; Arinzeh, T. L. Scaffolds Containing GAG-Mimetic Cellulose Sulphate Promote TGF-β Interaction and MSC Chondrogenesis over Native GAGs. *J. Biomed. Mater. Res. A* **2023**, *n/a* (n/a). https://doi.org/10.1002/jbm.a.37496.

(101)   Zeng, K.; Groth, T.; Zhang, K. Recent Advances in Artificially Sulphated Polysaccharides for Applications in Cell Growth and Differentiation, Drug Delivery, and Tissue Engineering. *Chembiochem Eur. J. Chem. Biol.* **2019**, *20* (6), 737–746. https://doi.org/10.1002/cbic.201800569.

(102)   Aggarwal, N.; Altgärde, N.; Svedhem, S.; Michanetzis, G.; Missirlis, Y.; Groth, T. Tuning Cell Adhesion and Growth on Biomimetic Polyelectrolyte Multilayers by Variation of pH During Layer-by-Layer Assembly. *Macromol. Biosci.* **2013**, *13* (10), 1327–1338. https://doi.org/10.1002/mabi.201300153.

(103)   Zeng, K.; Doberenz, F.; Lu, Y.-T.; Nong, J. P.; Fischer, S.; Groth, T.; Zhang, K. Synthesis of Thermoresponsive PNIPAm-Grafted Cellulose Sulfates for Bioactive Multilayers via Layer-by-Layer Technique. *ACS Appl. Mater. Interfaces* **2022**, *14* (43), 48384–48396. https://doi.org/10.1021/acsami.2c12803.

(104)   Lu, Y.-T.; Hung, P.-T.; Zeng, K.; Woelk, C.; Fuhrmann, B.; Zhang, K.; Groth, T. Surface Properties and Bioactivity of PNIPAm-Grafted-Chitosan/Chondroitin Multilayers. *Smart Mater. Med.* **2023**, *4*, 356–367. https://doi.org/10.1016/j.smaim.2022.11.008.

(105)   Picart, C.; Lavalle, Ph.; Hubert, P.; Cuisinier, F. J. G.; Decher, G.; Schaaf, P.; Voegel, J.-C. Buildup Mechanism for Poly(L -Lysine)/Hyaluronic Acid Films onto a Solid Surface. *Langmuir* **2001**, *17* (23), 7414–7424. https://doi.org/10.1021/la010848g.

(106)   Crouzier, T.; Picart, C. Ion Pairing and Hydration in Polyelectrolyte Multilayer Films Containing Polysaccharides. *Biomacromolecules* **2009**, *10* (2), 433–442. https://doi.org/10.1021/bm8012378.

(107)   Teixeira, R.; Reis, R. L.; Pashkuleva, I. Influence of the Sulfation Degree of Glycosaminoglycans on Their Multilayer Assembly with Poly- l -Lysine. *Colloids Surf. B Biointerfaces* **2016**, *145*, 567–575. https://doi.org/10.1016/j.colsurfb.2016.05.069.

(108)   Niepel, M. S.; Almouhanna, F.; Ekambaram, B. K.; Menzel, M.; Heilmann, A.; Groth, T. Cross-Linking Multilayers of Poly-l-Lysine and Hyaluronic Acid: Effect on Mesenchymal Stem Cell Behavior: *Int. J. Artif. Organs* **2018**. https://doi.org/10.1177/0391398817752598.

(109)   Zhu, H.; Liu, R.; Shang, Y.; Sun, L. Polylysine Complexes and Their Biomedical Applications. *Eng. Regen.* **2023**, *4* (1), 20–27. https://doi.org/10.1016/j.engreg.2022.11.001.

(110)   Mazia, D.; Schatten, G.; Sale, W. Adhesion of Cells to Surfaces Coated with Polylysine. Applications to Electron Microscopy. *J. Cell Biol.* **1975**, *66* (1), 198–200. https://doi.org/10.1083/jcb.66.1.198.

(111)   Hoffman, A. S. Stimuli-Responsive Polymers: Biomedical Applications and Challenges for Clinical Translation. *Adv. Drug Deliv. Rev.* **2013**, *65* (1), 10–16. https://doi.org/10.1016/j.addr.2012.11.004.

(112)   Wei, M.; Gao, Y.; Li, X.; J. Serpe, M. Stimuli-Responsive Polymers and Their Applications. *Polym. Chem.* **2017**, *8* (1), 127–143. https://doi.org/10.1039/C6PY01585A.

(113)   *Smart Polymers and Their Applications*, Second edition.; Aguilar, M. R., San Román, J., Eds.; Woodhead Publishing in materials; Woodhead Publishing is an imprint of Elsevier: Duxford, United Kingdom; Cambridge, MA, 2019.

(114)   Zhang, Q.; Hoogenboom, R. Polymers with Upper Critical Solution Temperature Behavior in Alcohol/Water Solvent Mixtures. *Prog. Polym. Sci.* **2015**, *48*, 122–142. http://dx.doi.org/10.1016/j.progpolymsci.2015.02.003.

(115)   Kudaibergenov, S.; Jaeger, W.; Laschewsky, A. Polymeric Betaines: Synthesis, Characterization, and Application. In *Supramolecular Polymers Polymeric Betains Oligomers*; Springer Berlin Heidelberg: Berlin, Heidelberg, 2006; Vol. 201, pp 157–224. https://doi.org/10.1007/12_078.

(116)   Arotçaréna, M.; Heise, B.; Ishaya, S.; Laschewsky, A. Switching the Inside and the Outside of Aggregates of Water-Soluble Block Copolymers with Double Thermoresponsivity. *J. Am. Chem. Soc.* **2002**, *124* (14), 3787–3793. https://doi.org/10.1021/ja012167d.

(117)   Seuring, J.; Agarwal, S. Polymers with Upper Critical Solution Temperature in Aqueous Solution. *Macromol. Rapid Commun.* **2012**, *33* (22), 1898–1920. https://doi.org/10.1002/marc.201200433.

(118)   Southall, N. T.; Dill, K. A.; Haymet, A. D. J. A View of the Hydrophobic Effect. *J. Phys. Chem. B* **2002**, *106* (3), 521–533. https://doi.org/10.1021/jp015514e.

(119)   Fujishige, S.; Kubota, K.; Ando, I. Phase Transition of Aqueous Solutions of Poly(N-Isopropylacrylamide) and Poly(N-Isopropylmethacrylamide). *J. Phys. Chem.* **1989**, *93* (8), 3311–3313. https://doi.org/10.1021/j100345a085.

(120)   Brun-Graeppi, A. K. A. S.; Richard, C.; Bessodes, M.; Scherman, D.; Merten, O.-W. Thermoresponsive Surfaces for Cell Culture and Enzyme-Free Cell Detachment. *Prog. Polym. Sci.* **2010**, *35* (11), 1311–1324. https://doi.org/10.1016/j.progpolymsci.2010.07.007.

(121)   Dai, S.; Ravi, P.; Tam, K. C. Thermo- and Photo-Responsive Polymeric Systems. *Soft Matter* **2009**. https://doi.org/10.1039/b820044k.

(122)   Schmaljohann, D. Thermo- and pH-Responsive Polymers in Drug Delivery☆. *Adv. Drug Deliv. Rev.* **2006**, *58* (15), 1655–1670. https://doi.org/10.1016/j.addr.2006.09.020.

(123)   Graziano, G. On the Temperature-Induced Coil to Globule Transition of Poly-N-Isopropylacrylamide in Dilute Aqueous Solutions. *Int. J. Biol. Macromol.* **2000**, *27* (1), 89–97. https://doi.org/10.1016/S0141-8130(99)00122-1.

(124)   Kubota, Kenji.; Fujishige, Shouei.; Ando, Isao. Single-Chain Transition of Poly(N-Isopropylacrylamide) in Water. *J. Phys. Chem.* **1990**, *94* (12), 5154–5158. https://doi.org/10.1021/j100375a070.

(125)   Pelton, R. Poly(N-Isopropylacrylamide) (PNIPAm) Is Never Hydrophobic. *J. Colloid Interface Sci.* **2010**, *348* (2), 673–674. https://doi.org/10.1016/j.jcis.2010.05.034.

(126)   de las Heras Alarcon, C.; Pennadam, S.; Alexander, C. Stimuli Responsive Polymers for Biomedical Applications. *ChemInform* **2005**, *36* (26). https://doi.org/10.1002/chin.200526252.

(127)   Alexandridis, P.; Alan Hatton, T. Poly(Ethylene Oxide)⬜poly(Propylene Oxide)⬜poly(Ethylene Oxide) Block Copolymer Surfactants in Aqueous Solutions and at Interfaces: Thermodynamics, Structure, Dynamics, and Modeling. *Colloids Surf. Physicochem. Eng. Asp.* **1995**, *96* (1–2), 1–46. https://doi.org/10.1016/0927-7757(94)03028-X.

(128)   Rassing, J.; Attwood, D. Ultrasonic Velocity and Light-Scattering Studies on the Polyoxyethylene—Polyoxypropylene Copolymer Pluronic F127 in Aqueous Solution. *Int. J. Pharm.* **1982**, *13* (1), 47–55. https://doi.org/10.1016/0378-5173(82)90141-7.

(129)   Vadnere, M.; Amidon, G.; Lindenbaum, S.; Haslam, J. L. Thermodynamic Studies on the Gel-Sol Transition of Some Pluronic Polyols. *Int. J. Pharm.* **1984**, *22* (2), 207–218. https://doi.org/10.1016/0378-5173(84)90022-X.

(130)   Wang, P.; Johnston, T. P. Kinetics of Sol-to-Gel Transition for Poloxamer Polyols. *J. Appl. Polym. Sci.* **1991**, *43* (2), 283–292. https://doi.org/10.1002/app.1991.070430207.

(131)   Wanka, G.; Hoffmann, H.; Ulbricht, W. Phase Diagrams and Aggregation Behavior of Poly(Oxyethylene)-Poly(Oxypropylene)-Poly(Oxyethylene) Triblock Copolymers in Aqueous Solutions. *Macromolecules* **1994**, *27* (15), 4145–4159. https://doi.org/10.1021/ma00093a016.

(132)   Schmolka, I. R. Physical Basis for Poloxamer Interactions. *Ann. N. Y. Acad. Sci.* **1994**, *720* (1), 92–97. https://doi.org/10.1111/j.1749-6632.1994.tb30437.x.

(133)   Cohn, D.; Sosnik, A.; Levy, A. Improved Reverse Thermo-Responsive Polymeric Systems. *Biomaterials* **2003**, *24* (21), 3707–3714. https://doi.org/10.1016/S0142-9612(03)00245-X.

(134)   Khan, S.; Minhas, M. U.; Tekko, I. A.; Donnelly, R. F.; Thakur, R. R. S. Evaluation of Microneedles-Assisted in Situ Depot Forming Poloxamer Gels for Sustained Transdermal Drug Delivery. *Drug Deliv. Transl. Res.* **2019**, *9* (4), 764–782. https://doi.org/10.1007/s13346-019-00617-2.

(135)   Almeida, H.; Amaral, M. H.; Lobão, P.; Lobo, J. M. S. Pluronic® F-127 and Pluronic Lecithin Organogel (PLO): Main Features and Their Applications in Topical and Transdermal Administration of Drugs. *J. Pharm. Pharm. Sci.* **2012**, *15* (4), 592. https://doi.org/10.18433/J3HW2B.

(136)   Cohn, D.; Sosnik, A.; Garty, S. Smart Hydrogels for in Situ Generated Implants. *Biomacromolecules* **2005**, *6* (3), 1168–1175. https://doi.org/10.1021/bm0495250.

(137)   Gioffredi, E.; Boffito, M.; Calzone, S.; Giannitelli, S. M.; Rainer, A.; Trombetta, M.; Mozetic, P.; Chiono, V. Pluronic F127 Hydrogel Characterization and Biofabrication in Cellularized Constructs for Tissue Engineering Applications. *Procedia CIRP* **2016**, *49*, 125–132. https://doi.org/10.1016/j.procir.2015.11.001.

(138)   Hospodiuk, M.; Moncal, K. K.; Dey, M.; Ozbolat, I. T. Extrusion-Based Biofabrication in Tissue Engineering and Regenerative Medicine. In *3D Printing and Biofabrication*; Ovsianikov, A., Yoo, J., Mironov, V., Eds.; Springer International Publishing: Cham, 2016; pp 1–27. https://doi.org/10.1007/978-3-319-40498-1_10-1.

(139)   Müller, M.; Becher, J.; Schnabelrauch, M.; Zenobi-Wong, M. Nanostructured Pluronic Hydrogels as Bioinks for 3D Bioprinting. *Biofabrication* **2015**, *7* (3), 035006. https://doi.org/10.1088/1758-5090/7/3/035006.

(140)   Dutta, S.; Cohn, D. Temperature and pH Responsive 3D Printed Scaffolds. *J. Mater. Chem. B* **2017**, *5* (48), 9514–9521. https://doi.org/10.1039/C7TB02368E.

(141)   Cortez-Lemus, N. A.; Licea-Claverie, A. Poly(N -Vinylcaprolactam), a Comprehensive Review on a Thermoresponsive Polymer Becoming Popular. *Prog. Polym. Sci.* **2016**, *53*, 1–51. https://doi.org/10.1016/j.progpolymsci.2015.08.001.

(142)   Lim, Y. M.; Jeun, J. P.; Lee, J. H.; Lee, Y. M.; Nho, Y. C. Cell Sheet Detachment from Poly(N-Vinylcaprolactam-Co-N-Iso- Propylacrylamide) Grafted onto Tissue Culture Polystyrene Dishes. 6.

(143) Lee, B.; Jiao, A.; Yu, S.; You, J. B.; Kim, D.-H.; Im, S. G. Initiated Chemical Vapor Deposition of Thermoresponsive Poly(N-Vinylcaprolactam) Thin Films for Cell Sheet Engineering. *Acta Biomater.* **2013**, *9* (8), 7691–7698. https://doi.org/10.1016/j.actbio.2013.04.049.

(144) Sala, R. L.; Kwon, M. Y.; Kim, M.; Gullbrand, S. E.; Henning, E. A.; Mauck, R. L.; Camargo, E. R.; Burdick, J. A. <sup/> Thermosensitive Poly(N-Vinylcaprolactam) Injectable Hydrogels for Cartilage Tissue Engineering. *Tissue Eng. Part A* **2017**, *23* (17–18), 935–945. https://doi.org/10.1089/ten.tea.2016.0464.

(145) Indulekha, S.; Arunkumar, P.; Bahadur, D.; Srivastava, R. Thermoresponsive Polymeric Gel as an On-Demand Transdermal Drug Delivery System for Pain Management. *Mater. Sci. Eng. C* **2016**, *62*, 113–122. https://doi.org/10.1016/j.msec.2016.01.021.

(146) Davis, E. C. Stability of Elastin in the Developing Mouse Aorta: A Quantitative Radioautographic Study. *Histochemistry* **1993**, *100* (1), 17–26. https://doi.org/10.1007/BF00268874.

(147) Meyer, D. E.; Chilkoti, A. Purification of Recombinant Proteins by Fusion with Thermally-Responsive Polypeptides. *Nat. Biotechnol.* **1999**, *17* (11), 1112–1115. https://doi.org/10.1038/15100.

(148) Urry, D. W.; Parker, T. M.; Reid, M. C.; Gowda, D. C. Biocompatibility of the Bioelastic Materials, Poly(GVGVP) and Its γ-Irradiation Cross-Linked Matrix: Summary of Generic Biological Test Results. *J. Bioact. Compat. Polym.* **1991**, *6* (3), 263–282. https://doi.org/10.1177/088391159100600306.

(149) Betre, H.; Ong, S. R.; Guilak, F.; Chilkoti, A.; Fermor, B.; Setton, L. A. Chondrocytic Differentiation of Human Adipose-Derived Adult Stem Cells in Elastin-like Polypeptide. *Biomaterials* **2006**, *27* (1), 91–99. https://doi.org/10.1016/j.biomaterials.2005.05.071.

(150) Annabi, N.; Mithieux, S. M.; Boughton, E. A.; Ruys, A. J.; Weiss, A. S.; Dehghani, F. Synthesis of Highly Porous Crosslinked Elastin Hydrogels and Their Interaction with Fibroblasts in Vitro. *Biomaterials* **2009**, *30* (27), 4550–4557. https://doi.org/10.1016/j.biomaterials.2009.05.014.

(151) Yeo, G. C.; Aghaei-Ghareh-Bolagh, B.; Brackenreg, E. P.; Hiob, M. A.; Lee, P.; Weiss, A. S. Fabricated Elastin. *Adv. Healthc. Mater.* **2015**, *4* (16), 2530–2556. https://doi.org/10.1002/adhm.201400781.

(152) Zhang, Y.-N.; Avery, R. K.; Vallmajo-Martin, Q.; Assmann, A.; Vegh, A.; Memic, A.; Olsen, B. D.; Annabi, N.; Khademhosseini, A. A Highly Elastic and Rapidly Crosslinkable Elastin-Like Polypeptide-Based Hydrogel for Biomedical Applications. *Adv. Funct. Mater.* **2015**, *25* (30), 4814–4826. https://doi.org/10.1002/adfm.201501489.

(153) Fletcher, E. E.; Yan, D.; Kosiba, A. A.; Zhou, Y.; Shi, H. Biotechnological Applications of Elastin-like Polypeptides and the Inverse Transition Cycle in the Pharmaceutical Industry. *Protein Expr. Purif.* **2019**, *153*, 114–120. https://doi.org/10.1016/j.pep.2018.09.006.

(154) Bessa, P. C.; Machado, R.; Nürnberger, S.; Dopler, D.; Banerjee, A.; Cunha, A. M.; Rodríguez-Cabello, J. C.; Redl, H.; van Griensven, M.; Reis, R. L.; Casal, M. Thermoresponsive Self-Assembled Elastin-Based Nanoparticles for Delivery of BMPs. *J. Controlled Release* **2010**, *142* (3), 312–318. https://doi.org/10.1016/j.jconrel.2009.11.003.

(155) MacEwan, S. R.; Chilkoti, A. Applications of Elastin-like Polypeptides in Drug Delivery. *J. Controlled Release* **2014**, *190*, 314–330. https://doi.org/10.1016/j.jconrel.2014.06.028.

(156)   Yamada, N.; Okano, T.; Sakai, H.; Karikusaa', F. Thermo-Responsive Polymeric Surfaces; Control of Attachment and Detachment of Cultured Cells. *Makromoleculare Chem. Rapid Commun.* **1990**, No. 11, 571–576.

(157)   Okano, T.; Yamada, N.; Sakai, H.; Sakurai, Y. A Novel Recovery System for Cultured Cells Using Plasma-Treated Polystyrene Dishes Grafted with Poly(N-Isopropylacrylamide). *J. Biomed. Mater. Res.* **1993**, *27* (10), 1243–1251. https://doi.org/10.1002/jbm.820271005.

(158)   Okano, T.; Yamada, N.; Okuhara, M.; Sakai, H.; Sakurai, Y. Mechanism of Cell Detachment from Temperature-Modulated, Hydrophilic-Hydrophobic Polymer Surfaces. *Biomaterials* **1995**, *16* (4), 297–303. https://doi.org/10.1016/0142-9612(95)93257-E.

(159)   Yamato, M.; Okuhara, M.; Karikusa, F.; Kikuchi, A.; Sakurai, Y.; Okano, T. Signal Transduction and Cytoskeletal Reorganization Are Required for Cell Detachment from Cell Culture Surfaces Grafted with a Temperature-Responsive Polymer. *J. Biomed. Mater. Res.* **1999**, *44* (1), 44–52. https://doi.org/10.1002/(SICI)1097-4636(199901)44:1<44::AID-JBM5>3.0.CO;2-X.

(160)   Kikuchi, A.; Okuhara, M.; Karikusa, F.; Sakurai, Y.; Okano, T. Two-Dimensional Manipulation of Confluently Cultured Vascular Endothelial Cells Using Temperature-Responsive Poly(N-Isopropylacrylamide)-Grafted Surfaces. *J. Biomater. Sci. Polym. Ed.* **1998**, *9* (12), 1331–1348. https://doi.org/10.1163/156856298X00424.

(161)   Nath, N.; Chilkoti, A. Creating "Smart" Surfaces Using Stimuli Responsive Polymers. *Adv. Mater.* **2002**, *14* (17), 1243–1247. https://doi.org/10.1002/1521-4095(20020903)14:17<1243::AID-ADMA1243>3.0.CO;2-M.

(162)   Teichmann, J.; Nitschke, M.; Pette, D.; Valtink, M.; Gramm, S.; Härtel, F. V.; Noll, T.; Funk, R. H. W.; Engelmann, K.; Werner, C. Thermo-Responsive Cell Culture Carriers Based on Poly(Vinyl Methyl Ether)—the Effect of Biomolecular Ligands to Balance Cell Adhesion and Stimulated Detachment. *Sci. Technol. Adv. Mater.* **2015**, *16* (4), 045003. https://doi.org/10.1088/1468-6996/16/4/045003.

(163)   Nagase, K.; Okano, T.; Kanazawa, H. Poly(N -Isopropylacrylamide) Based Thermoresponsive Polymer Brushes for Bioseparation, Cellular Tissue Fabrication, and Nano Actuators. *Nano-Struct. Nano-Objects* **2018**, *16*, 9–23. https://doi.org/10.1016/j.nanoso.2018.03.010.

(164)   Serpe, M. J.; Jones, C. D.; Lyon, L. A. Layer-by-Layer Deposition of Thermoresponsive Microgel Thin Films. *Langmuir* **2003**, *19* (21), 8759–8764. https://doi.org/10.1021/la034391h.

(165)   Glinel, K.; Sukhorukov, G. B.; Möhwald, H.; Khrenov, V.; Tauer, K. Thermosensitive Hollow Capsules Based on Thermoresponsive Polyelectrolytes. *Macromol. Chem. Phys.* **2003**, *204* (14), 1784–1790. https://doi.org/10.1002/macp.200350033.

(166)   Jaber, J. A.; Schlenoff, J. B. Polyelectrolyte Multilayers with Reversible Thermal Responsivity. *Macromolecules* **2005**, *38* (4), 1300–1306. https://doi.org/10.1021/ma0485235.

(167)   Le, P. N.; Huynh, C. K.; Tran, N. Q. Advances in Thermosensitive Polymer-Grafted Platforms for Biomedical Applications. *Mater. Sci. Eng. C* **2018**. https://doi.org/10.1016/j.msec.2018.02.006.

(168)   Yang, J.; Yamato, M.; Shimizu, T.; Sekine, H.; Ohashi, K.; Kanzaki, M.; Ohki, T.; Nishida, K.; Okano, T. Reconstruction of Functional Tissues with Cell Sheet Engineering. *Biomaterials* **2007**, *28* (34), 5033–5043. https://doi.org/10.1016/j.biomaterials.2007.07.052.

(169)   Zollinger, A. J.; Smith, M. L. Fibronectin, the Extracellular Glue. *Matrix Biol.* **2017**, *60–61*, 27–37. https://doi.org/10.1016/j.matbio.2016.07.011.

(170)   Mi, X.; Vijayaragavan, K. S.; Heldt, C. L. Virus Adsorption of Water-Stable Quaternized Chitosan Nanofibers. *Carbohydr. Res.* **2014**, *387*, 24–29. https://doi.org/10.1016/j.carres.2014.01.017.

(171)   Reinhardt, K. A.; Kern, W. Handbook of Silicon Wafer Cleaning Technology. 709.

(172)   Delgado, A. V.; González-Caballero, F.; Hunter, R. J.; Koopal, L. K.; Lyklema, J. Measurement and Interpretation of Electrokinetic Phenomena (IUPAC Technical Report). *Pure Appl. Chem.* **2005**, *77* (10), 1753–1805. https://doi.org/10.1351/pac200577101753.

(173)   Kaszuba, M.; Corbett, J.; Watson, F. M.; Jones, A. High-Concentration Zeta Potential Measurements Using Light-Scattering Techniques. *Philos. Transact. A Math. Phys. Eng. Sci.* **2010**, *368* (1927), 4439–4451. https://doi.org/10.1098/rsta.2010.0175.

(174)   Tudos, A. J.; Schasfoort, R. B. M. Chapter 1. Introduction to Surface Plasmon Resonance. In *Handbook of Surface Plasmon Resonance*; Schasfoort, R. B. M., Tudos, A. J., Eds.; Royal Society of Chemistry: Cambridge, 2008; pp 1–14. https://doi.org/10.1039/9781847558220-00001.

(175)   Tang, Y.; Zeng, X.; Liang, J. Surface Plasmon Resonance: An Introduction to a Surface Spectroscopy Technique. *J. Chem. Educ.* **2010**, *87* (7), 742–746. https://doi.org/10.1021/ed100186y.

(176)   Rodahl, M.; Höök, F.; Krozer, A.; Brzezinski, P.; Kasemo, B. Quartz Crystal Microbalance Setup for Frequency and Q -factor Measurements in Gaseous and Liquid Environments. *Rev. Sci. Instrum.* **1995**, *66* (7), 3924–3930. https://doi.org/10.1063/1.1145396.

(177)   Voinova, M. V.; Rodahl, M.; Jonson, M.; Kasemo, B. Viscoelastic Acoustic Response of Layered Polymer Films at Fluid-Solid Interfaces: Continuum Mechanics Approach. *Phys. Scr.* **1999**, *59* (5), 391. https://doi.org/10.1238/Physica.Regular.059a00391.

(178)   Alves, N. M.; Picart, C.; Mano, J. F. Self Assembling and Crosslinking of Polyelectrolyte Multilayer Films of Chitosan and Alginate Studied by QCM and IR Spectroscopy. *Macromol. Biosci.* **2009**, *9* (8), 776–785. https://doi.org/10.1002/mabi.200800336.

(179)   LeBlanc, J.; Brick, I. Morphologic Aspects of Adhesion and Spreading Behavior of Amphibian Blastula and Gastrula Cells. *Development* **1981**, *61* (1), 145–163. https://doi.org/10.1242/dev.61.1.145.

(180)   *NIH 3T3 Cell Line Origins, Characteristics, Transfection.* http://www.nih3t3.com/ (accessed 2022-02-09).

(181)   Donato, M. T.; Tolosa, L.; Gómez-Lechón, M. J. Culture and Functional Characterization of Human Hepatoma HepG2 Cells. *Methods Mol. Biol. Clifton NJ* **2015**, *1250*, 77–93. https://doi.org/10.1007/978-1-4939-2074-7_5.

(182)   *HepG2 liver hepatocellular carcinoma cells transfection.* https://www.hepg2.com/ (accessed 2022-02-09).

(183)   Seo, M.-D.; Kang, T. J.; Lee, C. H.; Lee, A.-Y.; Noh, M. HaCaT Keratinocytes and Primary Epidermal Keratinocytes Have Different Transcriptional Profiles of Cornified Envelope-Associated Genes to T Helper Cell Cytokines. *Biomol. Ther.* **2012**, *20* (2), 171–176. https://doi.org/10.4062/biomolther.2012.20.2.171.

(184)   Colombo, I.; Sangiovanni, E.; Maggio, R.; Mattozzi, C.; Zava, S.; Corbett, Y.; Fumagalli, M.; Carlino, C.; Corsetto, P. A.; Scaccabarozzi, D.; Calvieri, S.; Gismondi, A.; Taramelli, D.; Dell'Agli, M. HaCaT Cells as a Reliable In Vitro Differentiation Model to Dissect the Inflammatory/Repair Response of Human Keratinocytes. *Mediators Inflamm.* **2017**, *2017*, 7435621. https://doi.org/10.1155/2017/7435621.

(185)   Schindelin, J.; Arganda-Carreras, I.; Frise, E.; Kaynig, V.; Longair, M.; Pietzsch, T.; Preibisch, S.; Rueden, C.; Saalfeld, S.; Schmid, B.; Tinevez, J.-Y.; White, D. J.; Hartenstein, V.; Eliceiri, K.; Tomancak, P.; Cardona, A. Fiji: An Open-Source Platform for Biological-Image Analysis. *Nat. Methods* **2012**, *9* (7), 676–682. https://doi.org/10.1038/nmeth.2019.

(186)   Zhang, K.; Brendler, E.; Fischer, S. FT Raman Investigation of Sodium Cellulose Sulphate. *Cellulose* **2010**, *17* (2), 427–435. https://doi.org/10.1007/s10570-009-9375-0.

(187)   Bedini, E.; Laezza, A.; Parrilli, M.; Iadonisi, A. A Review of Chemical Methods for the Selective Sulfation and Desulfation of Polysaccharides. *Carbohydr. Polym.* **2017**, *174*, 1224–1239. https://doi.org/10.1016/j.carbpol.2017.07.017.

(188)   Bojanić, V.; Jovanović, S.; Tabaković, R.; Tabaković, I. Synthesis and Electrochemistry of Grafted Copolymers of Cellulose with 4-Vinylpyridine, 1-Vinylimidazole, 1-Vinyl-2-Pyrrolidinone, and 9-Vinylcarbazole. *J. Appl. Polym. Sci.* **1996**, *60* (10), 1719–1725. https://doi.org/10.1002/(SICI)1097-4628(19960606)60:10<1719::AID-APP24>3.0.CO;2-Y.

(189)   Bernkop-Schnürch, A.; Kast, C. E.; Richter, M. F. Improvement in the Mucoadhesive Properties of Alginate by the Covalent Attachment of Cysteine. *J. Controlled Release* **2001**, *71* (3), 277–285. https://doi.org/10.1016/S0168-3659(01)00227-9.

(190)   Shan, J.; Nuopponen, M.; Jiang, H.; Kauppinen, E.; Tenhu, H. Preparation of Poly(N-Isopropylacrylamide)-Monolayer-Protected Gold Clusters: Synthesis Methods, Core Size, and Thickness of Monolayer. *Macromolecules* **2003**, *36* (12), 4526–4533. https://doi.org/10.1021/ma034265k.

(191)   Costa, M. C. M.; Silva, S. M. C.; Antunes, F. E. Adjusting the Low Critical Solution Temperature of Poly(N-Isopropyl Acrylamide) Solutions by Salts, Ionic Surfactants and Solvents: A Rheological Study. *J. Mol. Liq.* **2015**, *210*, 113–118. https://doi.org/10.1016/j.molliq.2015.02.008.

(192)   Zhang, Y.; Furyk, S.; Bergbreiter, D. E.; Cremer, P. S. Specific Ion Effects on the Water Solubility of Macromolecules: PNIPAm and the Hofmeister Series. *J. Am. Chem. Soc.* **2005**, *127* (41), 14505–14510. https://doi.org/10.1021/ja0546424.

(193)   Wang, C.; Liu, M.; Yuan, L.; Wang, L.; Sun, D.; Wang, Z.; Li, D.; Liu, G.; Wang, B.; Han, J. Calorimetric and Spectroscopic Studies on Temperature- and pH-Dependent Interactions of Stimuli-Responsive Poly (N-Isopropylacrylamide) with Piceatannol. *J. Chem. Thermodyn.* **2016**, *98*, 186–192. https://doi.org/10.1016/j.jct.2016.03.022.

(194)   Wu, Q.-X.; Guan, Y.-X.; Yao, S.-J. Sodium Cellulose Sulphate: A Promising Biomaterial Used for Microcarriers' Designing. *Front. Chem. Sci. Eng.* **2019**, *13* (1), 46–58. https://doi.org/10.1007/s11705-018-1723-x.

(195)   Costa, R. R.; Custódio, C. A.; Arias, F. J.; Rodríguez-Cabello, J. C.; Mano, J. F. Layer-by-Layer Assembly of Chitosan and Recombinant Biopolymers into Biomimetic Coatings with Multiple Stimuli-Responsive Properties. *Small* **2018**, *7* (18), 2640–2649. https://doi.org/10.1002/smll.201100875.

(196)   Peter, M. G. Applications and Environmental Aspects of Chitin and Chitosan. *J. Macromol. Sci. Part A* **1995**, *32* (4), 629–640. https://doi.org/10.1080/10601329508010276.

(197)   Muthukumar, M. *50th Anniversary Perspective*: A Perspective on Polyelectrolyte Solutions. *Macromolecules* **2017**, *50* (24), 9528–9560. https://doi.org/10.1021/acs.macromol.7b01929.

(198)   Ahola, S.; Myllytie, P.; Österberg, M.; Teerinen, T.; Laine, J. EFFECT OF POLYMER ADSORPTION ON CELLULOSE NANOFIBRIL WATER BINDING CAPACITY AND AGGREGATION. *BioResources* **2008**, *3* (4), 1315–1328.

(199) Lu, Y.-T. Development of Biogenic Thermoresponsive Multilayers Based on Polysaccharides for Tissue Engineering Applications. Cumulativ, Martin-Luther-Universität Halle-Wittenberg, Halle (Saale), 2023.

(200) Silva, J. M.; Caridade, S. G.; Costa, R. R.; Alves, N. M.; Groth, T.; Picart, C.; Reis, R. L.; Mano, J. F. pH Responsiveness of Multilayered Films and Membranes Made of Polysaccharides. *Langmuir* **2015**, *31* (41), 11318–11328. https://doi.org/10.1021/acs.langmuir.5b02478.

(201) Halthur, T. J.; Claesson, P. M.; Elofsson, U. M. Stability of Polypeptide Multilayers As Studied by in Situ Ellipsometry: Effects of Drying and Post-Buildup Changes in Temperature and pH. *J. Am. Chem. Soc.* **2004**, *126* (51), 17009–17015. https://doi.org/10.1021/ja0464645.

(202) Boddohi, S.; Killingsworth, C. E.; Kipper, M. J. Polyelectrolyte Multilayer Assembly as a Function of pH and Ionic Strength Using the Polysaccharides Chitosan and Heparin. *Biomacromolecules* **2008**, *9* (7), 2021–2028. https://doi.org/10.1021/bm8002573.

(203) Sui, Z.; Salloum, D.; Schlenoff, J. B. Effect of Molecular Weight on the Construction of Polyelectrolyte Multilayers: Stripping versus Sticking. *Langmuir* **2003**, *19* (6), 2491–2495. https://doi.org/10.1021/la026531d.

(204) Dunér, G.; Thormann, E.; Dėdinaitė, A. Quartz Crystal Microbalance with Dissipation (QCM-D) Studies of the Viscoelastic Response from a Continuously Growing Grafted Polyelectrolyte Layer. *J. Colloid Interface Sci.* **2013**, *408*, 229–234. https://doi.org/10.1016/j.jcis.2013.07.008.

(205) Dzhoyashvili, N. A.; Thompson, K.; Gorelov, A. V.; Rochev, Y. A. Film Thickness Determines Cell Growth and Cell Sheet Detachment from Spin-Coated Poly(*N* -Isopropylacrylamide) Substrates. *ACS Appl. Mater. Interfaces* **2016**, *8* (41), 27564–27572. https://doi.org/10.1021/acsami.6b09711.

(206) Akiyama, Y.; Kikuchi, A.; Yamato, M.; Okano, T. Ultrathin Poly(*N* -Isopropylacrylamide) Grafted Layer on Polystyrene Surfaces for Cell Adhesion/Detachment Control. *Langmuir* **2004**, *20* (13), 5506–5511. https://doi.org/10.1021/la036139f.

(207) Canavan, H. E.; Cheng, X.; Graham, D. J.; Ratner, B. D.; Castner, D. G. Surface Characterization of the Extracellular Matrix Remaining after Cell Detachment from a Thermoresponsive Polymer. *Langmuir* **2005**, *21* (5), 1949–1955. https://doi.org/10.1021/la048546c.

(208) Lu, Y.-T.; Hung, P.-T.; Zeng, K.; Menzel, M.; Schmelzer, C. E. H.; Zhang, K.; Groth, T. Sustained Growth Factor Delivery from Bioactive PNIPAm-Grafted-Chitosan/Heparin Multilayers as a Tool to Promote Growth and Migration of Cells. *Biomater. Adv.* **2023**, *154*, 213589. https://doi.org/10.1016/j.bioadv.2023.213589.

(209) Altankov, G.; Richau, K.; Groth, T. The Role of Surface Zeta Potential and Substratum Chemistry for Regulation of Dermal Fibroblasts Interaction. *Mater. Werkst.* **2003**, *34* (12), 1120–1128. https://doi.org/10.1002/mawe.200300699.

(210) Fu, J.; Ji, J.; Yuan, W.; Shen, J. Construction of Anti-Adhesive and Antibacterial Multilayer Films via Layer-by-Layer Assembly of Heparin and Chitosan. *Biomaterials* **2005**, *26* (33), 6684–6692. https://doi.org/10.1016/j.biomaterials.2005.04.034.

(211) Zhou, Y.; Yang, H.; Liu, X.; Mao, J.; Gu, S.; Xu, W. Potential of Quaternization-Functionalized Chitosan Fiber for Wound Dressing. *Int. J. Biol. Macromol.* **2013**, *52*, 327–332. https://doi.org/10.1016/j.ijbiomac.2012.10.012.

(212)   Wang, W.; Meng, Q.; Li, Q.; Liu, J.; Zhou, M.; Jin, Z.; Zhao, K. Chitosan Derivatives and Their Application in Biomedicine. *Int. J. Mol. Sci.* **2020**, *21* (2), 487. https://doi.org/10.3390/ijms21020487.

(213)   Richert, L.; Arntz, Y.; Schaaf, P.; Voegel, J.-C.; Picart, C. pH Dependent Growth of Poly(L-Lysine)/Poly(L-Glutamic) Acid Multilayer Films and Their Cell Adhesion Properties. *Surf. Sci.* **2004**, *570* (1), 13–29. https://doi.org/10.1016/j.susc.2004.06.178.

(214)   Wu, J.; Wei, W.; Wang, L.-Y.; Su, Z.-G.; Ma, G.-H. A Thermosensitive Hydrogel Based on Quaternized Chitosan and Poly(Ethylene Glycol) for Nasal Drug Delivery System. *Biomaterials* **2007**, *28* (13), 2220–2232. https://doi.org/10.1016/j.biomaterials.2006.12.024.

(215)   Nilsen-Nygaard, J.; Strand, S.; Vårum, K.; Draget, K.; Nordgård, C. Chitosan: Gels and Interfacial Properties. *Polymers* **2015**, *7* (3), 552–579. https://doi.org/10.3390/polym7030552.

(216)   Naassaoui, I.; Aschi, A. Evaluation of Properties and Structural Transitions of Poly-L-Lysine: Effects of pH and Temperature. *J. Macromol. Sci. Part B Phys.* **2019**, *58*. https://doi.org/10.1080/00222348.2019.1638593.

(217)   Benito-Arenas, R.; Doncel-Pérez, E.; Fernández-Gutiérrez, M.; Garrido, L.; García-Junceda, E.; Revuelta, J.; Bastida, A.; Fernández-Mayoralas, A. A Holistic Approach to Unravelling Chondroitin Sulfation: Correlations between Surface Charge, Structure and Binding to Growth Factors. *Carbohydr. Polym.* **2018**, *202*, 211–218. https://doi.org/10.1016/j.carbpol.2018.08.120.

(218)   Vessella, G.; Vázquez, J. A.; Valcárcel, J.; Lagartera, L.; Monterrey, D. T.; Bastida, A.; García-Junceda, E.; Bedini, E.; Fernández-Mayoralas, A.; Revuelta, J. Deciphering Structural Determinants in Chondroitin Sulphate Binding to FGF-2: Paving the Way to Enhanced Predictability of Their Biological Functions. *Polymers* **2021**, *13* (2), 313. https://doi.org/10.3390/polym13020313.

(219)   Brotzel, F.; Chu, Y. C.; Mayr, H. Nucleophilicities of Primary and Secondary Amines in Water. *J. Org. Chem.* **2007**, *72* (10), 3679–3688. https://doi.org/10.1021/jo062586z.

(220)   Lee, H. Effects of Temperature, Salt Concentration, and the Protonation State on the Dynamics and Hydrogen-Bond Interactions of Polyelectrolyte Multilayers on Lipid Membranes. *Phys. Chem. Chem. Phys.* **2016**, *18* (9), 6691–6700. https://doi.org/10.1039/C5CP08039H.

(221)   Almodóvar, J.; Place, L. W.; Gogolski, J.; Erickson, K.; Kipper, M. J. Layer-by-Layer Assembly of Polysaccharide-Based Polyelectrolyte Multilayers: A Spectroscopic Study of Hydrophilicity, Composition, and Ion Pairing. *Biomacromolecules* **2011**, *12* (7), 2755–2765. https://doi.org/10.1021/bm200519y.

(222)   Câmara, P. C. F. da; C. Balaban, R.; Hedayati, M.; C. Popat, K.; F. Martins, A.; J. Kipper, M. Novel Cationic Tannin/Glycosaminoglycan-Based Polyelectrolyte Multilayers Promote Stem Cells Adhesion and Proliferation. *RSC Adv.* **2019**, *9* (44), 25836–25846. https://doi.org/10.1039/C9RA03903A.

(223)   Kumorek, M.; Kubies, D.; Riedel, T. Protein Interactions With Quaternized Chitosan/Heparin Multilayers. *Physiol. Res.* **2016**, S253–S261. https://doi.org/10.33549/physiolres.933427.

(224)   Mehrotra, S.; Hunley, S. C.; Pawelec, K. M.; Zhang, L.; Lee, I.; Baek, S.; Chan, C. Cell Adhesive Behavior on Thin Polyelectrolyte Multilayers: Cells Attempt to Achieve Homeostasis of Its Adhesion Energy. *Langmuir* **2010**, *26* (15), 12794–12802. https://doi.org/10.1021/la101689z.

(225)   Esmaeilzadeh, P.; Köwitsch, A.; Liedmann, A.; Menzel, M.; Fuhrmann, B.; Schmidt, G.; Klehm, J.; Groth, T. Stimuli-Responsive Multilayers Based on Thiolated Polysaccharides That Affect Fibroblast Cell Adhesion. *ACS Appl. Mater. Interfaces* **2018**, *10* (10), 8507–8518. https://doi.org/10.1021/acsami.7b19022.

(226)   Koetse, M.; Laschewsky, A.; Jonas, A. M.; Wagenknecht, W. Influence of Charge Density and Distribution on the Internal Structure of Electrostatically Self-Assembled Polyelectrolyte Films. *Langmuir* **2002**, *18* (5), 1655–1660. https://doi.org/10.1021/la011280e.

(227)   Duval, J. F. L.; Küttner, D.; Werner, C.; Zimmermann, R. Electrohydrodynamics of Soft Polyelectrolyte Multilayers: Point of Zero-Streaming Current. *Langmuir* **2011**, *27* (17), 10739–10752. https://doi.org/10.1021/la202292k.

(228)   Boudou, T.; Crouzier, T.; Ren, K.; Blin, G.; Picart, C. Multiple Functionalities of Polyelectrolyte Multilayer Films: New Biomedical Applications. *Adv. Mater.* **2010**, *22* (4), 441–467. https://doi.org/10.1002/adma.200901327.

(229)   Maroudas, N. G. Adhesion and Spreading of Cells on Charged Surfaces. *J. Theor. Biol.* **1975**, *49* (2), 417–424. https://doi.org/10.1016/0022-5193(75)90182-4.

(230)   Lotfi, M.; Nejib, M.; Naceur, M. *Cell Adhesion to Biomaterials: Concept of Biocompatibility*; IntechOpen, 2013. https://doi.org/10.5772/53542.

(231)   Cai, S.; Wu, C.; Yang, W.; Liang, W.; Yu, H.; Liu, L. Recent Advance in Surface Modification for Regulating Cell Adhesion and Behaviors. *Nanotechnol. Rev.* **2020**, *9* (1), 971–989. https://doi.org/10.1515/ntrev-2020-0076.

(232)   Ren, Y.-J.; Zhang, H.; Huang, H.; Wang, X.-M.; Zhou, Z.-Y.; Cui, F.-Z.; An, Y.-H. In Vitro Behavior of Neural Stem Cells in Response to Different Chemical Functional Groups. *Biomaterials* **2009**, *30* (6), 1036–1044. https://doi.org/10.1016/j.biomaterials.2008.10.028.

(233)   Palamà, I. E.; D'Amone, S.; Coluccia, A. M. L.; Gigli, G. Micropatterned Polyelectrolyte Nanofilms Promote Alignment and Myogenic Differentiation of C2C12 Cells in Standard Growth Media. *Biotechnol. Bioeng.* **2013**, *110* (2), 586–596. https://doi.org/10.1002/bit.24626.

(234)   Sanzari, I.; Buratti, E.; Huang, R.; Tusan, C. G.; Dinelli, F.; Evans, N. D.; Prodromakis, T.; Bertoldo, M. Poly(N-Isopropylacrylamide) Based Thin Microgel Films for Use in Cell Culture Applications. *Sci. Rep.* **2020**, *10* (1), 6126. https://doi.org/10.1038/s41598-020-63228-9.

(235)   Fischer, D.; Li, Y.; Ahlemeyer, B.; Krieglstein, J.; Kissel, T. In Vitro Cytotoxicity Testing of Polycations: Influence of Polymer Structure on Cell Viability and Hemolysis. *Biomaterials* **2003**, *24* (7), 1121–1131. https://doi.org/10.1016/S0142-9612(02)00445-3.

(236)   Hall, A.; Wu, L.-P.; Parhamifar, L.; Moghimi, S. M. Differential Modulation of Cellular Bioenergetics by Poly(L -Lysine)s of Different Molecular Weights. *Biomacromolecules* **2015**, *16* (7), 2119–2126. https://doi.org/10.1021/acs.biomac.5b00533.

(237)   Picart, C.; Mutterer, J.; Richert, L.; Luo, Y.; Prestwich, G. D.; Schaaf, P.; Voegel, J.-C.; Lavalle, P. Molecular Basis for the Explanation of the Exponential Growth of Polyelectrolyte Multilayers. *Proc. Natl. Acad. Sci. U. S. A.* **2002**, *99* (20), 12531–12535. https://doi.org/10.1073/pnas.202486099.

(238)   Wittmer, C. R.; Phelps, J. A.; Lepus, C. M.; Saltzman, W. M.; Harding, M. J.; Van Tassel, P. R. Multilayer Nanofilms as Substrates for Hepatocellular Applications. *Biomaterials* **2008**, *29* (30), 4082–4090. https://doi.org/10.1016/j.biomaterials.2008.06.027.

(239)   Chang, H.-Y.; Kao, W.-L.; You, Y.-W.; Chu, Y.-H.; Chu, K.-J.; Chen, P.-J.; Wu, C.-Y.; Lee, Y.-H.; Shyue, J.-J. Effect of Surface Potential on Epithelial Cell Adhesion, Proliferation and Morphology. *Colloids Surf. B Biointerfaces* **2016**, *141*, 179–186. https://doi.org/10.1016/j.colsurfb.2016.01.049.

(240)   Gomes, T. D.; Caridade, S. G.; Sousa, M. P.; Azevedo, S.; Kandur, M. Y.; Öner, E. T.; Alves, N. M.; Mano, J. F. Adhesive Free-Standing Multilayer Films Containing Sulphated Levan for Biomedical Applications. *Acta Biomater.* **2018**, *69*, 183–195. https://doi.org/10.1016/j.actbio.2018.01.027.

(241)   Bacakova, L.; Filova, E.; Parizek, M.; Ruml, T.; Svorcik, V. Modulation of Cell Adhesion, Proliferation and Differentiation on Materials Designed for Body Implants. *Biotechnol. Adv.* **2011**, *29* (6), 739–767. https://doi.org/10.1016/j.biotechadv.2011.06.004.

(242)   Chen, Y.-H.; Chung, Y.-C.; Wang, I.-J.; Young, T.-H. Control of Cell Attachment on pH-Responsive Chitosan Surface by Precise Adjustment of Medium pH. *Biomaterials* **2012**, *33* (5), 1336–1342. https://doi.org/10.1016/j.biomaterials.2011.10.048.

(243)   Gribova, V.; Auzely-Velty, R.; Picart, C. Polyelectrolyte Multilayer Assemblies on Materials Surfaces: From Cell Adhesion to Tissue Engineering. *Chem. Mater.* **2012**, *24* (5), 854–869. https://doi.org/10.1021/cm2032459.

(244)   Takahashi, H.; Nakayama, M.; Yamato, M.; Okano, T. Controlled Chain Length and Graft Density of Thermoresponsive Polymer Brushes for Optimizing Cell Sheet Harvest. *Biomacromolecules* **2010**, *11* (8), 1991–1999. https://doi.org/10.1021/bm100342e.

(245)   Martins, G. V.; Mano, J. F.; Alves, N. M. Dual Responsive Nanostructured Surfaces for Biomedical Applications. *Langmuir* **2011**, *27* (13), 8415–8423. https://doi.org/10.1021/la200832n.

List of figures

List of tables

A. Appendix

A.1. Images of live/dead staining for different cell types

The following images were taken after cells were stained using Calcein AM and Ethidium Homodimer III using a laser scanning microscope. Living cells were green fluorescent, while the cell nuclei of dead cells was red fluorescent. The different cell types on the different PEM films were combined in one montage each.
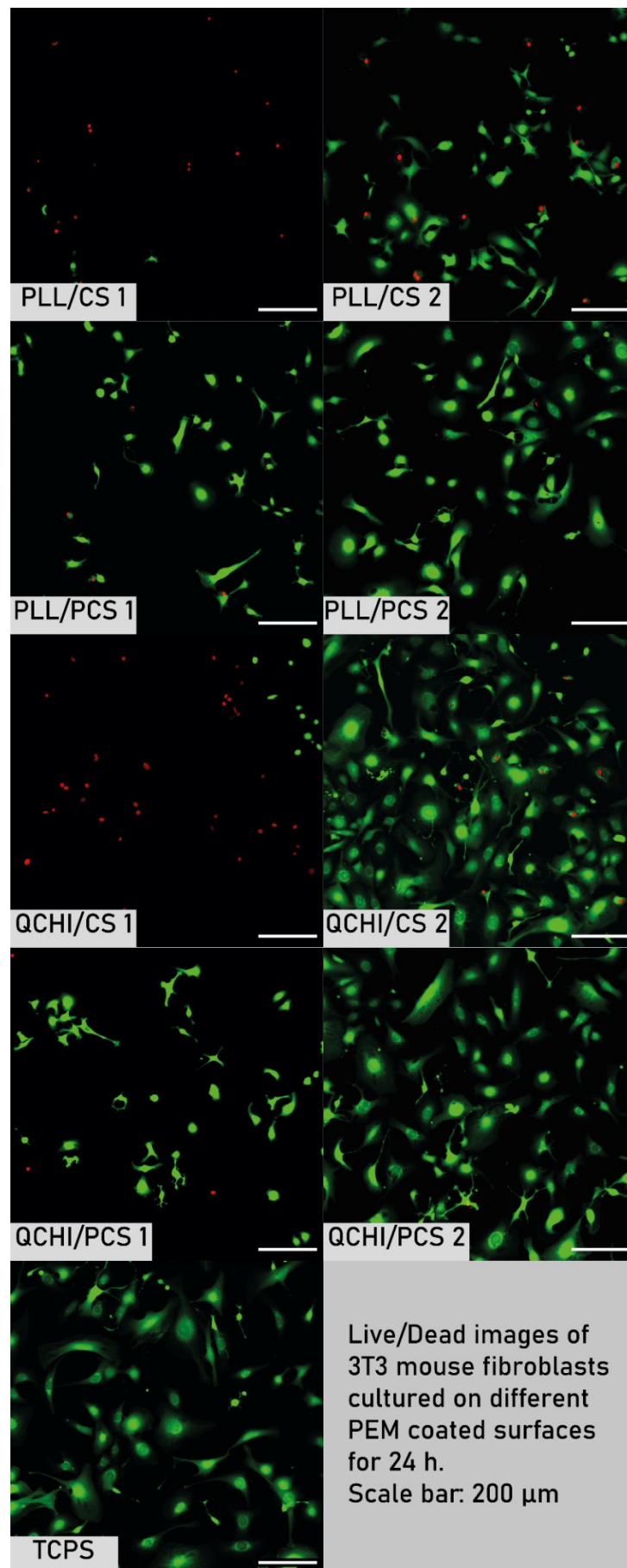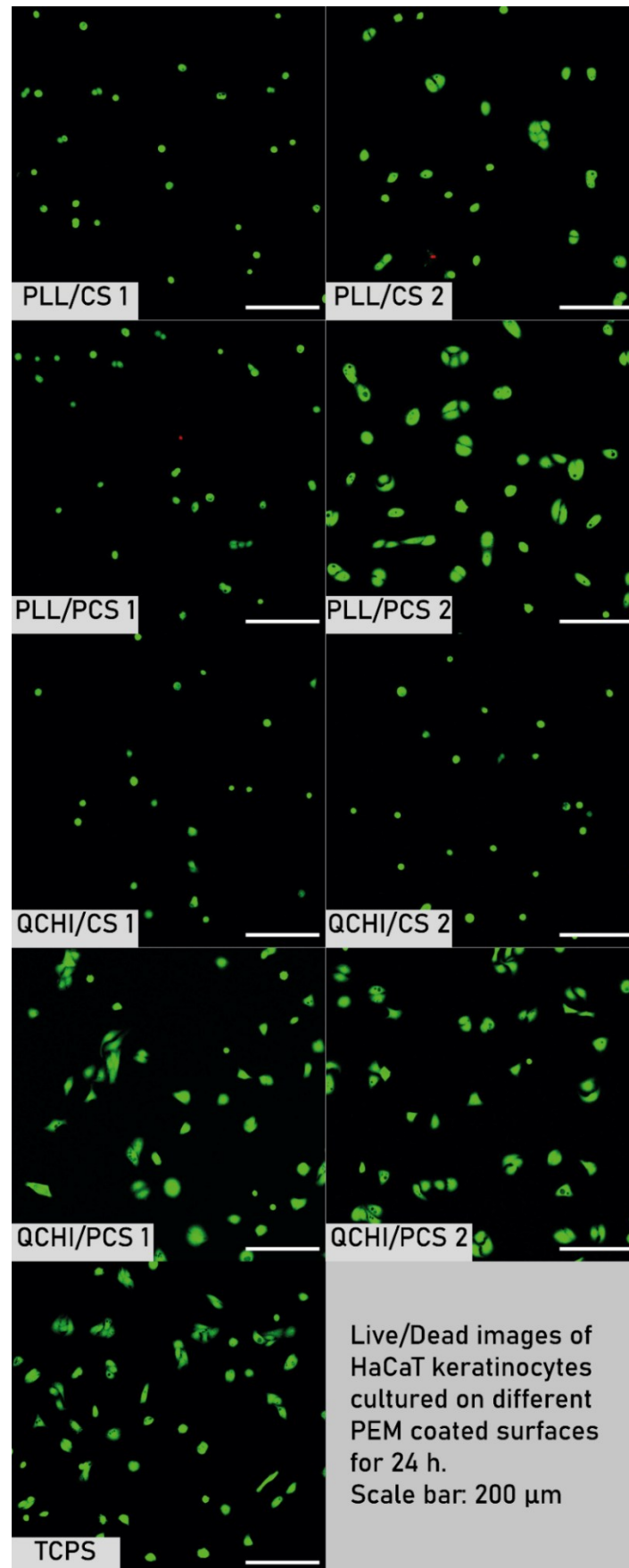
Appendix Fig. 1: Montage of Live/Dead staining images of 3T3 cells on different PEM films and TCPS. Cells were cultured for 24 h, living cell cytoskeleton is green, dead cell nuclei is red.
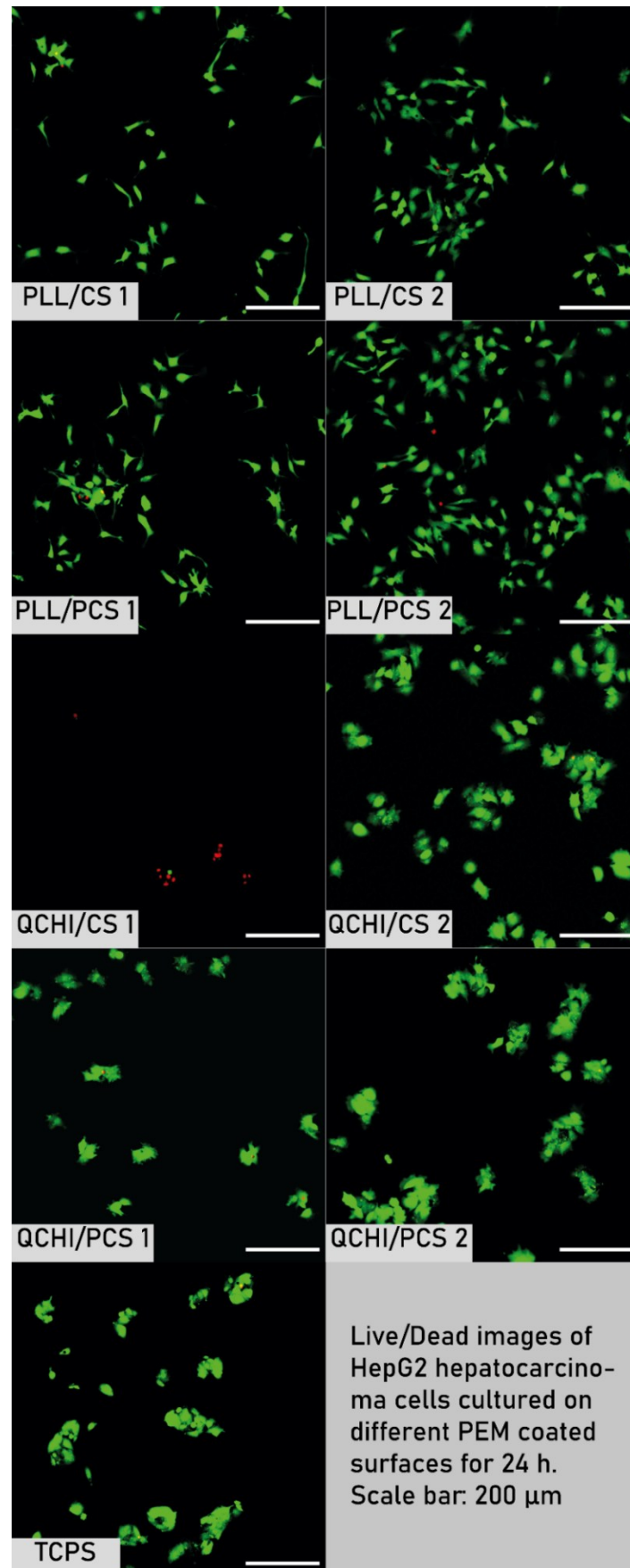
Appendix Fig. 2: Montage of Live/Dead staining images of HepG2 cells on different PEM films and TCPS. Cells were cultured for 24 h, living cell cytoskeleton is green, dead cell nuclei is red. Cells on PLL-containing PEM films developed an atypical phenotype for HEpG2 cells. On QCHI-PEM films, the aggregated and less extended phenotype classically ascribed to HepG2 cells was observable.

Appendix Fig. 3: Montage of Live/Dead staining images of HaCaT cells on different PEM films and TCPS. Cells were cultured for 24 h, living cell cytoskeleton is green, dead cell nuclei is red. Cell number distinctly lower compared to HepG2 or 3T3 cells seeded on the films. Surprisingly low cell attachment for QCHI/CS 2. Typical HaCaT aggregates are visible.
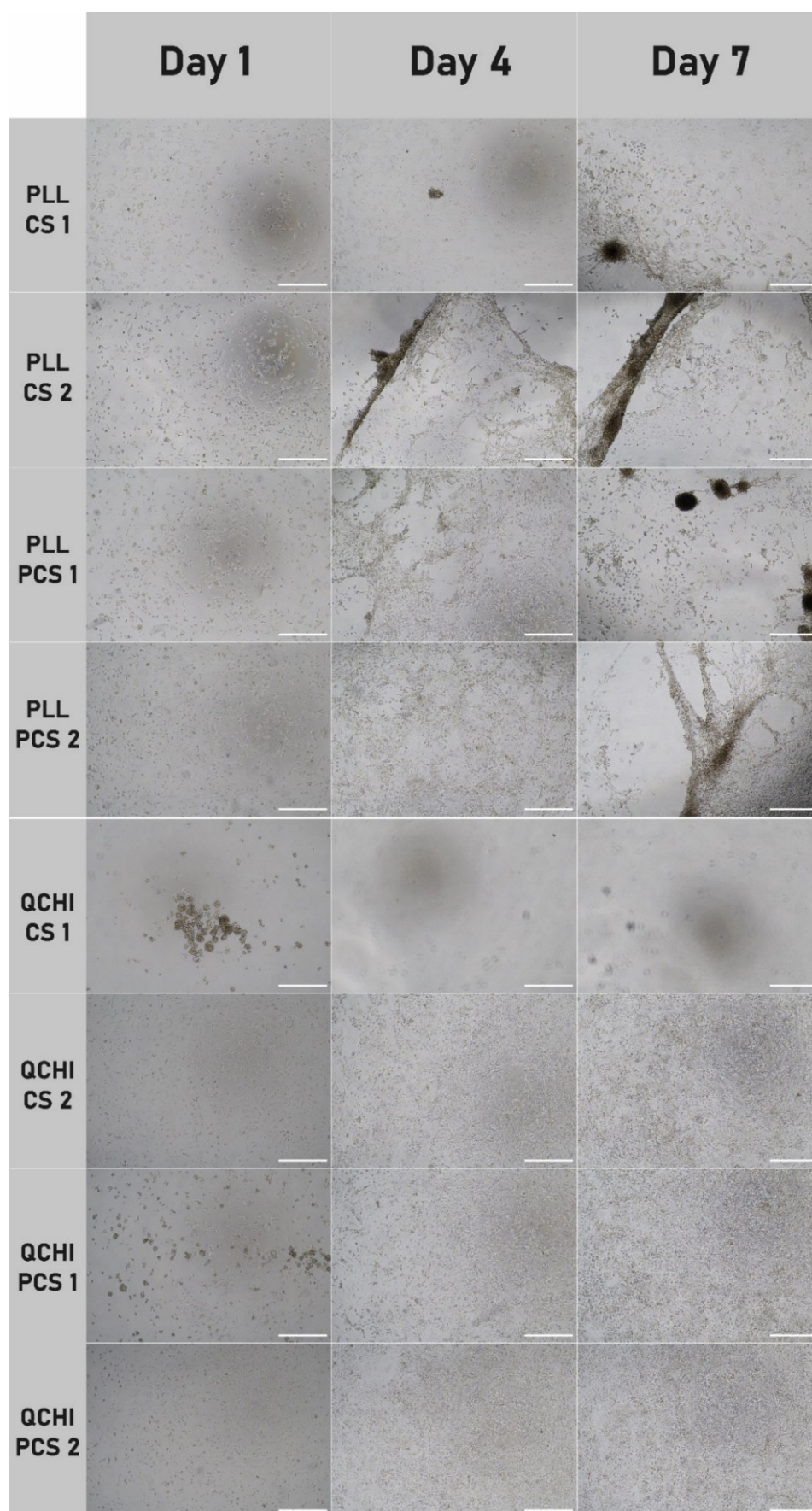
A.2.　Phase contrast images of different cell types

The following images were taken during the seven day Deep Blue assay using a phase contrast microscope. The three different cell types over the course of seven days on TCPS were summarized in one montage. The other image montages represent one of the used cell types each, combining the different PEM films upon which the cells were seeded over the course of seven days. The images show some artefacts due to the imaging conditions. The darker areas in the images are artefacts caused by the small wells the cells were seeded in when observed with the phase contrast microscope. The black dots visible in some images were droplets that formed due to condensation because the cells were taken from 37 ℃ cultivation temperature into room temperature and sealed (under sterile conditions) to reduce chance of contamination using parafilm.
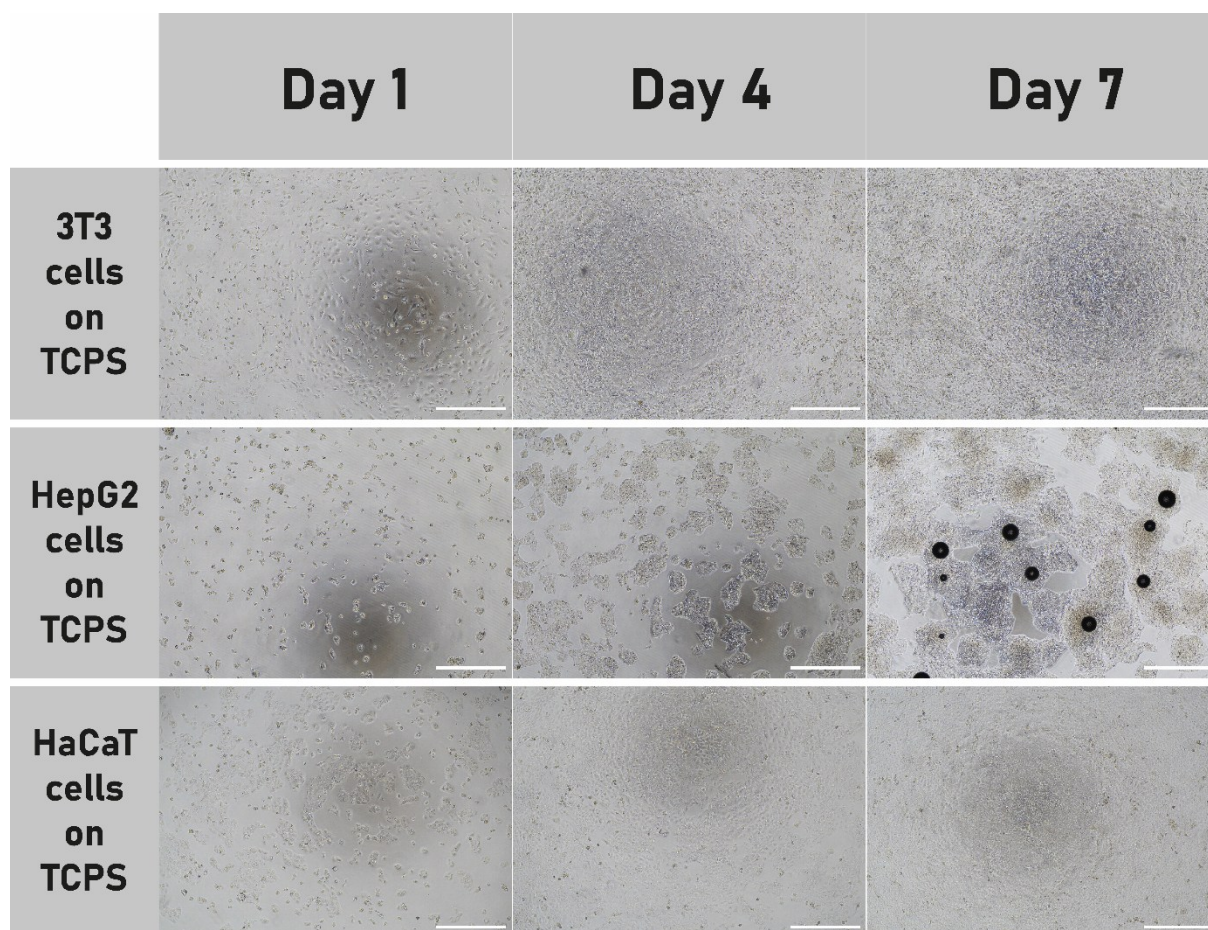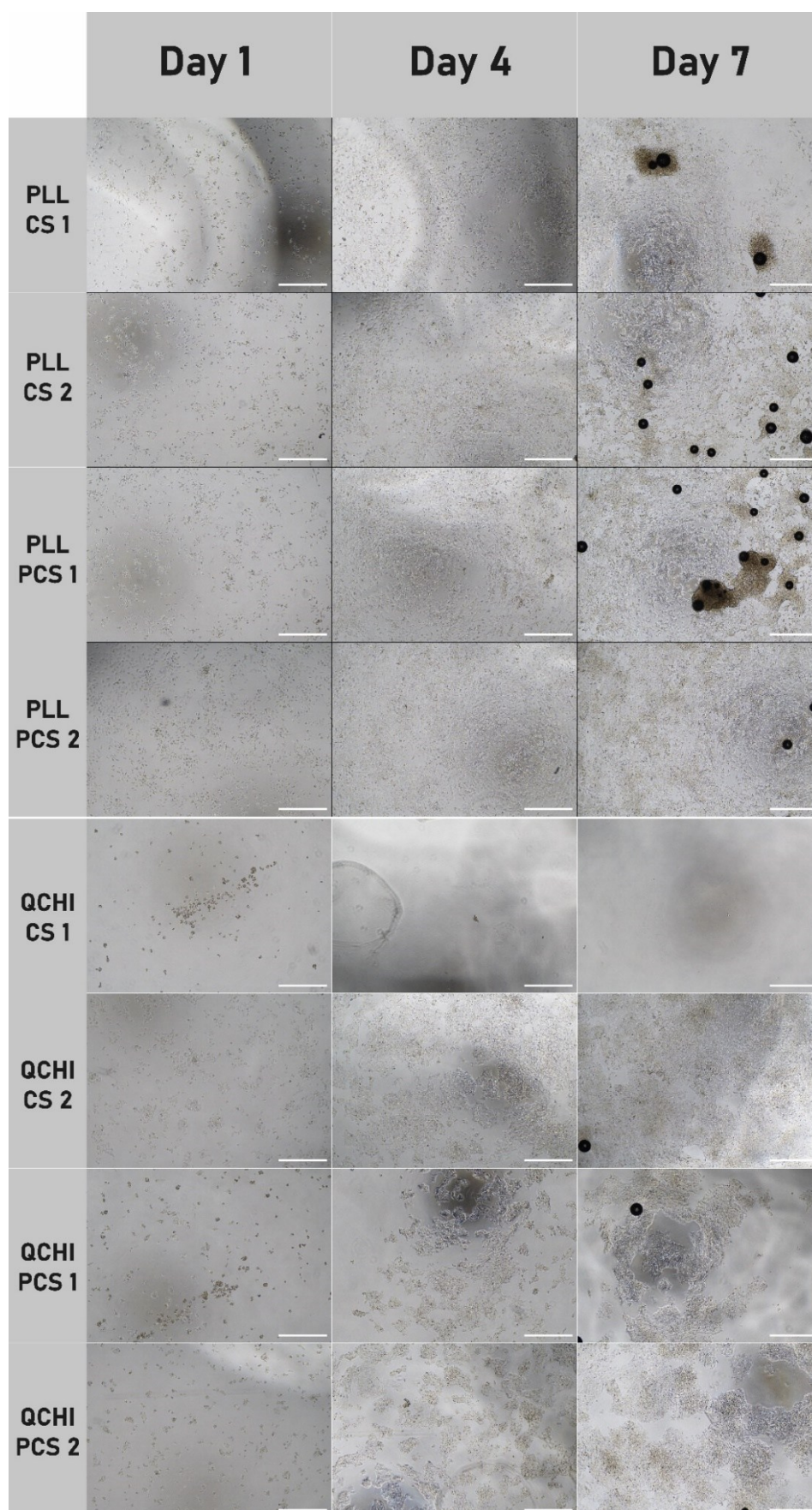

Appendix Fig. 4: Montage of phase contrast images of different cell types on TCPS substrates. Images were taken according to the Deep Blue assay measurement time points on day 1, 4 and 7 of cell culture. All cells grew well and in their typical manner on TCPS surfaces.
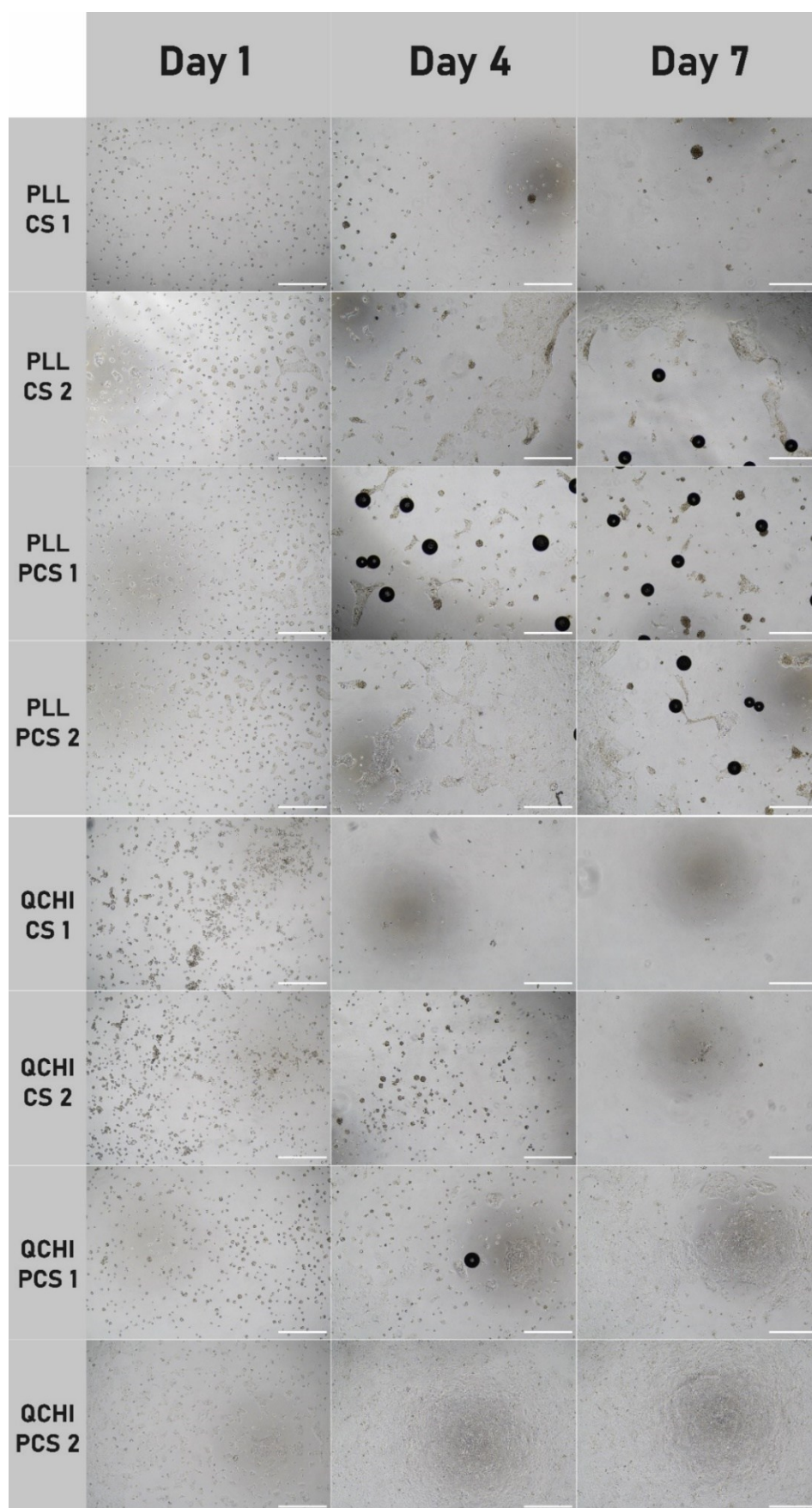
Appendix Fig. 5: Montage of phase contrast images of 3T3 mouse fibroblast cells seeded in well plates coated with different PEM compositions. Images were taken in parallel to the Deep Blue assay measurement time points on day 1, 4 and 7 of cell culture. The observed cell growth confirmed the results from the Deep Blue assay.

122

Appendix Fig. 6: Montage of phase contrast images of HepG2 human hepatoma cells seeded in well plates coated with different PEM compositions. Images were taken in parallel to the Deep Blue assay measurement time points on day 1, 4 and 7 of cell culture. The observed cell growth confirmed the results from the Deep Blue assay.

Appendix Fig. 7: Montage of phase contrast images of HaCaT human keratinocyte cells seeded in well plates coated with different PEM compositions. Images were taken in parallel to the Deep Blue assay measurement time points on day 1, 4 and 7 of cell culture. The observed cell growth confirmed the results from the Deep Blue assay.

Danksagung

Mit dieser Dissertation möchte ich das Kapitel Promotion abschließen. Es war eine wilde, anstrengende, lehrreiche und auch schöne Zeit, die ich sowohl mit der Arbeit, aber vor allem mit den Menschen in meinem Umfeld geteilt habe. Ich möchte mich bei all den Personen bedanken, die mich auf dem ganzen Weg oder auf Teilen des Weges unterstützt haben.

Zuallererst möchte ich mich bei Prof. Dr. Thomas Groth bedanken, der mir die Chance gegeben hat, diese Arbeit im Rahmen eines DFG-Projektes anzufertigen. Der mich als Doktorand in seiner Arbeitsgruppe aufgenommen hat und mich über viele Jahre mit vielen guten Diskussionen, lehrreichen Gespräch und viel Motivation unterstützt hat. Ich möchte mich für das entgegengebrachte Vertrauen und die stets gute Begleitung bedanken. In diesem Rahmen geht ein großer Dank an die Deutsche Forschungsgemeinschaft, welche mit ihren finanziellen Mitteln diese Arbeit erst ermöglicht hat. Durch die großzügige Förderung konnten wir viele unterschiedlichste Experimente durchführen und die Thematik aus vielerlei Winkeln durchleuchten.

Ein weiterer Dank geht an unsere Kollegen von der Georg-August-Universität Göttingen, Prof. Kai Zhang und vor allem Dr. Kui Zeng. Sie haben die chemischen Grundlagen und damit das Material zur Durchführung der Forschungsarbeit geliefert. Ich möchte mich bei Dr. Bodo Fuhrmann vom Interdisziplinären Zentrum für Materialforschung für die Hilfe und Einführung in vielerlei Messmethoden bedanken. Viele Erkenntnisse wäre ohne die freundliche Hilfe und Bereitstellung der Gerätschaften nicht erzielt wurden. In gleichem Maße geht der Dank and Dr. Christian Wölk und Dr. Catharina Husteden, welche beide sowohl durch fruchtvolle Diskussionen, aber auch durch die Ermöglichung einiger Messungen an Ihren Gerätschaften zum Gelingen dieser Arbeit beigetragen haben.

Ich möchte mich bei allen Mitgliedern der Forschungsgruppe bedanken. Ohne euch, eure vielen Diskussionen, Gespräche über Probleme und die gemeinsamen Motivationen, wäre diese Arbeit niemals vollendet wurden. Ich war und bin sehr dankbar, so kompetente, freundliche und unterstützende Kolleg*Innen als Wegbegleiter*Innen gehabt zu haben. Ein großes Dankeschön möchte ich an Marlis Porobin aussprechen. Ohne sie wären einige Versuche nicht möglich gewesen. Durch die tatkräftige Unterstützung, die Koordination von Bestellungen, die Unterstützung bei einer Vielzahl von Experimenten und den immer freundlichen Austausch war die Zeit im Labor mir Frau Porobin immer ein Vergnügen.

Neben den Unterstützern an der Universität gab es jede Menge außerhalb, dazu zählen vor allem die Menschen in meinem näheren Umfeld. Ein spezieller Dank geht an Frau Dr. Götter, ohne Sie und unsere zahlreichen Gespräche wäre ich nicht in der Lage gewesen, diese

125

Arbeit zu vollenden und dabei fröhlich, glücklich und zufrieden zu bleiben. Ich möchte mich bei meinen Freunden bedanken, die sich eins ums andere Mal meinen Frust anhören durften. Ich möchte mich für den Austausch, die Motivation und die vielen schönen Momente bedanken, die das Leben außerhalb der Universität mit euch bereichert haben. Aber vor allem der Ausgleich, beim Sport, am Spieletisch oder bei fröhlichen Runden im Park oder an diversen Küchentischen haben dafür gesorgt, bei diesem Vorhaben nicht komplett den Verstand zu verlieren.

Ich möchte mich bei meiner Freundin bedanken, die vor allem dazu beigetragen hat, dass ich die Arbeit auch final zu Ende bringe und mir selbst nicht im Weg stehe. Danke für dein offenes Ohr und deinen Antrieb. Du hast so viel Kraft, dass es für uns beide reicht. Ich bin schwer beeindruckt und dir immer dankbar.

Zum Abschluss möchte ich mich bei meiner Familie bedanken, die mich bei dem Vorhaben immer am meisten unterstützt hat, mich motiviert hat am Ball zu bleiben und mich durch die tiefen Täler der Demotivation begleitet und aufgerichtet hat, aber nie mehr Druck als nötig ausgeübte. Danke, dass ihr zu mir gehalten habt, egal wie ich mich entschieden habe. Danke, dass ihr mich immer unterstützt habt, wenn ich es am dringendsten gebraucht habe. Danke für alles!

Curriculum Vitae

Personal data

Name	Falko Doberenz
Address	
Date and place of birth	
Gender	male
Nationality	German
Academic degree	Dipl. Ing. (Diplom-Ingenieur)
Subject area of dissertation	Biomedical engineering

Education

03/2018 – ongoing	PhD student Biomedical Materials, Institute of Pharmacy, Biomaterial research, Martin-Luther-University, Halle-Wittenberg
10/2010 – 04/2017	Diploma Studies in Material Science, Advanced Modul: Biomaterials and Functional Materials, Technical University Dresden (TUD)
09/2002 – 06/2010	University qualification exam (Abitur), Ferdinand-Sauerbruch-Gymnasium, Großröhrsdorf

Work Experience

06/2022 – today	TÜV Süd Product Service GmbH, Medical Health Services, Client Manager/Conformity Assessment Responsible for Medical Devices Certification, Hamburg
03/2018 – 08/2021	Martin-Luther-University Halle-Wittenberg, Scientific Assistant in Halle, Working on research project of "Deutsche Forschungsgesellschaft "(DFG)
02/2015 – 03/2017	Centre for Translational Bone, Joint and Soft Tissue Research of the University Clinic Dresden, Student Assistant and Diploma Student, 3D-Plotting/Bioprinting

	"Max Bergmann Centre" on Biomaterial Research at Technical
10/2013 – 03/2014	University Dresden (TUD), Internship, Characterization of
	Biomaterials

List of publications

The following publications were written during the time at the Martin-Luther-University Halle-Wittenberg, relevant for this dissertation:

1) **Doberenz, F**.; Zeng, K.; Willems, C.; Zhang, K.; Groth, T. Thermoresponsive Polymers and Their Biomedical Application in Tissue Engineering – a Review. J. Mater. Chem. B 2020, 8 (4), 607–628

2) Husteden, Catharina, **Falko Doberenz**, Nathalie Goergen, Shashank Reddy Pinnapireddy, Christopher Janich, Andreas Langner, Frank Syrowatka, u. a. „Contact-Triggered Lipofection from Multilayer Films Designed as Surfaces for in Situ Transfection Strategies in Tissue Engineering". ACS Applied Materials & Interfaces 12, Nr. 8 (26. February 2020): 8963–77.

3) K. Zeng, **F. Doberenz**, Y.-T. Lu, T. Groth, K. Zhang, Synthesis of Thermoresponsive PNIPAM-Cellulose Sulfates for Fabrication of Bioactive Multilayers Using Layer-by Layer Technique. ACS Appl. Mater. Interfaces, 14 (2022), 43, 48384–48396

Selbstständigkeitserklärung

Hiermit erkläre ich gemäß § 5 der Promotionsordnung der Naturwissenschaftlichen Fakultät I der Martin-Luther-Universität Halle-Wittenberg, dass ich die Ergebnisse der vorliegenden monographischen Dissertation

Effect of polycations on stability and bioactivity of polyelectrolyte multilayers with thermoresponsive cellulose sulphate

am Institut für Pharmazie in der Arbeitsgruppe Biomedizinische Materialien unter Anleitung von Prof. Dr. rer. nat. habil. Thomas Groth selbständig erarbeitet und die Dissertation ohne fremde Hilfe verfasst habe. Weiterhin erkläre ich, dass ich keine anderen als die von mir angegebenen Quellen und Hilfsmittel zur Erstellung meiner Dissertation verwendet habe. Den benutzen Werken wörtlich oder inhaltlich entnommene Stellen sind als solche gekennzeichnet. Ferner erkläre ich, dass ich mich mit der vorliegenden Dissertationsarbeit erstmals um die Erlangung eines Doktorgrades bewerbe.

Hamburg, den 06.03.2024